Validation of Acoustic Simulations and Investigation of Aeroacoustic Flow Effects for Marine Exhaust Components using Finite Element Analysis

University of Turku
Department of Mechanical Engineering
Master of Science (Tech) Thesis
Wärtsilä Catalyst Systems

Author:
Eero Virtanen

20.04.2026
Turku

Master's thesis

Subject: Mechanical Engineering
Author: Eero Virtanen
Title: Validation of Acoustic Simulations and Investigation of Aeroacoustic Flow Effects for Marine Exhaust Components using Finite Element Analysis
Supervisors: Associate Professor Armin Wehrfritz, Jouni Kivi
Number of pages: 110 pages
Date: 20.04.2026

This work presents two methodologies for numerical acoustic finite element simulations of exhaust components. The methodologies are used to create a case study for a patented mixing silencer component.

First, a finite element method -based linear acoustics model for transmission loss calculations in exhaust components is validated. The results are compared to zero-flow measurements of the component, and the model is reported to achieve results that can be considered exact for engineering decision-making and dimensioning in cases where flow is negligible.

Second, the work also establishes a state-of-the-art complementary model, based on methods validated for other geometries: A linearised Navier-Stokes model combining computational fluid dynamics and the finite element method to incorporate the effects of a mean flow on the transmission loss of a component. This allows for evaluation of whether flow effects need to be considered in the design. The coupling is one-way, meaning that the fluid solution affects the acoustics, but not the other way around.

The main simulations are done on the patented mixing silencer geometry using Comsol 6.4. The silencer is a reactive quarter-wave chamber, which has been combined with another component for space-efficiency in marine applications. Computational fluid dynamics simulations are done using OpenFOAM v13.

The results indicate that exhaust flow causes a meaningful decrease in resonant frequency, where maximal transmission loss occurs. Thus, the flow conditions need to be considered in the design and tuning of large-scale exhaust components. Meaningful results are also obtained on the oscillatory nature of the flow through the component during the CFD studies.

The created models allow for a multitude of future studies to better understand, characterise and simulate various components from a design perspective.

Key-words: acoustics, finite element method, transmission loss, marine exhaust systems, linearised Navier-Stokes, reactive silencer, mean flow, CFD-FEM coupling, numerical validation, quarter-wave resonator, muffler acoustics

Table of contents

Table of symbols

Symbol	Unit	Explanation
∇	1	Nabla operator
c	m/s	speed of sound
d	m	diameter of a duct
dl	m	average element size
e	1	Euler's number
f	Hz	frequency
f_{cutoff}	Hz	cut-off frequency for a propagating wave mode
f_{in}	Hz	incoming frequency
f_r	Hz	resonant frequency for a component
g	m/s^2	gravitational constant
I	W/m^2	sound intensity
i	1	imaginary unit
k	rad/m	wave number
k_0	rad/m	convected wave number
$k_{mn}a$	1	constants related to cut-off of specific modes of order m, n
l	m	length of a quarter-wave resonator
L	m	length of the neck of a Helmholtz resonator
M	1	Mach number
$n_{nodes/\lambda}$	1	number of nodes per wavelength
p	Pa	acoustic fluctuation of pressure/sound pressure
p_b	Pa	background source pressure
p_{fluid}	Pa	absolute fluid pressure
p_{rms}	Pa	root-mean-square value of sound pressure
r	m	radius of the neck of a Helmholtz resonator
R	1	ratio for calculation of decibel levels
R_{gas}	J/(kg*K)	specific gas constant
S	m^2	cross-sectional area of the neck of a Helmholtz resonator

s	Pa/m^2	source term of inhomogeneous Helmholtz equation
$S(\boldsymbol{x}, t)$	Pa/m^2	source term of inhomogeneous wave equation
S_b	m^2	cross-sectional area of a quarter-wave resonator
S_{duct}	m^2	cross-sectional area of a duct
T	K	absolute temperature
t	s	time
T_{int}	s	integration period
TL	dB	transmission loss
u	m/s	acoustic fluctuation of particle velocity
$\boldsymbol{u}$	m/s	flow velocity vector
U_{flow}	m/s	mean speed of convecting flow
V	m^3	closed volume of a Helmholtz resonator
W	W	sound power
x	m	spatial coordinate direction
$\boldsymbol{x}$	m	spatial coordinate vector
y_+	1	y-plus value
z	m	axial direction of pipe
γ	1	ratio of specific heats
δ_{ij}	1	Kronecker delta
Δf	Hz	frequency reduction of attenuation peak
λ	m	wavelength
μ	Pa*s	dynamic viscosity
ν_t	m^2/s	turbulent viscosity
ρ	kg/m^3	density of a fluid
ω	rad/s	angular frequency

Table of acronyms

Acronym	Explanation
ABS	American Bureau of Shipping
ANSI	American National Standards Institute
ASTM	American Society for Testing and Materials
BEM	Boundary Element Method
BV	Bureau Veritas
CAD	Computer Aided Design
CFD	Computational Fluid Dynamics
CFL	Courant-Friedrichs-Lewy
CGNS	CFD General Notation System
CPU	Central Processing Unit
DNV	Det Norske Veritas
FE	Finite Element
FEM	Finite Element Method
FVM	Finite Volume Method
FFT	Fast Fourier Transform
IEC	International Electrotechnical Commission
IMO	International Maritime Organisation
ISO	International Organization for Standardization
KR	Korean Register
LNS	Linearised Navier-Stokes
LR	Lloyd's Register
MARPOL	International Convention for the Prevention of Pollution from Ships
MEPC	Marine Environment Protection Committee
MSC	Maritime Safety Committee
NVH	Noise, Vibration and Habitability
PDE	Partial Differential Equation
PML	Perfectly Matched Layer
RANS	Reynolds-Averaged Navier-Stokes
RMS	Root Mean Square
SCR	Selective Catalytic Reduction
SST	Shear Stress Transport

TL	Transmission Loss

1 Introduction

This thesis aims to validate a useful numerical simulation methodology for predicting the time- or frequency-dependent acoustic performance of mufflers and other components within a marine exhaust system for a diesel engine. The emphasis is on creating workflows that can be readily implemented in industrial design processes. The specific type of product studied in this thesis is a combined urea injection and reactive muffler component, called a mixing silencer.

This chapter establishes the context, motivation and trends for this research. First, the possibilities of numerical methods for engineering design and specifically exhaust silencers are discussed. Then, the importance of emission abatement systems is presented. Finally, the specific scope and objectives of this thesis are defined.

1.1 Possibilities of numerical methods

Static calculations and engineering approximations are often preferred in various engineering fields due to their applicability, simplicity and clarity. Assuming cases to be static or averaging over time naturally omits the time dependency of properties, making calculations simpler. On the other hand, it must be stated that this simplification leads to loss of information and often requires the use of various safety factors based on experiments or experience. This information loss includes both oscillatory and transient effects, both of which can be critical in practical applications.

Examples of these steady-state simplifications can be found across engineering disciplines. In the structural analysis of a building, loads can be calculated by assuming the building to be static, omitting wind loads for example. In electrical engineering or acoustics, where alternating waves are present, the quantities can be treated as constants by calculating the energy or power within the waves. In fluid mechanics, time-averaging unsteady turbulence allows for steady-state analysis.

It is important to understand when only steady analysis can be used. A popular example of a failure caused by oscillatory behaviour is the fall of the Tacoma Narrows Bridge [1], which was caused by wind-induced harmonic vibration that was not accounted for in the design.

Due to increased availability in both software packages and calculation resources, numerical methods offer a practical alternative to simpler calculation methods. All numerical methods

aim to somehow discretise the domain into smaller elements that can function as approximations of the continuous physical phenomena. Thus, the large, complex problem can be divided to many simple problems that can be solved by a computer. Exactly like a physical problem can be discretised in space, a time-dependent problem can be discretised in time or, in the case of harmonic behaviour, transformed into the frequency domain and solved in small steps.

Analytical methods simply do not allow for general solutions to complex time-dependent engineering problems. Comparatively, while time- or frequency-dependency does add computational cost in numerical methods, they are still possible and often very feasible. Numerical methods have only become more and more viable as the amount of available computational resources constantly increases [2]. This thesis aims to utilise the tools brought about by the current trends to improve design methods [3].

Based on these factors, numerical methods can clearly be beneficial for engineering design and virtual prototyping. We must still remember that a calculation is only valuable if the modelling methods are somehow validated.

1.1.1 Possibilities of numerical methods in exhaust acoustics

A practical example of the efficient use of numerical methods in the field of exhaust muffler acoustics is presented in [4] where the acoustics of multi-chamber perforated resonators were investigated. For a complex geometry, the analytical formulas get very complex, and the formulas need to be re-adapted for every new kind of geometry. Numerical methods remove this burden and make it easier to predict or replicate physical phenomena for engineering design based on only boundary conditions. The history and well-known examples of acoustic Finite Element Method (FEM) analyses of mufflers can be found in [5, Ch. 10.9].

Additionally, three-dimensional numerical methods like FEM and CFD (Computational Fluid Dynamics) allow for removal of geometric assumptions that would otherwise be needed to solve these problems. As an example, traditional modelling of an exhaust system often assumes that only plane waves, meaning plane-shaped wavefronts, propagate within ducts. An illustration of a plane wave propagating through a duct can be seen in Figure 1. In acoustics literature, this assumption is often referred to as the ducts functioning as a simple waveguide [5, Ch. 3.18]. With these models, any phenomenon in the radial direction is ignored, whereas FEM allows for the analysis of complex modal shapes.

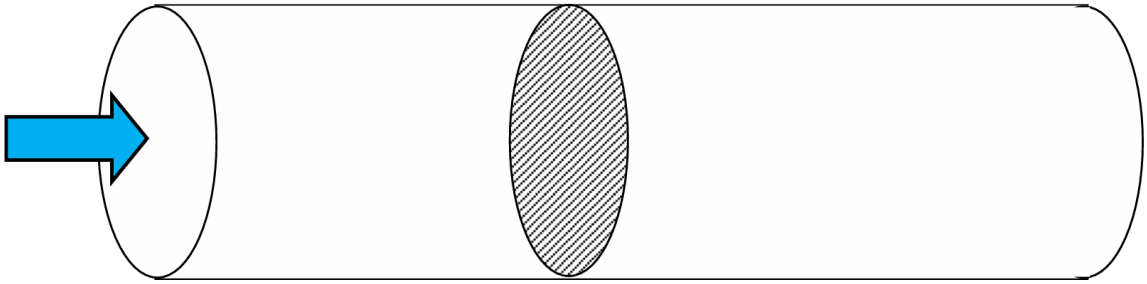

Figure 1: An illustration showing the shape of a single plane wavefront propagating in a pipe. The arrow indicates movement of the plane wave.

These advantages mean that acoustic numerical methods can be useful in design of new silencers. FEM-analyses give the additional benefit of also predicting phenomena that are not expected by the designer. The engineer setting up a simulation does not have to fully understand what will happen inside the simulation, as long as the boundary conditions are correct and physical. This might be the case when a part has been designed with something else than acoustics in mind or when dealing with complex designs. FEM-based evaluations of various silencer concepts have already been done in [6], [7], [8], where the manual set-up of a case consists of correct boundary conditions and a mesh of the domain.

1.2 Importance of emission abatement systems

In modern literature of emission abatement systems, the focus is often on technologies and methods to reduce exhaust gas emissions. In a combustion engine context, these include for example nitrogen and sulphur oxides, carbon dioxide, particulates and methane. This approach is immensely important to reduce the climate impact of running engines on fossil fuels, which is the main function of the various exhaust gas treatment systems. There are also regulations to adhere to, perhaps the most notable regulation in a marine context being the International Convention for the Prevention of Pollution from Ships (MARPOL) [9], which has been steadily updated and made stricter since 1973. MARPOL functions as a collection of annexes that set limits on various types of pollution from ships, including oil, chemicals, sewage, garbage, and air emissions.

While the importance of controlling exhaust gas emissions is undisputed, vibration and noise are also forms of pollution. On a mild level, they can be an annoyance to humans, but they can also pose a health risk at heavy exposure. There are also standards and classifications that determine the maximum noise levels on board ships [10], airborne noise radiated by ships [9], [11], and acceptable vibration levels aboard ships [12].

It is important to notice that acoustics is inherently linked to the physical behaviour of the exhaust system. Sound is simply longitudinal vibration, meaning the alternating compression and rarefication, of air. Thus, solid and acoustic vibrations are inherently connected. These vibrations are also affected by the flow through the exhaust components.

Vibrations caused by acoustic standing waves that match the modal frequency of a structure have the potential to cause mechanical failures through fatigue. As an example, a fluid-structure coupled FEM-analysis that assesses the structural effects of pipe shell vibration modes is performed in [13]. If a standing wave within the exhaust system happens to match a modal frequency of a component in the exhaust system, a comparatively small acoustic oscillatory pressure can cause measurable amplitudes in the solid parts through resonation [14]. This eventually leads to fatigue failures in structures and breakage in sensitive components like sensors.

To study marine exhaust systems, it is required to understand the functions of some common emission abatement components. A Selective Catalytic Reduction system (SCR) is the favoured option for reducing nitrogen oxides emissions [7], [15]. For sulphur oxides, various scrubber systems can be employed [16].

Functionally, an SCR system includes urea injection into the flow, which then travels through catalytic components within some kind of catalytic reactor.

Usually, mufflers and silencers are installed as components separate from the emission reduction systems. Because of this, the acoustic properties of SCRs or scrubbers are rarely considered in the design phase, which means that they are often suboptimal acoustically. To combat these challenges, a combined SCR and muffler has been designed and evaluated in [6], for example. The paper also notes that integrating a muffler with SCR is a good choice regarding space limitations on vessels.

In the specific case of Wärtsilä Catalyst Systems, an integrated urea injector and muffler component, called a mixing silencer, has been developed and patented [17]. This component is the focus of studies included in this thesis, and it is presented in Chapter 4 and in detail within the patent.

The idea of the mixing silencer is to integrate a reactive silencer into another component of the exhaust system to make the system more compact. The combining of components is also useful from a practical perspective; Often the design and routing of exhaust piping is done by

the shipyard, but components like the SCR are designed by the engine manufacturer or at least in collaboration with the engine manufacturer to ensure compatibility. With the integrated silencer, there is one component less to fit into the system, and the silencer will be tuned correctly to the engine. It should be noted that in the case of the mixing silencer, additional silencers are always needed as the mixing silencer is a narrowband quarter-wave reactive silencer that is tuned for specific engine excitation frequencies. The theory of how quarter-wave silencers behave is described in Chapter 2.3.

Whether one is trying to make a novel silencer for a specific engine or trying to integrate beneficial acoustic properties into another component, three-dimensional numerical methods have been proven to be beneficial due to the complexity of the geometry. Examples of these kinds of studies can be seen in [4], [6], [7], [8], [18], [19], [20], [21], [22].

Generally, it can be noted that numerical methods in their current state are able to provide useful and accurate information for silencer design. Implementing numerical methods has become simpler and more economical to ascertain the transmission loss of muffler in recent years [23].

The argument for the usage of numerical methods in designing emission abatement systems is supported by the increasing number of computational resources. High-performance computing and large-scale data analysis is becoming increasingly accessible, which will allow for the usage of computational resources to solve more complex problems in both academia and industry [2]. As most engineering problems concern linear acoustics [24], the computational requirements of acoustical FEM are low when compared to much more complicated simulations like CFD, which can also include acoustics [20]. Supported by these facts, this thesis will validate a practical FEM workflow for acoustics.

1.3 Thesis scope and objectives

The purpose of this thesis is to find a practical engineering workflow for simulations of the frequency- or time-dependent acoustic behaviour of marine exhaust systems based on three-dimensional CAD (Computer-Aided Design) geometry. The specific type of component studied, called the mixing silencer, in this thesis is defined by the patent [17].

The nature of the thesis is experimental and comparative; the simulation results are compared to analytical solutions and real-world experimental data.

This research is grounded in a postpositivist worldview. Thus, it is recognised that simulation results and knowledge of the exact phenomena within an exhaust system will always include approximations, as is typical for all engineering fields. The experimental approach strives to improve the level of understanding and allow for better engineering choices to be made, while considering the limitations of various models. This goal is reflected in the language, depth of theory, and methods of this thesis to make it more approachable for engineers and leadership not specialised in acoustics.

The physical size of the scope is restricted to allow for less costly calculations and due to limitations of obtaining and publishing geometry information. All analysis is confined to include only a single component of an exhaust system, the patented mixing silencer.

There are also requirements for the considered models regarding future studies. There should be no modelling restrictions on future expansion to simulate bigger or more complete marine exhaust systems. Additionally, there needs to be a method of coupling the acoustic simulation with vibration of solids, as the effect of acoustics creating vibration and fatigue in the solid parts of the system is of great importance.

The research can be divided into two parts: Firstly, a validation study is performed. Acoustic measurements without flow at atmospheric temperatures are compared to a lossless linear acoustics FEM simulation with a similar physical setup. Secondly, a more complex and computationally intensive aeroacoustic simulation that incorporates CFD results will be performed to quantify the effects of flow through the component and to determine if the flow should be considered in the design of silencers. The second study will not be validated, as there is no measurement data to compare against, but it is based on methods that have been validated for other acoustics cases.

2 Theory

This chapter will cover the theoretical basis of acoustics in mufflers and silencers, touching on both analytical and numerical methods. The contents are heavily focused around silencer acoustics. A more general and easy to read introduction to acoustics can be found, e.g. in [25]. The mathematics are presented using a similar notation as used in *Engineering Acoustics : Noise and Vibration Control* by M. J. Crocker and J. P. Arenas [5].

2.1 Acoustic quantities

The quantity humans hear is pressure fluctuations from the normal atmospheric pressure [26, Ch. 1]. Since the pressure is continuously fluctuating, it is often useful to refer to the Root Mean Square (RMS) of the sound pressure, defined as [5, Ch. 3.3.1]

$$p_{rms} = \sqrt{\frac{1}{T_{int}} \int_0^{T_{int}} p^2(t) dt} \,, \tag{1}$$

where p is the instantaneous acoustic fluctuation from the mean pressure, also known as instantaneous sound pressure. t is time and T_{int} is the integration period.

The intensity of sound represents the flow of sound energy per time and area. Thus, it can be used to evaluate acoustics from an energy flow perspective. The intensity I through a unit cross-sectional area is generally calculated as (adapted from [5, Ch. 3.3.3])

$$I = pu = \frac{1}{T_{int}} \int_0^{T_{int}} p \cdot u \, dt \,, \tag{2}$$

where u is the fluctuating particle velocity.

After defining intensity, sound power in a plane wave case within a duct can be simply calculated by intensity times the cross-sectional area of the duct.

The decibel is a crucial concept due to the large range of values in sound pressure, intensity and other acoustical measures. When a quantity is measured in decibels, the result is called a level. The decibel is defined as

$$\log_{10} R = 0.1 \rightarrow 10 \log_{10} R = 1 \text{ dB}. \tag{3}$$

R represents a ratio of the actual value to a pre-determined reference value [5, Ch. 3.4].

In practice, using decibels to represent absolute values requires reference values to be chosen. Various definitions for R can be seen in Table 1.

Table 1: Reference values for dB calculations of various quantities. Values taken from [5, Ch. 3.4].

Quantity	Reference value	Ratio to reference
Sound pressure p	$p_{ref} = 20\ \mu\text{Pa}$	$R = \frac{p_{rms}^2}{p_{ref}^2}$
Sound power W	$W_{ref} = 10^{-12}\text{W}$	$R = \frac{W}{W_{ref}}$
Sound intensity I	$I_{ref} = \frac{10^{-12}\text{W}}{\text{m}^2}$	$R = \frac{I}{I_{ref}}$

Special attention should be given to the fact that the pressure values are squared in the definition of R for sound pressure, but the same treatment is not present for power or intensity. This is to make the scales consistent; As the pressure values represent amplitude, they need to be squared to represent the power contained in the amplitude. Thus, all dB-levels represent ratios of power. As $10\log_{10} 2 \approx 3$ dB, every 3 dB represents a doubling of acoustic power, but for the same 3dB increase, the amplitude increases by a factor of $\sqrt{2}$.

Due to these factors, it is practical to understand that in harmonic cases where pressure is measured in dB-levels, RMS-values can be converted to peak values by adding 3 dB.

When decibels are used to calculate relative quantities such as Transmission Loss (TL), which quantifies how much sound power is transmitted through a component, reference values are not needed as R is then simply the ratio of two values. In the case of TL, R is the value of sound energy or power before a component over the sound energy or power after a component [5, Ch. 8.7.4].

2.2 Acoustics of ducts and pipes

Sound waves are always longitudinal, meaning that they compress and rarefy the air as they travel. It is important to distinguish that sound wave motion is a pressure disturbance on the general pressure of the surrounding material. One of the simplest and most useful ways to model acoustic behaviour is by analysing plane wave behaviour that is defined as “waves that have the same acoustical properties at any position on a plane surface drawn perpendicular to the direction of propagation of the wave” [5, Ch. 3]. The plane wave propagation is visualised in Figure 1. These kinds of waves are very realistic within a duct or an exhaust pipe, where

they can be modelled as a one-dimensional wave traveling along the pipe. When higher frequencies are involved, there are also radial waves present in the pipes, but for low frequencies, the one-dimensional plane wave assumption holds true. Various pipes and ducts that confine the wave propagation are often called waveguides [5, Ch. 3].

Eriksson [27] showed that the "cut-off frequency" where the plane wave assumption stops working for a circular duct is $f_{cutoff} = \frac{1.84c}{\pi d}$, where c is the speed of sound and d the diameter of the duct. The constant 1.84 emerges from the circular geometry and governing wave physics [27]. Above this frequency, there are more complicated waves that travel also in the radial direction of the pipe or duct.

As many methods of measurement and analysis rely on the wave assumption, it is noteworthy to specify the frequency criteria for various higher order modes. Although an infinite number of various modes are physically viable, only specific modes can propagate in a waveguide. A table listing values corresponding to the first cut-on frequencies in cylindrical waveguides of radius a is given, e.g., in the *Handbook of Acoustics* [28, p. 87]. The following equation is a condition for specific frequencies to be "cut-on":

$$\frac{\omega a}{c} > k_{mn}a, \tag{4}$$

where $\omega = 2\pi f$ and c is the speed of sound. $k_{mn}a$ are a list of constants for various orders (m, n) [28, p. 87]. For easy calculation of cut-off frequencies of specific orders, we can write

$$f_{cutoff,mn} = k_{mn}a \cdot \frac{c}{\pi d}, \tag{5}$$

where d is the diameter of the circular pipe and the propagating frequencies must be over f_{cutoff} for a specific higher order (m, n) mode to propagate. The results produced by Eriksson [27] and the *Handbook of Acoustics* [28, p. 87] are equivalent, as both list the first constant as $k_{10}a = 1.84$, although using slightly different notation.

In cases where we are under the lowest cut-off frequency, where $k_{10}a = 1.84$, disturbance in a thin cross-sectional element of fluid in a duct can be described by the one-dimensional wave equation

$$\frac{\partial^2 p}{\partial x^2} - \frac{1}{c^2}\frac{\partial^2 p}{\partial t^2} = 0, \tag{6}$$

where p is the sound pressure, c is the speed of sound, x is an axial coordinate direction and t is the time, with four assumptions: [5, Ch. 3.3]

1. Amount of fluid is conserved
2. The net longitudinal force is balanced by the inertia of the fluid in the element
3. Adiabatic system
4. No fluid flow

Equation (6) is called the one-dimensional acoustic wave equation. It can be expanded to three dimensions by adding second order partial derivatives of pressure over all cartesian coordinate directions. Transformations of Equation (6) to include relations to temperature, particle speed or density can be found in [29].

The speed of sound waves c for a perfect gas is given by [5, Ch. 3.3]

$$c = \sqrt{\gamma R_{gas} T}, \tag{7}$$

where γ is the ratio of specific heats, T the absolute temperature and R the specific gas constant.

In addition to wave acoustics, described by the wave equation, ray acoustics and energy acoustics offer alternative approaches to acoustic problems. In ray acoustics, rays that approximate the solutions to the exact acoustical solution are calculated. Ray acoustics are useful in cases where there are gradients in the fluid properties. In energy acoustics, calculations are based on acoustic energy density. Both ray and energy acoustics are useful in physically large high-frequency problems. [5, Ch. 3]

2.3 Acoustics in exhaust components

In the context of vibro-acoustics, the purpose of an exhaust system is generally to minimize the vibration effects of the flow. When the acoustic excitation frequencies match either the modal frequencies of the fluid within a system or the modal frequencies of the pipeline structure, there is potential for significant vibrations [14]. These kinds of resonance phenomena are to be avoided, as the vibrations cause noise and fatigue damage.

For complex systems, avoiding all fluid and structure resonances is a huge challenge. In Ref. [30], a simple system model for treating noise and vibration problems is presented. The model is visualised in Figure 2.

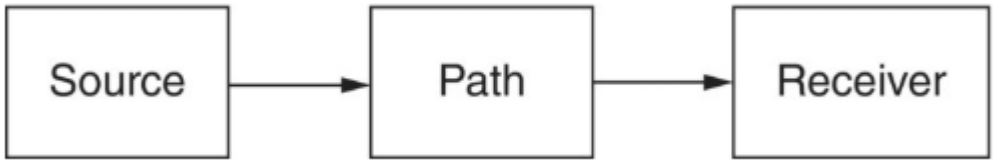

Figure 2: The source-path-receiver model for noise and vibration problems, presented in [30].

The idea of the model is that it gives the order in which the physical phenomenon happens, but also the order in which preventative measures should be taken. If applied to the problem of exhaust systems, the source would be the engine and attached turbomachinery. From the point of view of designing exhaust systems, the source cannot be modified.

For noise, the system formulated in Figure 2 is clear. The path is the exhaust system, and finally the receiver is whatever measuring device or position for a human is defined. Regarding structural vibrations, however, which we are also a pertinent part of the system as they can lead to mechanical breakages, the path and receiver in this problem are the same: The exhaust system itself. Additionally, there might be additional paths and sources on board a ship, for example. This complicates the situation compared to having a human receiver that can be equipped with hearing protection if everything else is too difficult to analyse.

The source-path-receiver model also defines that dominant sources, paths or receivers should be treated first, and then one should move on to the next one [30]. This allows for a practical way of thinking; As we can measure and gain information about the source, we should focus on amping the frequencies that are deemed to be the most critical within the exhaust system. If we can balance or dampen the frequency peaks present in the acoustic excitation, the benefits affect the entire system. This is very much applied in Catalyst System design in Wärtsilä, as exhaust components can be optimised to the specific Wärtsilä engine configuration.

In addition to being in accordance with the model, focusing on the excitations is also smart from a computational view. Entire systems will always be more complicated to model than single components, no matter how the model is built. Thus, focusing on a specific component that dampens the excitations from the source is also computationally efficient, and the benefits should affect the entire system.

Focusing on the excitations uncovers a new subject: What kinds of silencers or mufflers can attenuate various frequencies, and how can they be designed?

Silencers are often divided to dissipative and reactive silencers based on the working principle [5, Ch. 10]. Most silencers are a combination of the two. Reactive silencers, in accordance with their name, react to the incoming sounds, and reflect the waves resulting in absorption of energy in specific frequencies. Dissipative mufflers have some kind of absorptive material that converts sound energy into heat. These effects do overlap somewhat, and there are sources that state that even dissipative mufflers mostly function through reflection [31].

In the marine engine application, the low-frequency vibrations are of special interest. A review of noise and vibration reduction in marine applications states that the vibration and noise from a diesel engine is in the range of 1 – 1000 Hz [32]. It is also well-known that engine vibrations are focused on half-order multiples of the revolution speed of the engine [33]. The most important vibration orders of Wärtsilä engines studied in this work are also in the same range, under 1000 Hz.

Dissipative materials typically become less and less efficient for low frequencies [5, Ch. 9.5]. Thus, reactive geometries are useful in damping low frequencies around the mentioned frequency range.

An example of a reactive silencer that can be tuned to dampen a specific excitation frequency is the Helmholtz resonator, visualised in Figure 3.

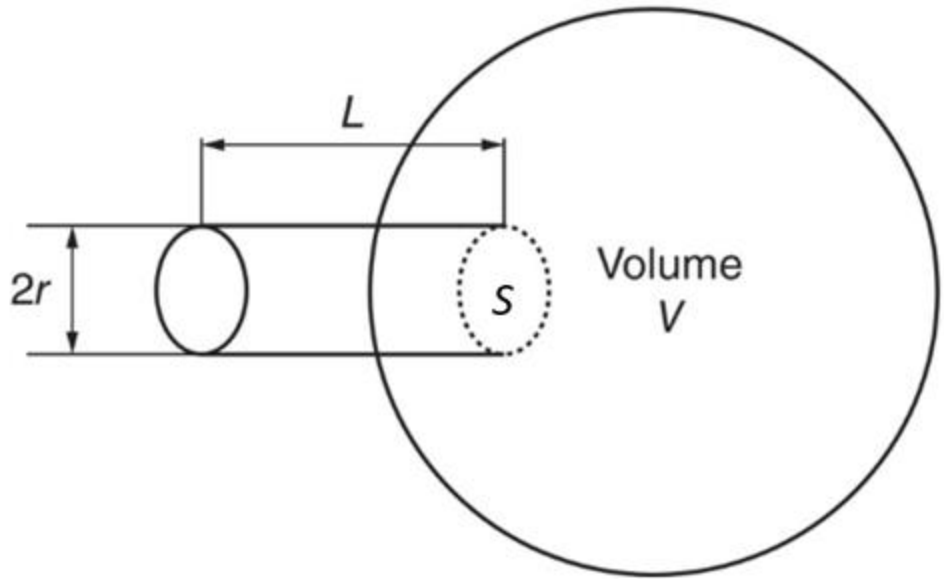

Figure 3: A Helmholtz resonator consists of a neck of radius *r*, length *L* and cross-sectional area *S*, and backed by a closed volume *V*. Adopted from [5, Ch. 9.5.5].

The Helmholtz resonator is effectively a mass-spring system, where a standing wave in the neck is the vibrating mass, and the air in volume V functions as a spring. For a circular neck and neglecting boundary effects, the resonance frequency f_r can be calculated by [5, Ch. 9.5.5]

$$f_r = \frac{c}{2\pi}\sqrt{\frac{S}{(L+1.7r)V}}, \tag{8}$$

where c is the speed of sound and other variables are visualised in Figure 3. The exact value of the factor $1.7r$ depends on the geometry of the ends of the neck and is called the end correction factor. Due to size constraints, Helmholtz-type silencers are mostly used in the frequency range $20 - 400$ Hz [5, Ch. 9.5.5].

It is interesting to note that the resonance frequency is also the one with maximum energy loss. This is due to there being a maximal amount of acoustic vibration within the reactive silencer, meaning maximal energy losses and maximal damping. It should also be noted that Helmholtz resonators have a sharp resonance peak, meaning that they function on a very narrow frequency band.

The quarter-wave resonator is a very similar concept to the Helmholtz resonator, except that it has multiple values of high-damping frequencies. These are given by [5, Ch. 9.5.5]

$$f_r = \frac{nc}{4l}, n = 1, 3, 5, \ldots \tag{9}$$

where *l* is the length of the silencer.

As an example for $n = 1$, as the wave of frequency f_r enters the resonator, and reflects from the end back to the inlet, it travels the length $2l$. Because *l is* a quarter of the wavelength, the reflected wave will have travelled half a wavelength. This means that it is in the exact opposite phase to the incoming wave and they interfere destructively. A similar process can be shown for all possible n. A simple construction can be seen in Figure 4. [5, Ch. 9.5.5]

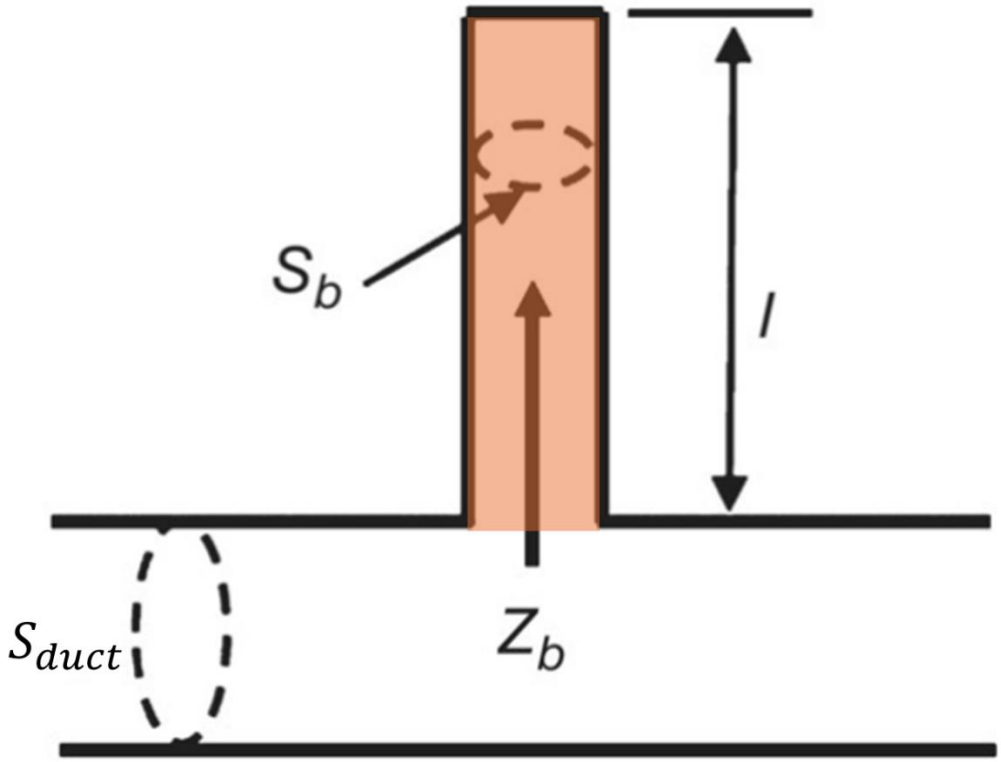

Figure 4: Simple quarter-wave silencer, highlighted with orange. *l* is the length of the silencer, S_b and S_{duct} are areas of the ducts and Z_b is the input impedance of the resonator. Adapted from [5, Ch. 9.5.5].

Generally, resonators with bigger ratios $\frac{S_b}{S_{duct}}$ allow for higher TLs. This can be seen from the formula regarding quarter-wave silencer TL as a side branch from [5, Ch. 10.6.2]:

$$TL = 10 \log \left[\frac{\tan^2(kl) + 4\left(\frac{S_{duct}}{S_b}\right)^2}{4\left(\frac{S_{duct}}{S_b}\right)^2} \right] \tag{10}$$

k represents the wave number, TL the transmission loss and the length and areas are defined in Figure 4. TL is defined in Chapter 2.4.

Both quarter-wave and Helmholtz silencers offer approaches to attenuating specific engine excitation frequencies to prevent problems in marine exhausts. There are some notes in literature that their resonance peaks can be somewhat widened by including dissipative or porous materials [34]. As a development concept, this would be useful to allow for small variance in engine rpm or to account for changes in the speed of sound due to temperature changes.

It is notable that Equations (9) and (10) do not include any end correction terms. End correction is required due to the three-dimensional effects at discontinuities in a pipe, and they are used to change the lengths of components in the one-dimensional analysis. An example of how end correction can be utilised to make one-dimensional modelling more accurate can be seen in [35]. The process is visualised in Figure 5.

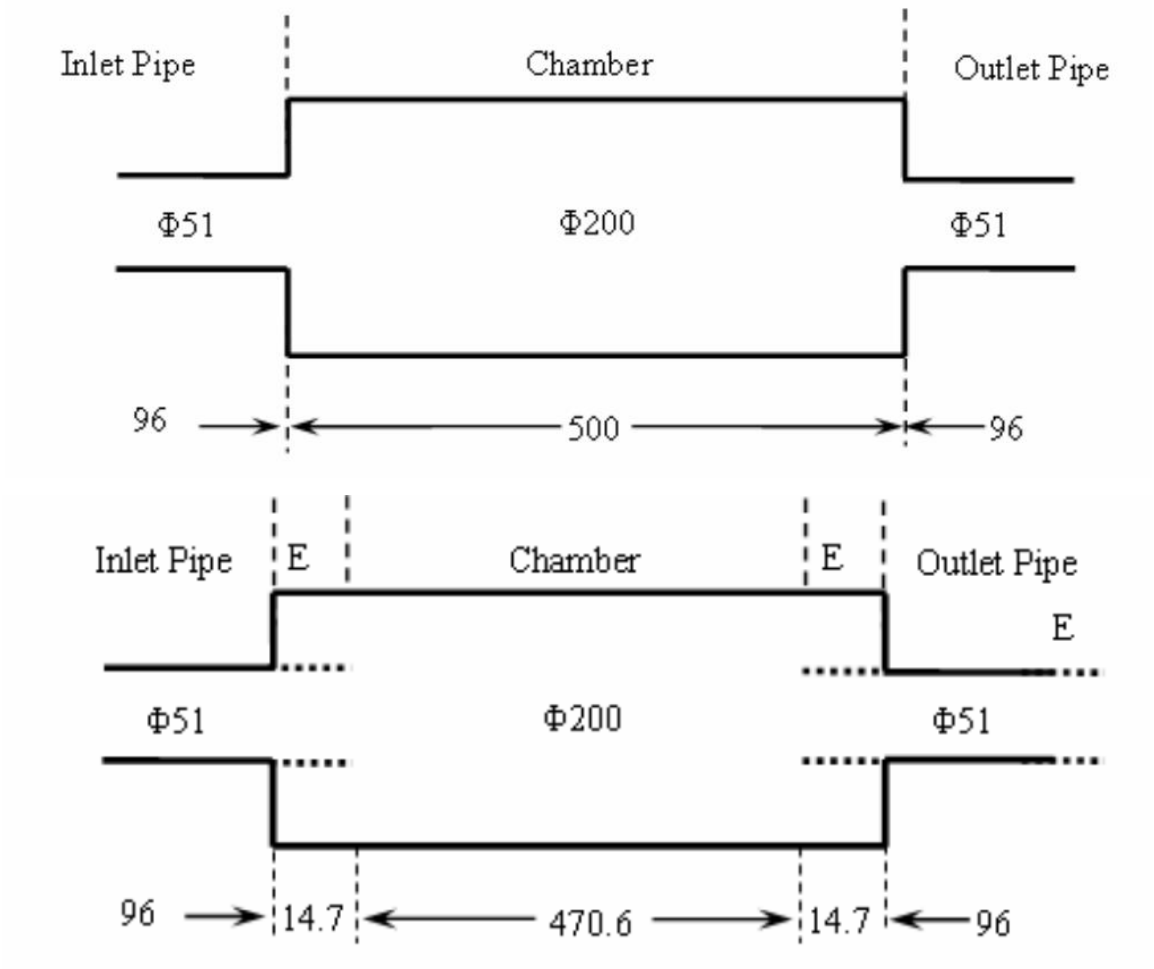

Figure 5: A simple expansion chamber component. On the top, the real geometry can be seen. On the bottom, end corrections that are required with one-dimensional models are shown with dashed lines. Adapted from [35].

It should be noted that having to manually determine end corrections for every component is exactly what this thesis is trying to prevent by validating a numerical method that is inherently three-dimensional.

Thus far we have omitted the effects of the mean flow on the acoustics of an exhaust component. Multiple sources suggest that using the theory that does not account for the effects of the flow starts to have errors when the mean flow Mach number is 0.1 or higher [5, Ch. 10], [36], with the effects and exact values varying based on the application. The error naturally increases as the Mach number increases. The effects of mean flow are included in this research scope, and they are numerically investigated. The numerical approach on mean flow effects is described in Chapter 2.5.1.

2.4 Measurement methods for obtaining data about performance of silencers

The main parameter of a muffler is naturally the amount of attenuation at various frequencies. Thus, it is useful to be able to define the acoustic attenuation and frequency response of a single component. For this purpose, TL can be used. It is defined in [5], as "10 times the logarithm (to base 10) of the ratio of the sound power incident on the dividing structure to the sound power radiated on the receiving side". Referring to Table 1, we can write $R = \frac{W_{in}}{W_{out}}$. An example transmission loss figure for a quarter-wave silencer can be seen in Figure 6.

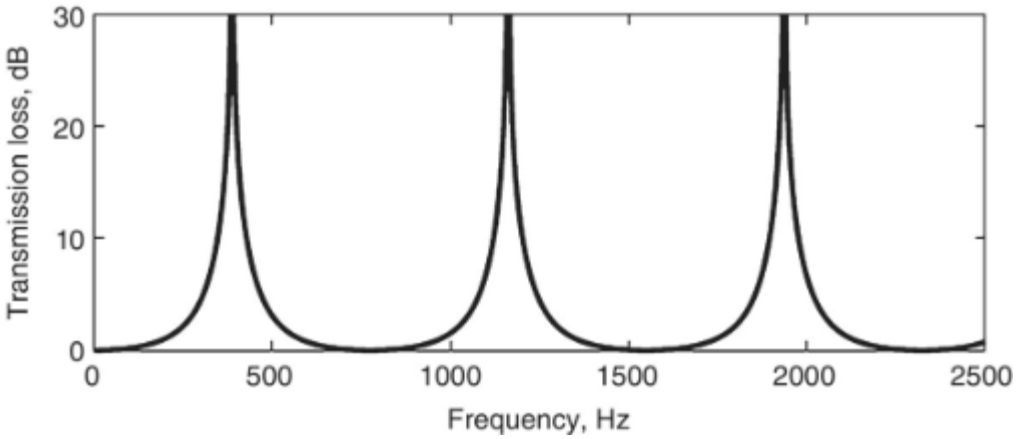

Figure 6: Transmission loss for side-branch quarter-wave resonator. Note the higher order spikes for n=3 and n=5. Adopted from [5, Ch. 10.6.2.].

The exact terminology varies in literature, but intuitively the TL graph shows which frequencies are attenuated, and by how much, by comparing the sound power before and after a component using the decibel scale.

The TL results are usually measured or simulated at a single constant temperature. Once the behaviour in one temperature has been determined, it is simple to transform the results into another temperature. From the perspective of simple linear acoustics, the only quantity that varies with temperature is the speed of sound. Looking at the problem from another perspective, we can say that the wavelength that is attenuated by a component (quarter-wave resonator, for example) is constant as the length l is constant, and the resonant frequency only changes because the speed of sound varies. Thus, we can write

$$\lambda = const. \leftrightarrow \frac{c_1}{f_1} = \frac{c_2}{f_2}, \tag{7.1}$$

where λ is a wavelength with certain behaviour, and c_i and f_i represent speed of sound and corresponding frequency at various temperatures. Combining Equation 7 with 7.1, we can

achieve the following result for evaluating the transformation of frequencies from one temperature to the next.

$$f_2 = \sqrt{\frac{T_2}{T_1}} \cdot f_1 \tag{7.2}$$

T_i represents the temperature in Kelvin for the two cases. This methodology allows for a single calculation or measurement of TL to be easily transformed into the temperature of interest with the assumption of linear acoustics.

The two-source method is one of the possible measurement procedures to experimentally determine the TL of a component. The mathematical background and principles are presented in [37], but it should be noted that the method assumes only plane waves at the inlet and outlet. The measurement setup can be seen in Figure 7. Two measurements are made: White noise, or in some cases a sine wave sweep, is input first upstream of the muffler, and then downstream of the muffler in the second measurement. Then, the data from the four microphones can be used to calculate a four-pole transfer matrix and the TL can be plotted. While not identical in execution, the two-source method preserves the core methodological approach of the standard measuring technique for absorptivity of materials described in [38].

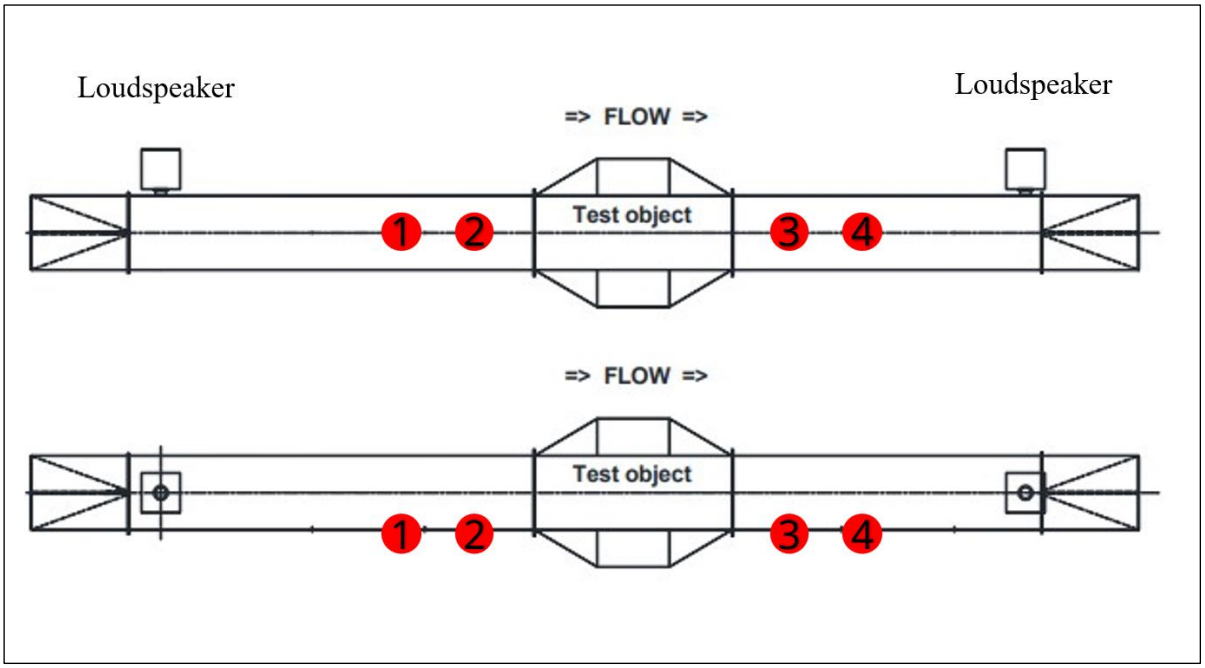

Figure 7: Measurement setup for two-source method. Four microphones marked in red.

The same basic methodology using plane wave inlet and outlet conditions has been extended to FEM-simulations [39]. If we use this methodology to extract TL figures from our

simulations, they will be a great asset in comparing whether the simulation results match what is measured in real life. In FEM, one could simulate microphones similarly to the two-source method, but it is simpler to just integrate the sound power over the inlet and outlet, as the fields are known.

Finding the TLs for specific components also allows for building a model for the whole exhaust system part-by-part by connecting blocks defined by TL matrixes to each other using one-dimensional duct models. This function is included in the acoustic modelling software Actran, for example [40, p. 771].

There are also other areas of interest that may be obtained from the simulations but not measured: As the purpose of this thesis is to find a method to be expanded upon in the future, behaviour of waves and other field data within the system is also of interest. Due to confidentiality reasons, they will not be analysed in this work.

2.5 Numerical methods used for acoustics in exhaust components

For cases where the assumptions of Equation (6) are not true, formulae that account for additional physical phenomena exist. The formulae are introduced first, then a FEM solution method for the equations is generally described.

As acoustics is simply the vibration of a fluid, it can theoretically be represented by the general form of the Navier-Stokes equation. The following formulation is a combination of equations (3.11) and (4.44), presented in [41]:

$$\rho \frac{du_i}{dt} = -\frac{\partial p_{fluid}}{\partial x_i} + \rho g_i + \frac{\partial}{\partial x_j}\left[\mu\left(\frac{\partial u_i}{\partial x_j} + \frac{\partial u_j}{\partial x_i}\right) - \frac{2}{3}\mu\left(\frac{\partial u_k}{\partial x_k}\right)\delta_{ij}\right] \tag{11}$$

In Equation (11), ρ is the density of the fluid, u is the flow speed, p_{fluid} the fluid pressure, g is the gravitational acceleration, μ is the viscosity, x is the spatial coordinate, indexes i, j and k represent Cartesian directions, and δ_{ij} is the Kronecker delta. $\frac{\partial u_k}{\partial x_k}$ represents the divergence of the velocity field.

If the fluid in Equation (11) can be treated as incompressible, the divergence of the velocity is zero and the equation simplifies somewhat. However, as acoustic waves are only made possible by air compressing and decompressing, this simplification is intuitively not useful in an acoustic context.

Equation (11) includes many other phenomena that often are not of particular interest in acoustics. Therefore, to reduce the computational load, calculations of acoustic behaviour are often based on the acoustic wave equation [42], a simple formulation of which was presented in Equation (6). A three-dimensional inhomogeneous version of the wave equation that can account for spatially varying density is presented in [42], using vector notation. It is called the linearized wave equation. The equation is rewritten here using the unified notation adopted throughout this work.

$$\rho\boldsymbol{\nabla}\cdot\left(\frac{1}{\rho}\boldsymbol{\nabla}p\right)-\frac{1}{c^2}\frac{\partial^2 p}{\partial t^2}=S(\boldsymbol{x},t), \tag{12}$$

where p is the sound pressure, ρ the density, c the speed of sound, and S a source term dependent on space $\boldsymbol{x}$ and time t. For the case of time harmonic disturbances that fulfil

$$P(\boldsymbol{x},t)=p(\boldsymbol{x})e^{i\omega t}, \text{where } i^2=-1 \text{ and } \omega=2\pi f, \tag{13}$$

the inhomogeneous Helmholtz equation can be obtained [42]

$$\rho\boldsymbol{\nabla}\cdot\left(\frac{1}{\rho}\boldsymbol{\nabla}p\right)+k^2p=s, \text{where } i\omega\boldsymbol{u}=-\frac{1}{\rho}\boldsymbol{\nabla}p \text{ and } k=\frac{\omega}{c}. \tag{14}$$

k is the wavenumber, and omega the radian frequency. s is a source term. This frequency formulation is useful for researching how components act under various frequency excitations instead of over time.

It is especially important to understand that in Equation (11), p_{fluid} is the absolute pressure, whereas in all other equations in this thesis, p refers to the sound pressure that is a variance from the mean conditions.

As it is linear, Equation (12) is much easier to solve both analytically and numerically when compared to the Navier-Stokes Equation (11).

It should also be noted that the linearised wave equation (12) is only an approximation of the true behaviour. When looking into higher sound levels, higher temperatures and closer to sound sources or other non-linearly behaving structures, the nonlinear effects become larger [43, Ch. 2]. The B/A ratio is used to quantify how much the sound speed deviates from its linear (small-amplitude) value due to finite-amplitude (nonlinear) effects [43, Ch. 2.3]. Despite this, linear acoustics “does an outstanding job of explaining most acoustical phenomena” [43, Ch. 1.1]. The mathematics of nonlinear acoustics are outside the scope of

this thesis, but nonlinear models simply include higher-order approximations of the phenomena.

According to [42], Equations (12) and (14) are often the starting point for Finite Element (FE) models. For another perspective, the documentation of two commercially available software, Comsol Multiphysics and Actran FFT, with a vast amount of vibroacoustic capabilities was consulted.

From the Actran User's guide [40], the acoustic propagation in a medium at rest can be rewritten with the notation used in this work as:

$$\frac{1}{\rho c^2}\frac{\partial^2 p}{\partial t^2} - \boldsymbol{\nabla}\cdot\left(\frac{1}{\rho}\boldsymbol{\nabla} p\right) = s, \tag{15}$$

which is clearly similar to Equation (12).

In the Comsol documentation [44], the same "wave equation for pressure waves in a lossless medium" is shown as

$$\frac{1}{\rho c^2}\frac{\partial^2 p}{\partial t^2} + \boldsymbol{\nabla}\cdot\left(-\frac{1}{\rho}\left(\boldsymbol{\nabla} p - \boldsymbol{q_d}\right)\right) = s, \tag{16}$$

which is also similar to (12) and (15), except that they have included two source terms, $\boldsymbol{q_d}$ and s.

Thus, we can note that the two software solve the exact same equations and are focused on the implementation of source terms. This is natural, as the boundary conditions are the main modelling consideration in numerical simulation. Going further into the Partial Differential Equations (PDEs) that allow for considering mean flow, for example, is out of scope for this thesis, but they can be found in [40], [44].

Now that we know the nature of the acoustic PDEs that we are trying to solve, we can have a brief look at how a numerical solution can be achieved.

Since the 1970s, there have been two main numerical methods that try to solve wave equations similar to Equations (12), (15) and (16) [5, Ch. 3.19.2], [42]. In addition to the already mentioned FEM, the Boundary Element Method (BEM) allows for a different approach; FEM divides the (fluid) domains into small subregions, whereas BEM discretises only the bounding surfaces of the domains.

FEM models are recognised for their robustness, capability to accommodate spatially varying material properties, and compatibility with structural coupling applications [42]. It is also found that FEM is more useful for TL calculations, in comparison to BEM [45]. As one of the objectives of this thesis is to compare TL measurements to numerical simulations, it can be concluded that this thesis should focus on FEM.

FEM discretises the computational domain using an unstructured mesh that provides flexibility in handling complex geometries [40],[46]. The nodes where properties are solved for are strategically positioned within the mesh elements, where field variables such as acoustic pressure serve as degrees of freedom. Spatial distribution of acoustic quantities between nodes is determined through interpolation using shape functions, which ensure continuity across element boundaries. The solution process involves solving for these degrees of freedom at each time instant in transient analyses or at each frequency of interest in frequency-domain calculations. A critical consideration in acoustic FEM modelling is maintaining adequate mesh resolution. In practice, there is usually a target number for “nodes per wavelength", the target value for which is typically between 5 and 10 [40],[46]. A similar requirement is presented by the Courant–Friedrichs–Lewy (CFL) condition regarding the timestep in transient simulations [40].

The fact that we are targeting a frequency-dependent mesh resolution means that the computational cost increases as the frequency increases. Because engine excitations are most prominent in low frequencies and reactive silencers are also best suited to low frequencies, the mesh resolution can be kept fairly low for this work.

Another parameter regarding the mesh is the choice of shape functions, also called interpolation functions. They are mathematical functions that relate field variables within a FEM element to the nodal values that are solved for. Similarly, they allow for interpolation in space to create curved edges for elements to more closely represent geometry. The most relevant shape functions for acoustics, linear and quadratic, are visualised in Figure 8.

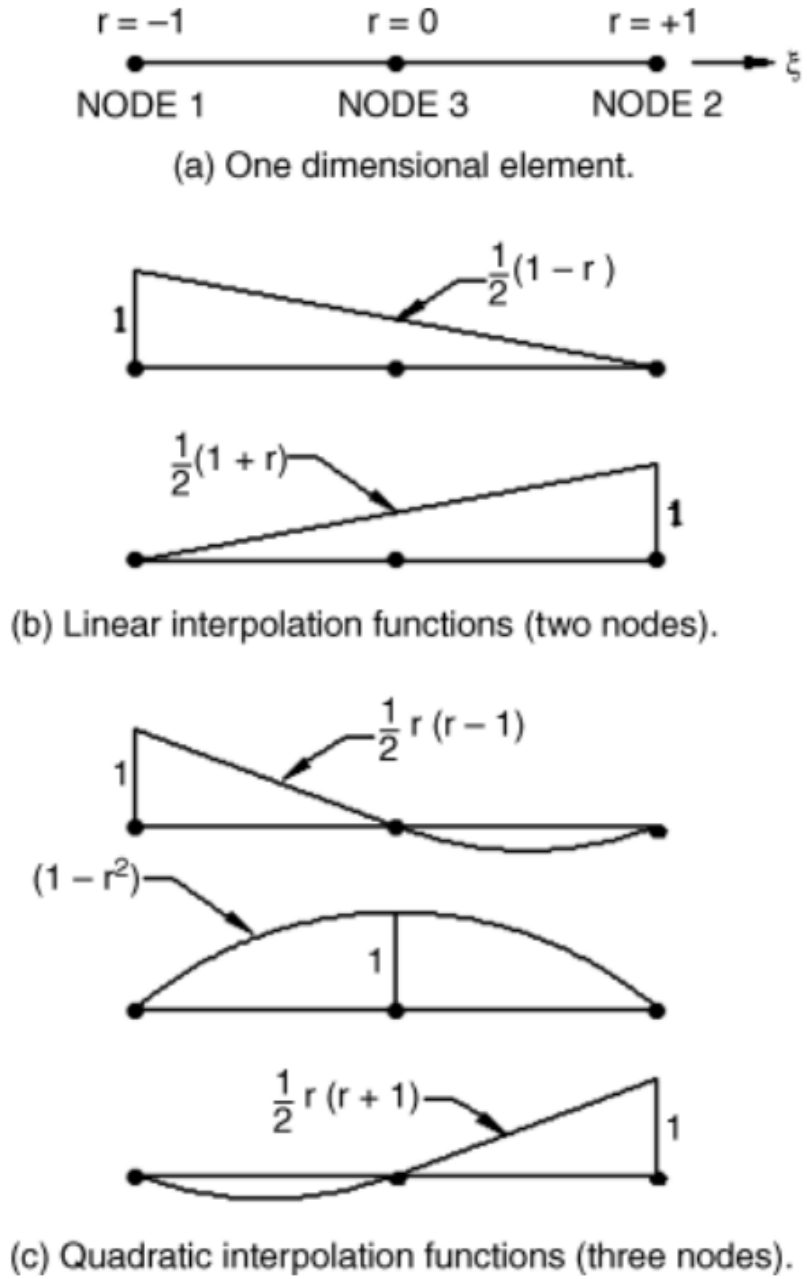

Figure 8: Linear and quadratic interpolation functions visualised. Adopted from [36].

With the theoretical background established, it is appropriate to outline the scope of problems that can be addressed using acoustic FEM. Table 2 presents the various types of analyses that can be performed by FEM codes, based on [42]. It should be noted that the list is not exhaustive, and that these capabilities were already available as of 2007.

Table 2: A list of traditional acoustical analysis types

Type of analysis	**Use case**
1. Natural frequencies and eigenmodes of closed domains	Study the resonant frequencies of both solids and fluids, coupling between the two is possible.
2. Response of closed domains to excitations	Either structural or acoustic excitations and their effects on the domain. Structural-acoustic coupling is possible
3. Additional model for porous media and absorption	Show the effects of porous media and acoustically treated surfaces in analyses of Types 1. and 2.
4. Radiation and scattering in unbounded domains	Types 1. and 2. are usually closed volumes, but this analysis allows for open areas
5. Transmission in ducts and waveguides	Simplified models that allow for connecting more complicated components to each other without building a full FEM model
6. Mean flow analysis	Considers the effects of mean flows on the acoustic propagation. [42, Ch. 9] Can be combined to any one of the above.

To define the boundaries of the FEM computational domain, various boundary conditions are used [40], [42], [44]. These can include coupling to structural vibration models, for example. The boundary conditions can be used to define physical components such as walls, but they are also used to truncate the domain. An example of truncation would be using non-reflective boundary conditions to simulate an open outlet where no sound is reflected.

For the purposes of this thesis, it is not useful to delve deeper into the mathematical or computational aspects regarding discretisation and solving of acoustic FEM. For a comprehensive introduction to acoustic FEM, the reader is referred to the textbook by Atalla and Sgard [47].

2.5.1 Mean flow in acoustic FEM analysis

When mean flow is introduced to an acoustical system, the problem of linear acoustics becomes much more complex. Firstly, the CFD computation to obtain the mean flow requires a large amount of expertise and more computational resources when compared to acoustics due to the nature of Equation (11). In addition to the equation being nonlinear, the velocity, pressure, density and temperature all must be solved for in CFD instead of just pressure in linear acoustics.

Theoretically, acoustic results could be obtained straight from CFD, as the pressure is solved for. In practice, this requires a cautious problem setup and multi-step as shown in Ismail et al. [20]. In the paper, they first run a steady calculation and then two unsteady temporal studies that are then compared to find the acoustic behaviour and TL. The transient data is finally transformed to the frequency domain. Solving a simpler acoustic equation directly in the frequency domain using flow data from the steady CFD would be a computationally lighter approach.

The decoupled approach is also suggested by the Comsol User's guide [44]: "Aeroacoustic simulations would ideally involve solving the fully compressible continuity, momentum (Navier–Stokes equations), and energy equations in the time domain. The acoustic pressure waves would then form a subset of the fluid solution. This approach is often impractical for real-world computational aeroacoustics applications due to the required computational time and memory resources. Instead, for solving many practical engineering problems, a decoupled two-step approach is used: first solve for the fluid flow, then the acoustic perturbations of the flow."

Assuming that we can obtain a good CFD solution, the physics of linear acoustics are somewhat more complicated with mean flow. In [36, Ch. 1.4], it is shown that acoustic waves are convected downstream by a mean flow. In [36, Ch. 1.5], it is deduced that the cut-off frequency for higher order mode propagation also becomes lower when there is flow within a pipe. On the other hand, acoustic waves are attenuated when propagating through a region with turbulent flow [48].

In the *Handbook of Noise and Vibration Control,* a chapter written by Astley [42, pp. 101–115] differentiates between rotational and irrotational mean flows, saying that irrotational cases can be solved simply by acoustic velocity potential formulations that only account for

convection of waves, whereas rotational cases require the linearized Euler equations, which can have stability problems. The velocity potential formulations are only rough estimations of the flow, as they do not model flow separation and boundary layers [41]. The two methods are offered by the Comsol software package, with the option of expanding to the Linearised Navier-Stokes (LNS) equations that include true viscous losses, eddy viscosity losses and thermal effects [44]. The LNS equations are presented excellently in [49].

3 Literature review

In this chapter, the current state of the field will be examined to produce a basis for the experiments. The historical development and current state of general acoustics research is reviewed. The state of specifically exhaust acoustics and reactive silencers are studied from the perspectives of analytical, experimental and numerical methods. The different variables, methods used to treat them and relationships that have been discovered in existing studies are presented. Related standards are briefly listed. Finally, the review is concluded with a general description of the state of field, which is connected to the purposes of this thesis.

Note that mathematical formulations and theoretical foundations are presented separately in Chapter 2, and this chapter focuses on the methods used and conclusions instead of showing the theoretical basis.

3.1 State of general acoustics research

Acoustics is by no means a new research topic, which is natural as it is directly related to the human sense of hearing. The start of modern acoustics research can be said to have happened with the invention of the microphone during the 1920s (then described as a “reliable electroacoustic transducer”), which allowed for quantifiable measurements of sound. Eventually this led to the development of reliable sound intensity probes around 1980 [5, Ch. 8.3]. Development of measurement capabilities is more widely discussed in Chapter 3.5.

The ability to measure acoustics phenomena led to the ability to create and validate models based on physical behaviour, some of which are included in Chapter 2. Development of computational acoustics methods naturally followed with the advancement of FEM in the 1980s, with the first commercial product for acoustics (Sysnoise) being launched in 1988 [5, Ch. 10.9].

Generally, based on the research conducted for this thesis, I would conclude that the physics of acoustics, especially linear acoustics, which is enough for most engineering use cases, are well understood and can be modelled accurately [43, Ch. 1.1]. Main challenges lie in choosing methods and creating products that best utilize the existing information. A challenge is also presented by applications where surrounding phenomena affect the acoustic behaviour, as in cases where acoustics is coupled with a fluid flow or structural vibrations.

The validation study described in Chapter 4.2 should thus produce good results, as it uses well-established methods and only linear acoustics. The mean flow investigation described in Chapter 4.3 on the other hand is more intensive and includes much more uncertainty.

3.2 State of exhaust system acoustics and reactive silencers

The behaviour of wave propagation in pipes as it is described in Chapters 2 and 4 of this thesis was well understood already in the 1980s [27]. In the paper, Eriksson presents a methodology for indexing higher-order modes that can propagate in a duct and revises the definition of the cut-off frequencies of the various modes. The established mathematical definitions are still used in modern literature and state-of-the-art software (Chapters 2 and 4). The paper measures TLs for various expansion chambers and uses the analytical theory to explain the behaviour.

The theory and applications of quarter-wave resonators are presented in the 1997-paper by Field and Fricke [50]. Again, the results and shown methodology are identical to Chapter 2, and to what has is widely used in industry for dimensioning of silencers. Another approach is to think of a quarter-wave resonator as a simplified example of a Helmholtz resonator, for which a much more thorough approach has been outlined already in 1953 [51]. The paper includes end correction coefficients, design considerations for various geometries and even effects of nonlinearity. It is thus clear that the scientific information behind the ideas of this thesis have been well-known for decades.

A more modern take on the state of muffler acoustics can be found from a review by Haghighi et al. [23]. The review examines advances in muffler acoustics and design, highlighting the extensive research conducted on reactive mufflers using various analytical, numerical, and experimental approaches. TL is demonstrated to be the primary metric for evaluating acoustic performance across different muffler geometries. The review notes that for reactive resonators, “the mufflers' acoustic performance is frequency-selective, requiring them to be developed or changed to accommodate the broad frequency characteristics of the intended sound in most applications”. They also suggest active (or commonly known as active noise-cancelling) techniques for very low frequencies, where the wavelengths and thus the size of components becomes large. However, the spatial constraints are less significant in the marine context of this thesis when compared to automotive mufflers, for example. Thus, active techniques are not usually needed.

According to the source-path-receiver model presented in Chapter 2.3, a muffler should naturally be tuned to the excitation frequencies coming from the engine. Nakada et al. [33] show how the sound and vibration excitations from a combustion engine are multiples, also known as orders, of the engine running frequency. Knowing the most prominent excitation orders and the revolution speed of the engine gives a target for the design of a reactive muffler or resonator.

The automotive industry has been perhaps the leading industry driving practical muffler research. An example of this can be seen in Ref. [35], which provides insight into the practical validation and one-dimensional modelling approaches used in automotive exhaust system design, and into the various kinds of mufflers that are considered in an automotive context.

To conclude, the concepts used in this thesis are nothing new, but the correct implementation of them has potential to result in clear improvement for acoustic performance of marine exhaust components.

3.3 Usage of numerical methods for silencer acoustics

This subchapter is divided into parts based on the various computational methods that can be used to simulate the behaviour of exhaust mufflers. The focus is heavily on which methods could be used for the purposes of this thesis.

3.3.1 Finite Element Method (FEM)

FEM is the default tool for numerical analysis of acoustics, and the theory basis has been introduced in Chapter 2.5. The application of FEM in acoustics has been mentioned to be a "relatively mature technology", with its advantages being robustness, material property handling and simple structural coupling [42, p. 113]. This chapter discusses acoustics FEM solutions that do not incorporate the effects of the flow on the acoustic performance.

One of the earliest implementations of acoustic FEM was published in 1975 by Young and Crocker [39]. The results for a simple expansion chamber were comparable to proven analytical methods using only 24 elements up to a certain frequency limit.

The paper by Cazzolato et al. [21] Includes a design process based on FEM analysis for a complicated multi-Helmholtz silencer already in 1997. Similarly to other models, good correlation is found between FEM predictions and measurements.

The papers by Andersen [52] and Jokandan et al. [22] compare measured TL of multiple automotive silencers to FEM simulations created with Comsol with good results, noting that differences between simulations and measurements usually come from false boundary or initial conditions. As examples, false material properties or impedance properties for perforates are mentioned. For mesh resolution, a target of five elements per wavelength is recommended and used in both cases.

Zhang and Xin [34] perform a similar study to Andersen [52], comparing FEM results to measurements, but the concept is much more relevant to this thesis. The paper studies how a Helmholtz resonator can be lined with porous material to widen the sound absorption coefficient peak. If a similar material was implemented to the mixing silencer, the exhaust gas temperature wouldn't have to be predicted exactly, but the silencer could have instead a temperature range where certain frequencies are attenuated.

In [8], Kheybari et al. utilise coupled structural and acoustic FEM in Comsol to analyse a muffler with structural mass-spring resonators with multiple target frequencies instead of fluid-based resonators within a muffler. To obtain pressure drop data, an additional simple CFD case that does not resolve acoustics is run. With this approach, CFD and FEM are kept separate so that each can be used based on the methods' strengths, but there is no coupling between the two.

Coulon et al. [13] characterise structural piping problems caused by acoustic excitations, with similar coupling as is used in [8]. An example case, where a real-life pipe developed cracks due to flow-induced acoustic excitation shows good agreement with the simulated FEM model. The paper works as a good illustration of the risks present when piping systems have high levels of acoustic excitations. The paper by Gaul et al. [53] is another study comparing various FEM methods and showing that good agreement between measurements and FEM simulations can be achieved in automotive mufflers.

For the papers mentioned in this chapter, used and/or suggested mesh densities vary between five and eight elements per wavelength, confirming the range of five to ten suggested in Chapter 2.5.

3.3.2 Boundary Element Method (BEM)

BEM was developed around the same time as FEM and is still available in many commercial programs. Based on only meshing the boundaries of the domains, it is often considered to be more flexible than FEM, but less robust [5, Ch. 10.9].

Bilawchuk and Fyfe [45] compare FEM and BEM specifically for TL calculations. The paper determines that BEM is often slower than FEM and should only be used when the flexibility is required.

3.3.3 One-dimensional methods

The idea behind one-dimensional modelling and end correction methods are presented already in Chapter 2.3. The goal with these methods is to simplify the system and enable efficient calculation for specific geometries.

A paper by Guo et al. [4] is a comparison of one-dimensional transfer matrix method against FEM for a perforated resonator. The transfer matrix method is determined to be limited to frequencies under the cut-off frequency of plane wave behaviour as higher-order modes are not one-dimensional. Additionally, it is mentioned that the impedance modelling of perforation and evaluation of end-corrections is a challenge. They recommend that FEM is used for the most accurate calculations.

Calton and Sommerfeldt [54] compare three different one-dimensional modelling methods for a complex combination of resonators, with the impedance translation method determined to be the most accurate, with about 1 Hz of error for the an example resonator attenuation peak between 67 and 68 Hz. These models are all still dependent on the plane-wave assumption and simple cylindrically symmetric geometries.

A more practical paper on one-dimensional acoustic simulation methods is in [35], where the software “BOOST SID” was used to create one-dimensional models for various practical muffler geometries with results that would be useable in an engineering context. Still, higher order modes are not considered accurately, and the models must be built block by block, where various elements represent the real geometry. This method of modelling restricts the used geometries to be combinations of various simple geometries. A mixing silencer, as presented in [17], for example, would not be straightforward to model with the software.

One-dimensional simulation methods inherently restrict the geometries that can be used in muffler design, as they require the model to be constructed with accurate representations for combinations of various simple geometric elements. This approach demands substantial manual work in setting up and validating each model configuration. Furthermore, as these are fundamentally one-dimensional methods, they cannot calculate higher-order mode behaviour that becomes significant at higher frequencies or in complex geometries. For cases where flow is considered, one-dimensional methods cannot correctly account for spatial gradients in flow properties. Given that the primary objective of this thesis is to improve simulation accuracy for complex muffler geometries, one-dimensional methods are not suitable and will not be employed in this work.

3.3.4 Computational Fluid Dynamics (CFD)

Computational Fluid Dynamics (CFD) represents a theoretically complete approach to acoustic simulation, particularly when using transient methods that can directly resolve both the fluid flow and the resulting acoustic phenomena. In pure CFD approaches, the full compressible Navier-Stokes equations are solved in the time domain, capturing all physical interactions between flow structures and acoustic waves without the need for the extreme simplifications done in linear acoustics [20]. Note that various simplifications regarding turbulence modelling and resolution are still almost always made.

Using CFD is necessary for aeroacoustic source applications, such as wind/flow noise prediction [54], where the noise generation mechanisms are directly linked to complex three-dimensional turbulent flow patterns.

In [20], a pure CFD Reynolds-Averaged Navier-Stokes (RANS) approach is applied to a reactive silencer. The silencer is simulated in the time domain and acoustic frequency properties are identified with the Fast Fourier Transform (FFT). The results in the specific case match very well with measurements. It is not explicitly mentioned in the study, but despite the good results, this kind of study should be much more computationally intensive than frequency domain methods, as the timestep must be small enough to be able to resolve the acoustic waves.

Jena and Panigrahi [55] suggest frequency domain FEM for static TL calculations and transient CFD to account for flow effects.

In a similar effort, Liu et al. [14] use similar methodology to [20]. The authors use transient RANS CFD to solve flow-induced acoustics and vibration in compressor exhaust pipelines. The CFD approach highlights that the pressure pulsation in a pipeline is the same phenomenon as acoustic sound travelling in a pipe, although one should keep in mind that CFD shows also various non-acoustic pulsations. A Fourier transform is again used to get the results into the frequency domain. The method allows us to model the complete physical behaviour of the aeroacoustic system at a higher computational cost. FEM is also conducted to find static resonance frequencies in the pipe structure. Finally, the compressor excitation frequency and fluid and structural natural frequencies can be compared to identify risks for resonance.

CFD can, in principle, be used for acoustic simulation and thus to obtain TL values; however, the associated computational cost is prohibitive for industrial applications and thus not further considered in this thesis. Instead, the hybrid CFD/FEM methods presented in Chapter 3.3.5 will be employed for the study that includes mean flow.

3.3.5 CFD/FEM hybrid solutions

The hybrid method of using a steady-state CFD solution as a background field for frequency-domain TL FEM calculations is a well-known process, and it efficiently uses the strengths of each method. CFD can be used to calculate an average flow for the component, using various methods freely. Then, the mean flow from the steady solution is one-way coupled to acoustic FEM, allowing for frequency-domain acoustics simulations. This approach allows to examine how the flow affects TL characteristics more efficiently than in direct CFD simulations.

Perhaps the most topical paper for this thesis is [7], where CFD and FEM are combined to optimize acoustic properties for marine exhaust line components using Actran. The paper shows that combined FEM/CFD approaches are almost two orders of magnitude more efficient than pure CFD, when comparing CPU (Central Processing Unit) times. The exact simulation methods, like which fields are transferred from CFD to FEM and which equations are solved, are not described, but the results match experiments well.

Huang et al. [56] and Chu et al. [57] utilise only the flow velocity data being mapped from a CFD simulation to FEM for a perforated silencer. This only considers the convection of acoustic waves, but does not include effects of turbulence, for example. Huang et al. [56] include comparisons to measurements with flow, and the results are somewhat accurate, but

not exact. It is also noted that the flow effects are comparatively small in low frequencies. Both studies ignore flow generated noise.

The paper by Zhirong et al. [49] is an improvement upon the previously mentioned studies [56], [57], as it solves the LNS equations. Quoting the paper: “In an effort to accurately and quickly determine the acoustic attenuation performance of two-pass perforated hybrid mufflers in the presence of complex airflow, the frequency-domain LNS equations with consideration of eddy viscosity are firstly applied to predict the TLs of the mufflers in the present work, where the sound-absorbing material is treated as an equivalent fluid with complex sound speed and density.” According to the research done for this thesis, this approach is the most accurate currently available option for frequency-domain acoustic FEM that considers flow effects. The results of Zhirong et al. [49] are validated based on measurements with good consistency. The general observations made in the paper are that airflow increases TL for lower frequencies and that low-frequency resonance peaks (like the peaks produced by the mixing silencer) are flattened.

Huang and Ji [58] utilise the same workflow as Zhirong et al. [49]. Steady CFD results are used as input for LNS in Comsol for dual-chamber mufflers. Huang and Ji generalise three main flow effects: “(1) the shift of resonance frequencies, (2) the decrease of amplitude of TL at resonance frequencies and the increase of amplitude of TL at some frequencies, (3) the decrease of amplitude of TL in the low frequency range for some configurations”. It is noticeable that effect (3) is the opposite of what was found in [49], but the difference might be explained by the different geometries and flow parameters.

Huang and Ji [58] also highlight a numerical problem with Perfectly Matched Layers (PMLs) at the outlet failing to absorb low frequency sound completely at Mach numbers over 0,2. The TL graphs to look noisier instead of being smooth and continuous, which is due to the reflections from PML interfaces.

Zhang et al. [59] introduce a more complicated metamaterial muffler that functions by the Helmholtz resonator principle. The multi-resonator is investigated with LNS with included flow, while the design itself is based on analytical methods. The paper also includes an additional CFD-based analysis to determine the noise produced by the flow, which is not accounted for by the Comsol LNS model.

A common theme across the various studies, even the ones using the best available methods like LNS CFD-FEM hybrids, is that most silencers aim to reduce the general sound level. This means that researchers focus on much higher frequencies and broadband attenuation, whereas for the mixing silencer use case we are interested in only the low frequencies. Based on literature, it seems like adding flow to a resonator component tends to flatten out the resonance peaks, but other clear trends are not seen. The behaviour seems to be very dependent on the specific geometry. Therefore, this phenomenon has to be quantified with a new simulation for correct dimensioning of the mixing silencer.

3.4 Development of measurement protocols and standards

It is a natural relationship that to do any kind of useful work, whether related to simulations or analytical formulas, one must have good enough measurement capabilities. A thorough history of measuring sound pressure and intensity, from the early papers in the 1870s to modern methods, is given in [5, Ch. 8.2]. The academic interest is largely on measuring sound intensity, as the vector quantity allows for easier in-situ measurements of sound power radiated by a machine, for example. Sound pressure measurements depend massively on the environment, whereas intensity measurements make it possible to calculate sound power of specific components within a room independently of the room geometry and other sources.

In the context of this thesis, it is important to understand measuring methods for the acoustic excitations coming from an engine and for the TL measurements of components.

The earliest papers on acoustics relied on human senses and sensitive flames, for example [60, pp. 217–252]. An example figure attempting to characterise the nature of sound through the behaviour of flames is shown in Figure 9.

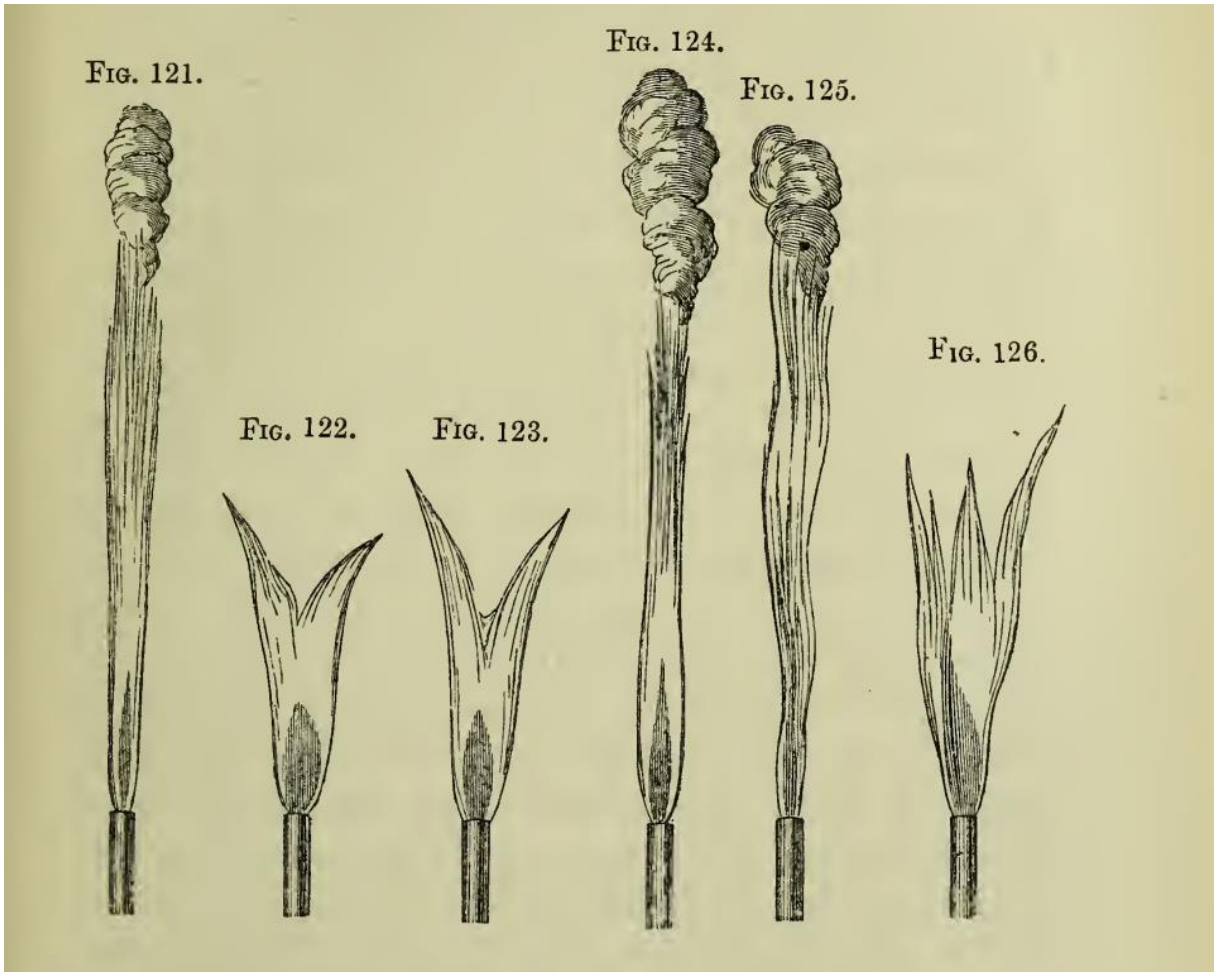

Figure 9: Illustrations of how flames look before and after blowing into a whistle. Adopted from [60].

The most notable invention for sound intensity and pressure measurement was the microphone, two of which can be combined to calculate the sound intensity [5, Ch. 8.2]. On the simplest level, a microphone can be defined as a device capable of converting sound pressure fluctuations to voltage.

An important mention is that practical, accurate and calibrated devices for measurements were shown only around 1979 [61] and during the 1980s they were adapted to various applications, as shown in [62], [63], [64].

The developments in measurement equipment led to the creation of standards for various measurements. The historical background of the standards can be found in [5, Ch. 8.9]. For convenience, the standards are listed in Table 3.

Table 3: Various standards for measurement of sound. Standards published by ISO (International Organization for Standardization), IEC (International Electrotechnical Commission), ANSI (American National Standards Institute) and ASTM (American Society for Testing and Materials)

Standard identifier	Purpose of standard
ISO 266 [65]	Defining values for and one-third-octave measurement bands
ISO 354 [66]	Measuring sound absorption in a reverberation room
ISO 3744 [67]	Measuring sound power and energy using sound pressure (free field)
ISO 3745 [68]	Measuring sound power and energy using sound pressure (rooms)
ISO 3746 [69]	Measuring sound power and energy using sound pressure (survey method)
ISO 9614 [70]	Measuring sound power levels of noise sources using sound intensity
ISO 10534 [71]	Determining acoustic material properties using intensity or standing wave method
ISO 15186 [72]	Measuring of sound insulation in buildings and building elements
IEC 61043 [73]	Defining instruments for the measurement of sound intensity
ANSI S12.12-1992 [74]	Defining instruments for the measurement of sound intensity
ASTM E2249-02 [75]	Measuring sound insulation in buildings and building elements

Currently, the environmental impacts of ships are widely investigated and various requirements have been set for the noise and vibration emissions. Park et al. [32] present a review of operational insights and experience regarding vibration and noise in a marine context, while considering the effects on passengers, crew, marine life and humans on land. Biot et al. [11] have a similar research idea, and they present a numerical model for quantifying the airborne noise emitted by ships based on a noise emission classification by Lloyd's Register.

Stemming from environmental research, there exists a category of standards and methods related to acoustics and vibrations more specifically in marine applications. As they are more specific, there is more variation in the publishers, and some of the references in Table 4 are just papers suggesting methods instead of being official standards. Some optional classifications are also listed. Many but not all of the referenced standards are also listed by Park et al. [32]. Note that all listed International Maritime Organization (IMO) standards are a part of MARPOL.

Table 4: Various standards and classifications regarding marine acoustics and vibration. Published by ISO (International Organization for Standardization), IMO (International Maritime Organization), MSC (Maritime Safety Committee), MEPC (Marine Environment Protection Committee), DNV (Det Norske Veritas), BV (Bureau Veritas), ABS (American Bureau of Shipping), KR (Korean Register) and LR (Lloyd's Register).

Identifier	Purpose
ISO 20283-5 [12]	Determine measurement methods and acceptable levels of solid vibration on ships
ISO 21984 [76]	Guidelines for measurement and evaluation of vibration regarding habitability of specific ships
IMO MSC.337 [10]	Code for measuring and limiting maximum acceptable noise levels on ships
IMO MEPC.1/Circ.833 [77]	Guidelines for the reduction of underwater noise from commercial shipping to address adverse impacts on marine life
IMO MEPC 74/INF.28 [78]	Ship underwater radiated noise technical report and matrix
IMO MARPOL [9]	A convention for the prevention of pollution from ships by IMO. Includes a huge number of requirements and all other IMO standards in this table. Constantly updated.
DNV Noise and Vibration Classes [79]	Comfort, vibration of machinery/equipment and underwater noise classifications
BV NR 636 [80]	Comfort and health on-board offshore units, noise and vibration aspects
ABS noise and vibration control for inhabited spaces [81]	Noise and vibration control for inhabited spaces
KR GC-21-E [82]	Noise, Vibration and Habitability (NVH) guidance for ships
KR GL-0031-E [83]	Guidelines for eliminating vibration problems on ships
LR-GN-31 [84]	Guidance and an overview of ship structural vibration problems

As is clear from Table 4, especially the more human-centric classifications and guidelines are provided by multiple different classification organisations. The critical takeaway is that the importance of controlling vibration and noise, which is the goal of this thesis, is recognised globally to be an important factor, showing the importance of this work. [84] and [83] even offer guidance for remedying vibration problems on ships. These are the kinds of challenges, which this work is trying to prevent at the source.

No standards were found for measuring the acoustic excitation of the engine, but a methodology aiming to minimize the effects of pipe resonances in the excitation measurements can be seen in [85]. A similar methodology, created within Wärtsilä, combined with a special silencer designed to attenuate the pipe resonances is presented in [86]. This method is the one that will be used in practice to evaluate the acoustic engine sources.

For the TL measurements in this work, the two-load method described in Chapter 2.4 is used.

3.5 Literature review summary and conclusions

The problem of linear acoustics is well established, and FEM methods for linear acoustics are widely adopted. Thus, creating and validating a FEM linear acoustics model is described in Chapters 4.1 and 4.2 and accurate results are to be expected.

Linear acoustics itself is not a full description of muffler behaviour, as it ignores flow effects. To capture these, a more comprehensive model with a hybrid CFD-FEM approach should be created. This model can then be used to determine whether the flow effects are large enough to have to be considered in the design and dimensioning of the mixing silencer.

The LNS computation method offered by Comsol is one of the most intricate, accurate and modern ways of doing these kinds of simulations in the frequency domain. The simulation process itself also requires CFD and field data mapping, and there are reports of challenges with non-reflecting outlet conditions mentioned in literature. This means that the setup of the model must be done extremely carefully to replicate physical behaviour in a component that has flow through it. This approach is described in Chapter 4.3.

Generally, there is a lot of research on exhaust mufflers, but the research focuses mainly on automotive mufflers designed to effectively reduce the total sound transmission, whereas the marine components studied in this thesis are much larger in scale, and focus heavily on tuning the resonator to attenuate specific low frequencies excited by the engine. Thus, the general

descriptions of muffler behaviour are largely not applicable, and conclusions should be made largely on the results of the simulations.

For the reactive silencer tuning, the availability of accurate engine excitation data is also highlighted, as it is the parameter that determines the frequency that the resonator will be tuned for. This data can be gathered by the methodology presented in [86], among other sources.

4 Research methods

In this chapter, an initial comparative test case is run to support modelling choices for the main validation experiments in terms of both practicality of setting up the simulation and comparing the results between software. Afterwards, the methods and modelling choices related to the validation case and the second aeroacoustic investigation are presented.

All research geometries will be variations of the silencer described in the Wärtsilä patent EP3707355B1 [17]. The component is called a mixing silencer, as it includes both urea injection and mixing with a surrounding silencer. A general view of the component can be seen in Figure 10.

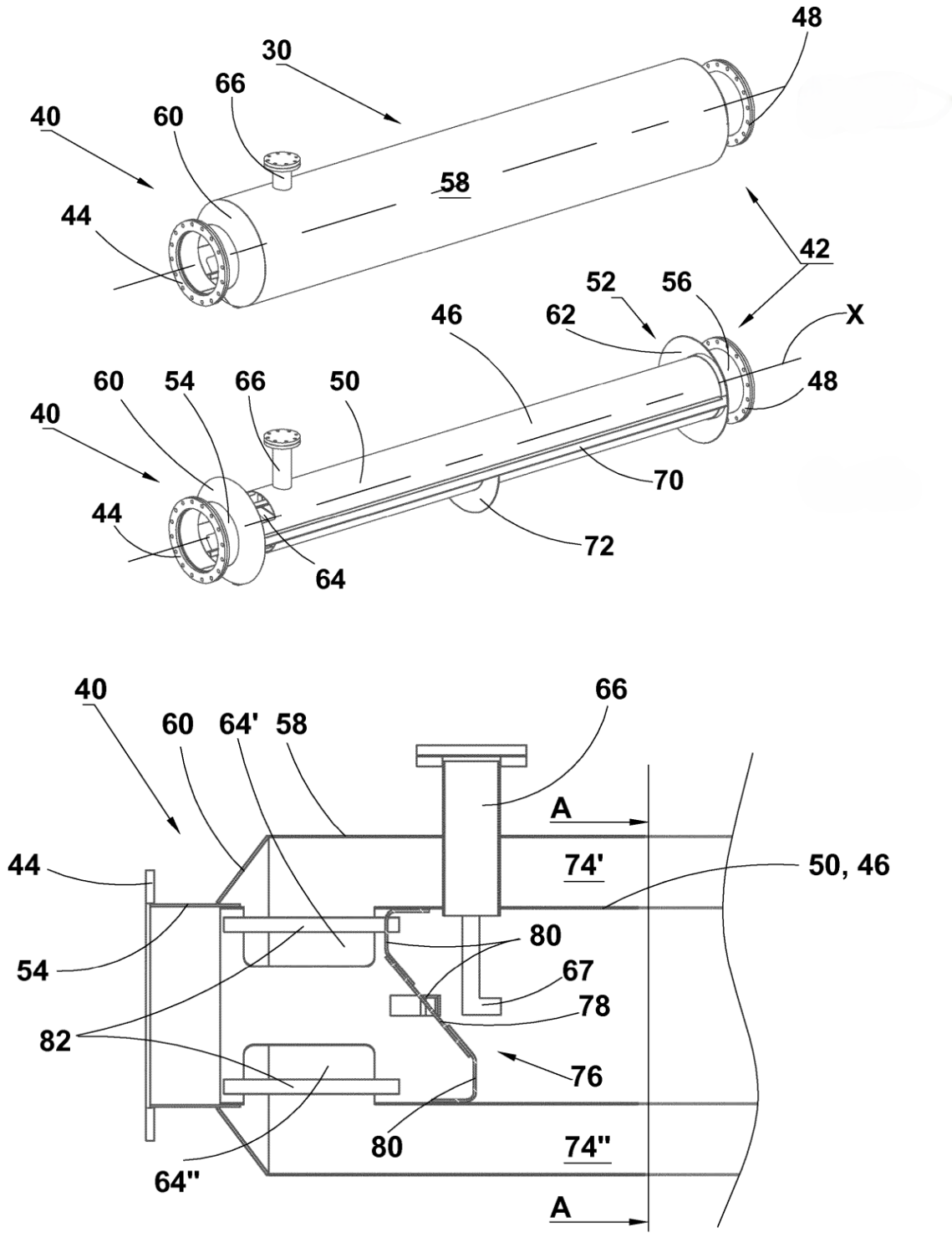

Figure 10: Patent drawings of the mixing silencer geometry. Part numbers are in accordance with the patent. Adopted from [17].

Referencing the numbers in Figure 10, the component is composed of a central pipe 46 that includes the urea injection and mixing components 67, 78 and 80, and a surrounding cavity, formed by 58 and 60, which functions as a quarter-wave resonator. This design allows for a large cross-section for the resonator while being efficient with the space around the

component. A bigger transverse area in the resonator leads to a bigger TL, as noted earlier in Chapter 2.3, Equation (10). This kind of compact component is beneficial in marine applications, where space is a constraint.

4.1 Initial test case in Comsol and Actran

To evaluate the user experience and capabilities of both Comsol and Actran, and to determine whether they produce similar results, identical simulations using the same simple mesh geometry are performed in both software packages. The two software packages are chosen based on availability and the requirements set in Chapter 1.3. This investigation also serves to determine the validity of the hypothesis that as linear acoustics is not an overly complex numerical problem, various software supplied with the same data should reach very nearly the same results.

Additionally, the test case functions as an introduction to the practical side of setting up FEM for duct acoustics.

4.1.1 Introduction to simulation methods

The simulations do not include any mean flow through the component, as they are a simple simulation of the lossless linear acoustic behaviour of the silencer at rest in ambient pressure and temperature. The outputs of the simulations are TL data.

The fluid geometry is created based on the patent shown in Figure 10, but the presented simple case is not an actual product. The test case geometry, seen in Figure 11, is drawn for testing purposes and omits the urea injection and mixing components. The dimensions do not correspond to any real delivery project and are chosen in a general way for demonstration purposes. As the real muffler geometries used for validation will be inherently three-dimensional, all simulations are kept three-dimensional even though the used geometry could be modelled by a two-dimensional sector mesh.

As a dimensional reference, the pipe geometry has a total length of 2.5 m and a main pipe diameter of 800 mm.

The mesh is an auto-generated tetrahedral mesh, created with Altair HyperMesh. The mesh size is defined by an average element size of 0.1 meters. It is generated based on a CAD

geometry. The mesh geometry can be seen in Figures 11 and 12, where grey surfaces represent hard walls, blue surface is the inlet and red surface is the outlet.

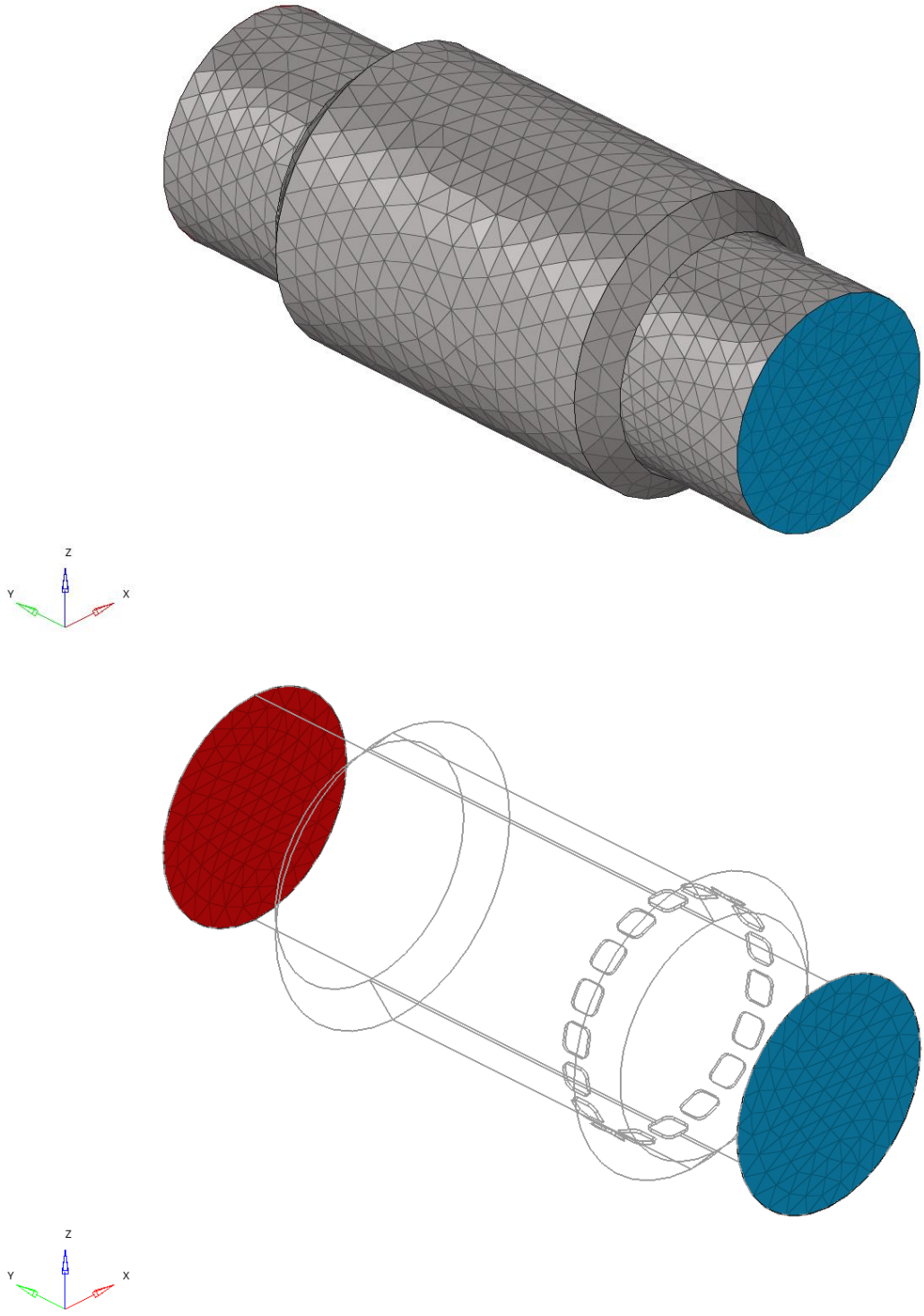

Figure 11: Isometric views of simplified example mixing silencer domain. Grey surfaces are hard walls, blue surface is the inlet, and red surface is the outlet.

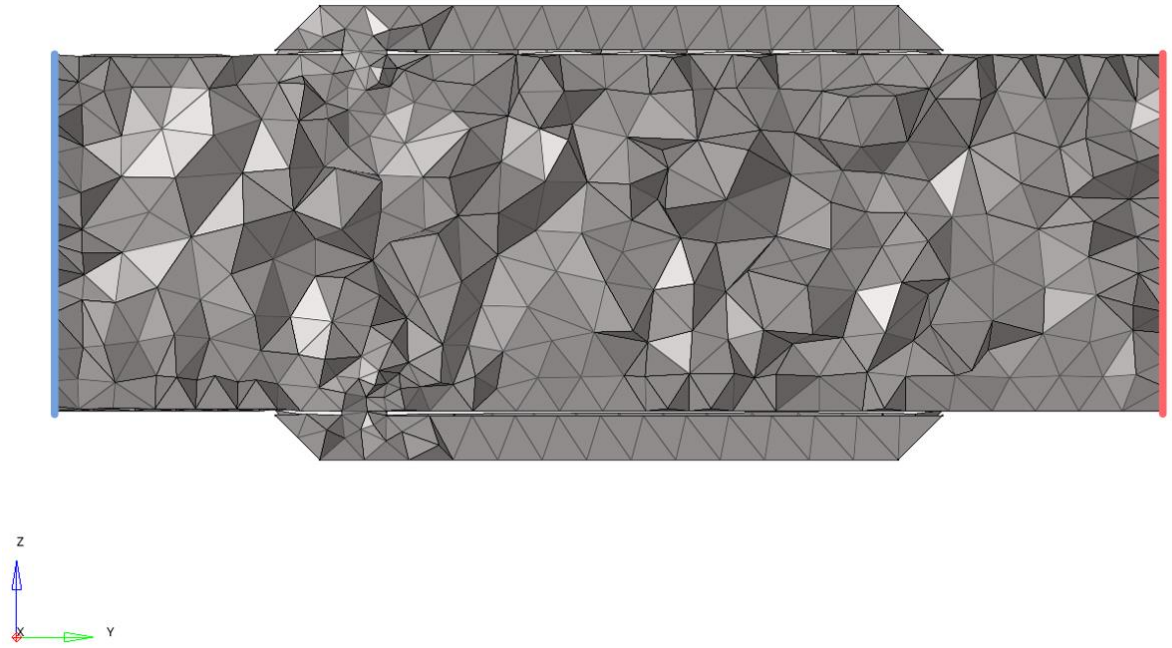

Figure 12: Plane cut from the centre of the silencer. Note the reactive silencer chambers around the main pipe. Grey surfaces are fluid elements, the blue surface is an inlet, and the red surface is an outlet.

The geometry has a concentric annular reactive silencer that is located around the main pipe, allowing for a compact quarter-wave silencer with maximal area for the acoustic wave to travel in. A bigger transverse area in the resonator leads to a bigger TL, as noted earlier in Chapter 2.3, Equation (10).

The simulations are in the frequency domain, with a frequency range of 10 Hz to 300 Hz with a 1 Hz step size, creating 291 data points. The measured quantity is TL as it is defined in Chapter 2.4. The compared values for TL are acoustic power through the inlet and the power exiting through the outlet. In other words, referencing Equation (3) and Table 1, we can note $R = \frac{W_{in}}{W_{out}}$.

When the respective temperature and pressure values are set to atmospheric values of 293.15 K and 101330 Pa, the Comsol built-in ideal gas model calculates speed of sound and fluid density values ($\frac{343.20\text{m}}{\text{s}}$ and $\frac{1.2043\text{kg}}{\text{m}^3}$). The same exact values of density and sound propagation speed are manually input into the material model used by Actran to remove variations produced by different material model properties.

No FEM damping is used. The mesh shape functions that interpolate the solution [40], [44] within the discrete elements are set to be linear in both cases. Using the average element size of $dl = 0.1$ m, we can calculate the minimum nodes per wavelength at the highest frequency

of 300 Hz as $n_{\frac{nodes}{\lambda}} = \frac{\lambda}{dl} = \frac{c}{f_{max} \cdot dl} = \frac{343.20 \frac{\mathrm{m}}{\mathrm{s}}}{300\ \mathrm{Hz} \cdot 0.1\ \mathrm{m}} = 11.44$. The value of 11.44 is well above the recommended values from literature that range from 5 to 10 nodes per wavelength. Therefore, it can be determined that the mesh density is high enough to accurately model the linear acoustics in the system.

Most of the simulation settings are identical between the software. The only clear difference is in how the inlet and outlet are defined. The software packages have specialised boundary conditions built specifically for simulating acoustically infinite (non-reflective) inlet and outlet ducts, but they are defined somewhat differently.

Actran utilises a concept called duct modes for setting up the inlet and outlet [87]. For a circular cross-section, like in our case, Actran includes tools to automatically calculate the axis and two radial coordinate directions for the inlet or outlet. Based on these, incident modes of various circumferential and radial orders can be defined. The plane wave is set to be 1 Pa in amplitude, as scaling this value does not affect the TL results in linear acoustics. Waves propagating out of the domain can be formatted as being “Free” within a specific frequency range [87]. This means that one does not manually have to check cut-off frequencies of specific outgoing modes, as the software does it automatically. The excitation could also be set to “Free”, but this would reduce the comparability of our results as Comsol does not include this behaviour.

A similar utility within Comsol is called ports [44]. The basic idea of modelling a duct outside of the domain is the same as in Actran, but Comsol does not include the “Free” condition that automatically chooses the required orders based on frequency. Instead, every single mode has to be defined using its own port. For modes that are not axisymmetric, two ports are needed with “circular port reference axes” that are perpendicular to each other to capture all possible shapes. Examples of non-axisymmetric modes can be seen in Figure 13, specifically modes (1,0), (1,1) and (2,0).

Comsol provides a postprocessing variable that shows the cut-off frequency of the ports [44]. This can be used to determine whether the used modes are appropriate for the considered frequency range, but the values can only be seen after running the case. Other methods also exist for specifying acoustic inlets and outlets, but the Comsol documentation advices to use ports, if possible [44].

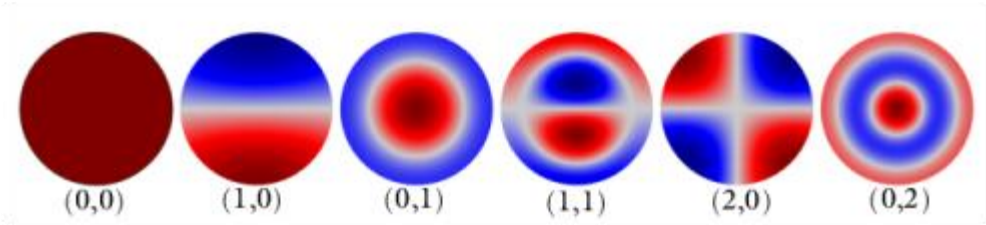

Figure 13: The first 6 modes using Comsol notation (azimuthal or circumferential order, radial order) of a waveguide with circular cross section. Adopted from [44].

As visualised in Figure 13, Comsol notates the plane wave order as (0,0), where the first number corresponds to the azimuthal direction and the second to the radial direction [44]. The same definition is often used in literature, and the paper by Eriksson [27] attempts to unify this notation. Despite this, Actran defines the wave orders using different indexing, where the plane wave is noted as (1,0) [40]. This work uses the common notation seen in Figure 13.

For the Comsol simulation, incident wave excitation can simply be toggled on for a port, and otherwise the ports function as non-reflective exits for waves. 1 Pa of amplitude excitation is added to the plane wave order for the inlet port, similarly to what is done in the Actran simulation. In addition to the plane wave, two ports with order (1,0) but orthogonal directions are added to both the inlet and outlet without any excitations.

Using Equation (5) and tabulated values from [28, p. 87], we can determine cut-off frequencies for various orders, using the notation seen in Figure 13 and literature [27], [28]. With $c = \frac{343.20\text{m}}{\text{s}}$ and $d = 0.8$ m, we get $f_{cutoff(1,0)} = 251.26$ Hz and $f_{cutoff(2,0)} = 416.5$ Hz. As these are the two lowest cut-off frequencies, we can establish that we need to only consider the (1,0) mode in our simulation inlet and outlet. Thus, the setups described earlier are physically correct as our range is only up to 300 Hz.

The earlier calculations can be verified, as Comsol automatically calculates cutoff frequencies. For the included order (1,0) the software evaluates $f_{cutoff(1,0)} = 251.43$ Hz. My hypothesis is that the small difference to Equation (5) comes from the discretisation of the geometry, as the linear elements cannot fully represent a circle.

To summarize, the two cases are built with the same mesh geometry, material properties and boundary conditions representing the same physical behaviour. The solver parameters used on both simulations were kept as the defaults.

The parameters used in the test case are summarised in Table 5.

Table 5: Properties used to setup the simple test Cases in Comsol and Actran.

Property	**Value**
Type of analysis	Acoustic transmission loss in the frequency domain
Frequency range	0 Hz to 300 Hz with a step of 1 Hz
Excitation	1 Pa amplitude plane wave at the inlet
Damping	No damping
Atmospheric pressure	101330 Pa (functions only as a basis for the Comsol ideal gas model)
Air temperature	293.15 K (functions only as a basis for the Comsol ideal gas model)
Material	Air, linear elastic or lossless model
Used properties, ideal gas	Density $\rho(101330\ \text{Pa}, 293.15\ \text{K}) = \frac{1.2043\text{kg}}{\text{m}^3}$ Speed of sound $c(293.15\ \text{K}) = \frac{343.20\text{m}}{\text{s}}$
Interpolation/shape functions	Linear
Walls	Sound Hard Boundary
Inlet	1 Pa plane wave amplitude excitation, all modes under 300 Hz considered.
Outlet	All modes under 300 Hz considered, no excitations
Mesh	Shown in Figures 11 and 12. Nodes per wavelength 11.44 at the highest frequency.
Solution methods	Software defaults

4.1.2 The results of the initial test case simulation and comparison to analytical method

For an additional comparison to the FEM results, we calculate the damping spike frequency with a simple analytical method. Using Equation (9), we can estimate the first resonant frequency of the resonator by omitting all end correction phenomena and simply taking the distance l as the distance from the middle of a resonator inlet to the end of the resonator. As the resonator end is at an angle, the distance is measured to the middle of the end plate, as shown in Figure 14.

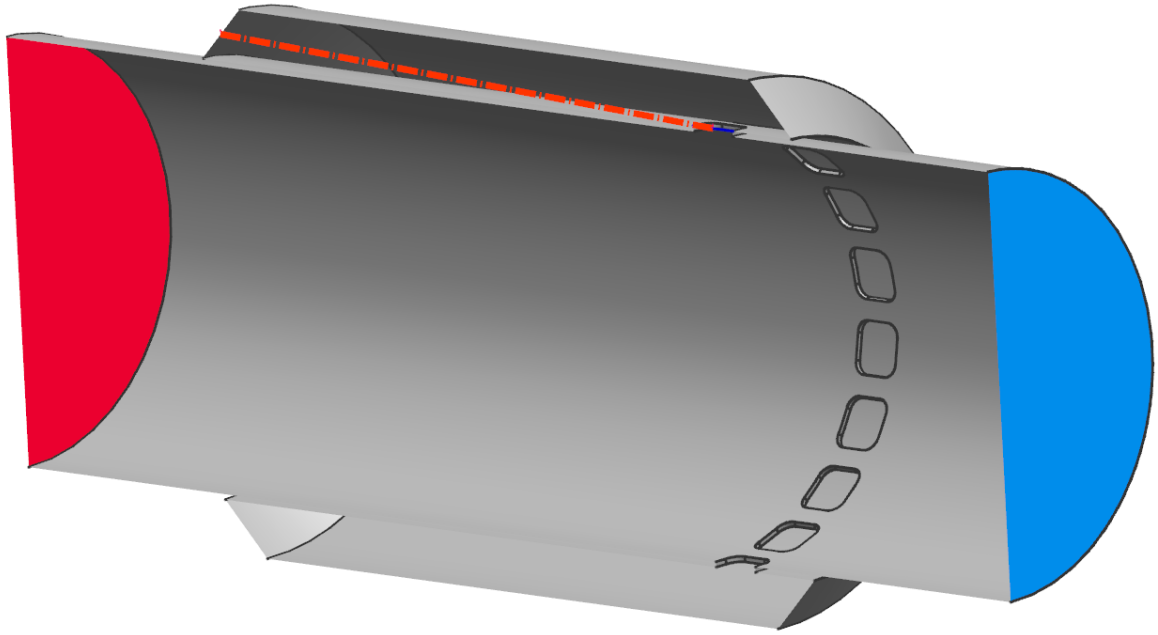

Figure 14: Section from the middle of the test case geometry, also depicted in Figures 11 and 12. Orange line that is situated on the central cut plane shows the length l measured for the reactive silencer.

Using this approximation and Equation (9), we get $f_{r_{analytical}} = \frac{1 \cdot 343.20 \frac{\mathrm{m}}{\mathrm{s}}}{4 \cdot 1.251\ \mathrm{m}} \approx 68.59$ Hz. The second spike is simply three times the frequency of the first one, also based on Equation (9).

TL results of the two simulations and the locations of the analytical TL peaks are plotted in Figure 15.

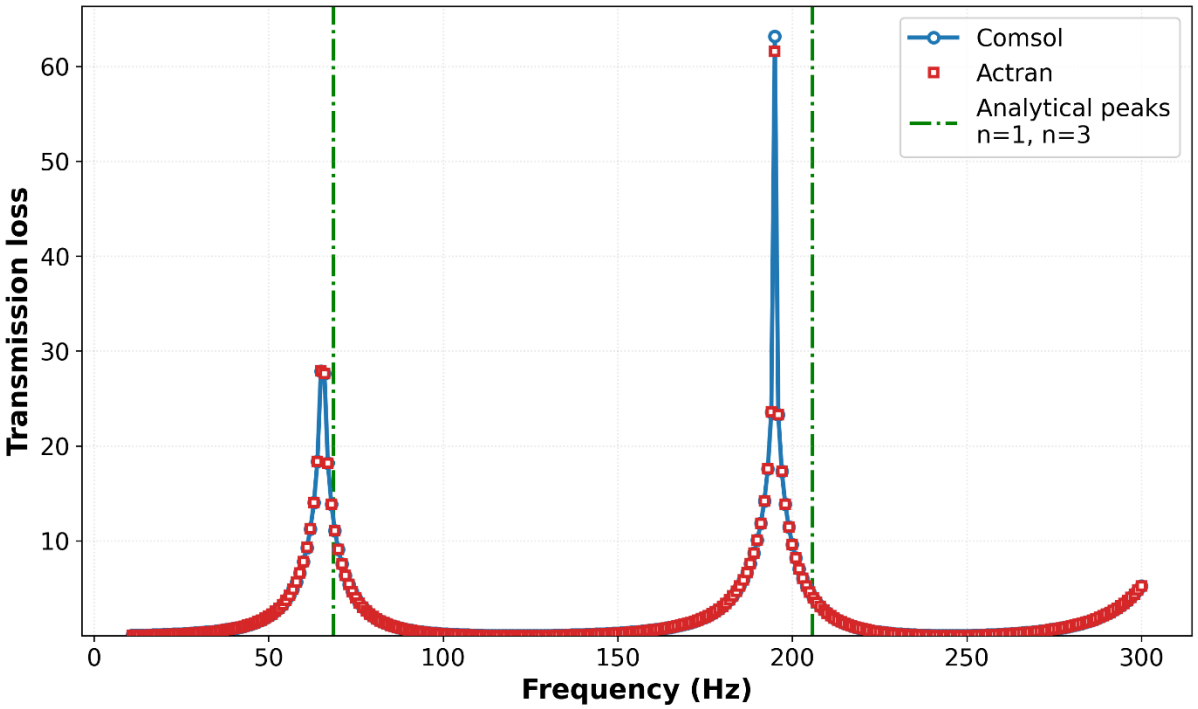

Figure 15: Transmission losses for the simple test Cases in Actran and Comsol.

There are many ways of analysing the data from Figure 15, but the two software packages produced nearly identical results. The only marked difference is in the amplitude of the attenuation spike at roughly 200 Hz, but as the spikes are theoretically infinite, their maximum height should not be something to focus on. The same phenomenon explains why the second spike is much higher; The values produced by the 1 Hz step just happen to be closer to the resonating frequency of the reactive muffler at that point.

Referencing Table 6 for the exact values around the peaks of the simulations, the first peak is likely centred between 65 and 66 Hz, as these data points have very similar dB values in both datasets. The second spike is roughly at 195Hz, as that is the highest value. It should be noted that the simple analytical calculation gives a value that is roughly three Hz away from what is predicted by the FEM for the first spike. Our hypothesis is that the difference is the result of FEM taking three-dimensional end correction effects into account, which will produce a difference when compared to the analytical formula. Thus, the FEM-analysis allows to Tablecalculate the true acoustic length of the quarter-wave silencer. This is supported by the results found in the literature review, which conclude these kinds of linear acoustics FEM simulations to be very accurate.

The marked difference between the analytical formula and FEM calculations illustrates the fact that there are three-dimensional effects or so-called end corrections that should be

considered in the case related to the mixing silencer. It may also be that the length of the reactive silencer should be measured from different points than the ones used for this comparison.

Table 6: The exact data around the TL maxima in Figure 15. Rounded to three significant figures.

Frequency [Hz]	**Comsol TL result [dB]**	**Actran TL result [dB]**
64	18.3	18.3
65	27.9	27.9
66	27.6	27.6
67	18.2	18.2
194	23.6	23.6
195	63.2	61.6
196	23.3	23.3

If one wanted to obtain more exact frequency spikes, more simulations with smaller steps around the spikes could be run. There is likely also a way mathematical way to interpolate the exact frequency of the TL maxima.

Regarding the objectives of this simulation and comparison, the results show that the choice of software seems to not affect the results on a practical level, and that the physical accuracy of the models should be the focus of the validation study.

Both software packages showed similar computational speeds around half a minute on a 12-thread laptop for the ~5000 degrees of freedom problem, indicating very manageable computational costs for this type of simulation.

4.2 Methods of validation study

The validation study serves to verify that linear acoustics FEM can accurately predict TL. The setup is very similar to the simulations seen in Chapter 4.1, but the geometries are based on real mixing silencer products. The general mixing silencer geometry can be seen in patent EP3707355B1 [17] and in Figure 10.

The simulation results are compared to measurements taken in constant temperature and pressure environment, and without flow. Therefore, the simulations are set up in the same way

as described in Chapter 4.1, except for adjusting the temperature values to match measurement temperatures.

Comsol is chosen to be the software used in the validation study due to practical considerations, as it is determined in Chapter 4.1 that both Comsol and Actran produced the same results with similar inputs, and that the software have similar capabilities. On the practical side, Comsol has the advantage in terms of the available technical support, better meshing capabilities, available example cases and user-friendly notation. These considerations are naturally subjective and should be treated as such.

The objective of the validation study is to create a practical acoustic FEM simulation model for a reactive silencer, which in this case is the mixing silencer.

4.2.1 Validation comparison data

As there is measurement data from three different mixing silencers in ambient conditions without flow, there are three validation cases. The mixing silencers are part of different delivery projects, and will be referred to as Components 1, 2 and 3. All three Components are mixing silencers, so the topology is identical to the patent [17] and Figure 10. Only the dimensions and tuning frequencies vary between the components.

The measurement data is collected by the two-load method, described in Chapter 2.4, except that two additional microphones are used to reduce noise and increase the measurement frequency range. Using the two-load method means that the measurement can have inaccuracies above the cut-off frequency.

Practically, the measurement data is gathered using the proprietary software Sidlab [88], which takes the measurement data from the microphones and calculates TL curves for the Components. The measurements are conducted by JTK Power Oy [89].

The measurement results can be transformed to represent behaviour in various exhaust gas temperatures, as shown in Equation (7.2). Thus, simulating or measuring the Components at various temperatures does not provide additional information, as the results will be just a scaled version of the same results, according to the theory of linear acoustics.

4.2.2 Methods of validation simulations

As noted previously, the simulation methods are the same as in Chapter 4.1. Gas properties are matched to measurement conditions, and the geometry and therefore meshes are changed. The methodology is thus described briefly, using the notation from the Comsol documentation [44].

Corresponding to the three different measured mixing silencers (Components 1-3), three simulation cases will be run, one for each Component. The parameters used for all validation simulations can be seen in Table 7.

The simulations are in the frequency domain, with a specified frequency range and with a step size of order 10^{-1} [Hz]. The step size is identical to the one used in the measurements data. The measured quantity is TL between the inlet and outlet as it is defined in Chapter 2.4.

The Comsol built-in lossless ideal gas model for air is used. Thus, the input parameters are the atmospheric pressure and temperature, which are matched to measurement conditions.

The boundaries are defined as follows: All walls function as sound hard boundaries, and the inlet and outlet are defined using ports with plane wave modes and all higher order modes that have cut-off frequencies under the upper frequency limit, as described in Chapter 4.1. Thus, it can be said that all modes that can physically propagate in the pipe are considered. The system is excited by an incident plane wave with 1 Pa amplitude at the inlet.

To allow for better representation of the circular geometries present in the components, the quadratic Lagrangian geometry shape function is used. This allows for the edges of the elements to be curved, as visualised in Figure 8(c). To increase accuracy, second order quadratic Lagrangian shape functions are also used for the interpolation within elements.

The shape functions influence what density is required from the mesh. To find a suitable balance between computational requirements and accuracy and ensure overall validity of the meshing procedure, a mesh sensitivity study is performed in Chapter 4.3.

Table 7: Properties used in the three validation simulations. Air temperature between components varies to match measurement conditions.

Property	**Values for simulations**		
Software	Comsol		
Type of analysis	Acoustic transmission loss in the frequency domain		
Frequency range	Lower limit to higher limit of order 10^2 [Hz] with a step size of order 10^{-1} [Hz]		
Excitation	1 Pa amplitude plane wave at the inlet		
Damping	No damping		
Atmospheric pressure	101330 Pa		
Air temperature	18°C for Component 1	25°C for Component 2	21°C for Component 3
Material	Air, linear elastic lossless model		
Used properties, ideal gas	Ideal gas for air		
Interpolation/shape functions	Quadratic Lagrange		
Walls	Sound hard boundary		
Inlet	1 Pa plane wave amplitude excitation. All propagating modes under the upper frequency limit considered but not excited.		
Outlet	All propagating modes under the upper frequency limit considered, no excitations.		
Mesh	Meshing procedure is determined in Chapter 4.2.3		
Solution methods	Software defaults		

4.2.3 Methods of mesh sensitivity study for validation cases

To verify a correct meshing strategy, a mesh sensitivity study and comparison to experimental results is conducted with Component 1 at the real measurement temperature of 18°C. The study serves as a basis for the meshing methodology used for the validation cases to determine a targeted nodes per wavelength value. As literature suggests 5-10 elements per wavelength, the hypothesis is that the mesh sensitivity study results are somewhere on the same scale, possibly on the low side as we are using quadratic elements that interpolate the solution better within an element.

All simulations are run with mesh that fully represents all surfaces present in the real product. This means that the present thin surfaces and associated mesh quality settings will restrict the mesh to be smaller than the targeted value in all the meshes.

For the first mesh, the target density is set to be on the high side based on the literature at $n_{\frac{nodes}{\lambda}} = 10$. This data is then compared to the measurement data that has been obtained and used as a starting point for simplifying the calculations.

Secondly, the mesh is made coarser while keeping the geometry fully represented by reducing the targeted $n_{\frac{nodes}{\lambda}}$-value.

Using the gathered data, a suitable meshing workflow and parameters are suggested and used in calculation of all the validation cases, meaning the two temperatures for both Components 1 and 2.

Some of the mesh sensitivity studies are run using a lower frequency step to reduce the computational burden, as the comparisons between datasets are still valid even if the frequency resolution is lower.

The meshing is done entirely within Comsol. The general process for creating meshes that include all surfaces but vary in density is described as follows:

1. Import CAD geometry.
2. Set minimum and maximum allowable element sizes and mesh quality parameters. The minimum element size is defined by the thin surfaces that are only as wide as the thickness of the plates used to construct the product. To be able to include all faces, the minimum mesh size must be smaller than the thinnest surface. Maximum mesh size is defined so that it does not restrict the targeted mesh size.
3. Calculate a target value for the number of nodes per smallest wavelength, which is used as a “Size Expression” for the process.
4. Create a free unstructured tetrahedral mesh that targets the specified $n_{\frac{nodes}{\lambda}}$ -value.

The created meshes are then used as the input to a simulation that is described in Chapter 4.1 using properties in Table 7. The mesh sensitivity study will only be conducted for Component 1 at room temperature. Five meshes are created, with Mesh 1 serving as an overly accurate

baseline $n_{\frac{nodes}{\lambda}} = 10$ and Mesh 5 being the coarsest mesh. This study is then used to establish a suitable target value for the number of nodes per smallest wavelength. The studied values are focused around the lower bound of $n_{\frac{nodes}{\lambda}} = 5$ in the values suggested in literature, as quadratic elements should require less elements per wavelength. The entire parameter set can be seen in Table

Table 8: Values of $n_{\frac{nodes}{\lambda}}$ for the mesh sensitivity study

Mesh number	$\boldsymbol{n_{\frac{nodes}{\lambda}}}$
1	10 (overly dense)
2	6
3	5
4	4
5	2

To illustrate the effect of $n_{\frac{nodes}{\lambda}}$, a dimensionally generic mixing silencer geometry was meshed using the described methods. In Figure 16, the coarsest and densest meshing results are visualised.

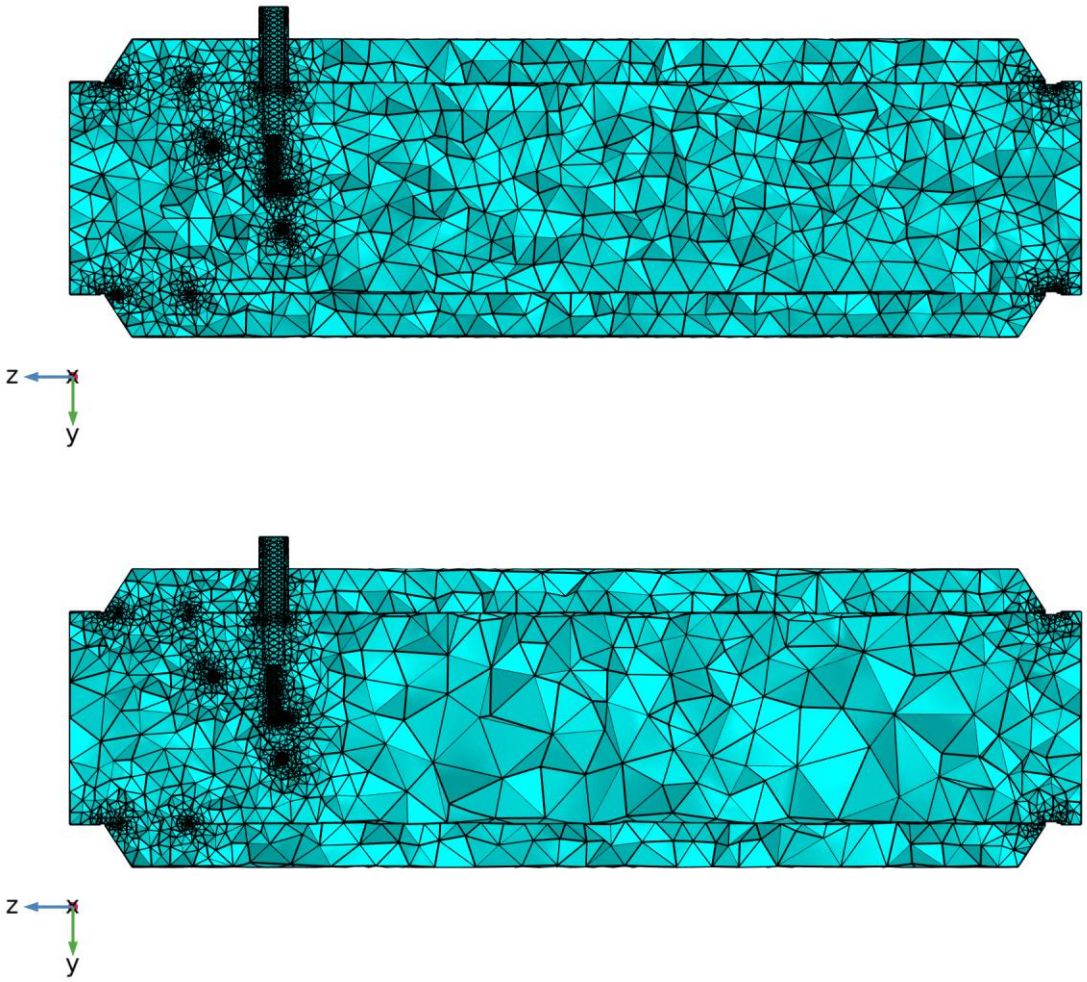

Figure 16: A middle slice view of generic mixing silencer mesh. Target mesh sizes are $n_{\frac{nodes}{\lambda}} = 10$ on the top, and $n_{\frac{nodes}{\lambda}} = 2$ on the bottom. The cut from the middle is created by filtering by elements whose centroids are in the negative x direction from the central axis of the component.

As can be seen from Figure 16, the element size is greatly restricted by the fact that the setup requires small surfaces to be modelled. Thus, the element size difference is mostly seen in the middle of the mesh, where there are no spatial restrictions and the elements can grow.

The automatic mesh generation will fail or behave unpredictably, if the CAD geometry given as input is somehow faulty. As the procedure always tries to mesh the geometry that it is given, care must be taken in CAD to avoid accidental small gaps and/or surfaces, while including the several small features in an otherwise large volume.

The most useful part about this specific meshing procedure is that it will produce a valid mesh even for the difficult thin plate geometries, which include every single detail that exists in the

real component. The mesh sensitivity study also verifies if the behaviour of the automatic meshing affects the results.

To conclude, the hypothesis is that the used target mesh size might not affect the results as much as what can be seen in more theoretical studies, where all elements are exactly the size of the target. This sensitivity study serves also as a verification that this meshing procedure creates acceptable results, even if there is something unpredictable happening with the mesh size.

4.3 Methods of mean flow study

Separately from the validation study, a second study is conducted. In contrast to the earlier methods, this simulation investigates effects of the mean flow on the mixing silencer geometry. A separate CFD solution is calculated using OpenFOAM v13 [90]. The field results from the CFD simulation will then be imported into Comsol. The sound waves are convected by the mean flow and attenuated or dissipated by the turbulence, which is modelled by additional turbulent viscosity using the LNS interface in Comsol [91, Ch. 1–2]. The exact theory and equations are out of the scope of this thesis, but the theory behind the LNS equations is well-composed in [91], along with other sources cited in this chapter.

4.3.1 Motivation

The mean flow study serves to answer the question of how the flow effects the acoustic performance of the muffler, and whether flow needs to be considered during the design of mufflers. There are practical experiences in Wärtsilä that show that the practical measured attenuation is always lower than simulated, but there are no proper data points to validate against.

The fields that are imported from OpenFOAM into the Comsol mean flow study are flow velocity, pressure, turbulent viscosity, density and temperature. The case is solved in the frequency domain. It does not consider aerodynamic noise produced by eddy currents generated by flow through the geometry. This is an acceptable simplification, as the flow effects on the TL are the main interest. If needed in the future, sound sources from a separate simulation could be added as background acoustic pressure fields.

The geometry is simplified to allow for a simpler meshing procedure using snappyHexMesh, a meshing tool included with OpenFOAM. In practice, this means that some connections

between plates are simplified. The urea injector and the attaching structure for the mixing plate are also removed, meaning that the geometry is formed by the pipe walls with the circular mixing plate “floating” in the middle of the inner pipe as seen in Figure 17. The shape of the geometry makes the case very suitable for a cylindrical background mesh instead of the traditional cartesian background. The simplified geometry is evaluated and compared to the original in terms of its linear acoustics properties in Chapter 5.2.2. The simplification is done so that the meshing quality is higher.

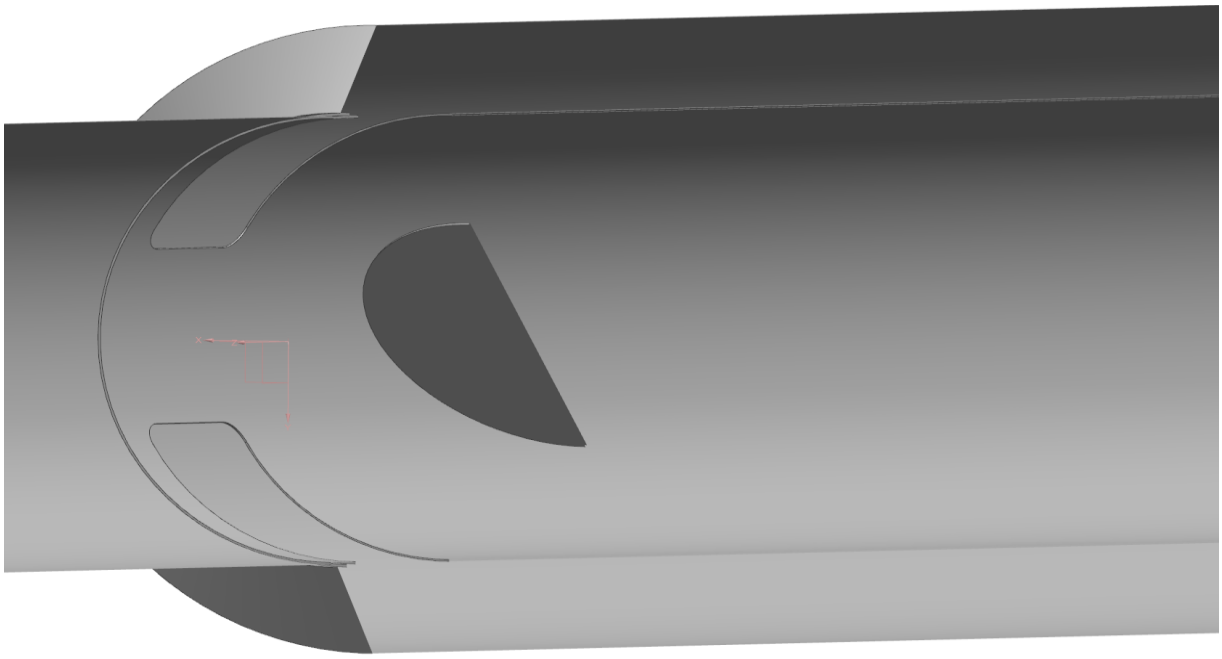

Figure 17: A cut from a simplified generic mixing silencer geometry, showing the mixing plate floating within the pipe.

4.3.2 CFD methods

The CFD is conducted with OpenFOAM v13. The governing equations for an incompressible fluid flow are briefly introduced in Chapter 2.5, and for a comprehensive introduction, the textbook by Versteeg and Malalasekera [92] is recommended. The specific model choice and settings will be introduced next. As is done with the FEM simulation descriptions, the text will focus on modelling choices and physical correctness instead of solver-related aspects like discretisation schemes and solution methods.

Case files for both steady and transient simulations are provided in a public GitHub repository [93]. Various values like the flow rate and running scripts have been removed for confidentiality reasons.

Theoretically, only a steady-state solution is necessary for the mean flow study, as the FEM will be in the frequency domain, and it will use static CFD fields. Transient simulations are still of interest due to the nature of the flow over the mixing plate in the mixing silencer. The plate causes oscillatory, inherently transient behaviour, which means that a steady-state solution with low residuals cannot be obtained. This challenge is solved by modelling the behaviour over time with a more expensive transient simulation and calculating average fields over multiple oscillations to get correct, averaged results.

While Comsol and many other FEM codes offer potential-flow approximations and FEM-based CFD, OpenFOAM utilises the Finite Volume Method (FVM) and allows for more flexible and transparent methodology. The CFD results will be mapped onto a FEM mesh to be used by Comsol. Various solutions are compared; a steady-state solution, a single timestep of a temporal simulation and a time-averaged solution.

Note that to avoid non-physical values during the mapping, the CFD mesh should be finer than the FEM one. Also, if we want to capture the gradients near walls, the FEM mesh should have boundary layers and refinement similarly to the CFD mesh. The accuracy of the mapping can be visualised by plotting values of original and mapped values over a line, as is done in Chapter 5.2.1.

The physical boundary conditions used in the CFD are listed in Table 9. Fields related to turbulence modelling and heat transfer were set up in a physical way using wall functions, and their exact definitions can be seen in [93].

Table 9: Physical boundary conditions of CFD for the mean flow study.

Boundary	Velocity	Pressure	Temperature
Inlet	constant flowrate	zero gradient	constant 350°C
Outlet	zero gradient	constant total pressure	zero gradient
Walls	no-slip	zero gradient	zero gradient

The turbulence modeling approach is based on the RANS approach. Therefore, turbulent fluctuations are not visible in the flow field results and only the mean flow field is solved for. From a practical standpoint, RANS-simulations require choosing a turbulence model that is used to calculate the turbulent kinetic energy to represent the turbulent fluctuations. The turbulence model used in this simulation is k-omega-SST (Shear Stress Transport) model

[94]. The k-omega-SST model is chosen as it is recommended as the standard turbulence model for industrial simulations [95].

The working fluid is modelled as air with temperature-dependent properties. The incompressible perfect gas equation allows for density to vary with temperature, but not with local pressure, meaning that the flow is considered incompressible. This setup allows taking temperature variations in the flow into account, and enables conjugate heat transfer simulations in the future.

4.3.3 Comsol methods

As noted in Chapter 4.3.1, five CFD fields are imported into the Comsol LNS interface to account for the background mean flow. The iterative solver suggested by Comsol is then used to solve for the acoustic variations in velocity, pressure and temperature in the frequency domain, using the simplified geometry that is similar to Figure 17. Quoting Comsol documentation: “The equations are formulated in the frequency domain and assume harmonic variation of all sources and fields. The equations include viscous losses and thermal conduction as well as the heat generated by viscous dissipation, if relevant. The coupling between the acoustic field and the background flow does not include any predefined flow induced noise.”[96]

For this case, acoustic boundary effects are ignored similarly to the validated Helmholtz example by Comsol [97]. This means that the walls are set to enforce slip and adiabatic conditions.

LNS allows for modelling the impact of turbulence on the acoustic wave. It is shown in [98] that acoustic waves are attenuated by turbulence by an amount that corresponds to extending the value of the dynamic viscosity to include the eddy viscosity calculated by CFD turbulence models. SST turbulence models, which are used in this thesis, are suggested by the Comsol documentation to best estimate the eddy viscosity [99]. In effect, the turbulence is modelled as additional local viscosity. LNS was chosen, as it allows for modelling of the effects of both convection and turbulence on the acoustics of the muffler.

The equations solved by the Comsol LNS interface are linearised continuity, momentum and energy equations. The resulting fields show acoustic variations in pressure, velocity and temperature [96].

The linearised functions assume that the perturbations are small compared to the background values, allowing for linearity assumptions. This should be accurate for the case at hand just like it is for most acoustics.

The mean flow LNS case is setup similarly to the Comsol tutorial "Helmholtz Resonator with Flow: Imported Fluid Flow from CGNS (CFD General Notation System) Data" [97], the results of which are in good agreement with a reference measurement [100].

The various domains in the LNS simulation are shown in Figure 18. PMLs are placed on either end of the domain to absorb transmitted waves without reflection. The source domain is defined as a constant background field and the main LNS domain that includes the simplified mixing silencer geometry is in the middle.

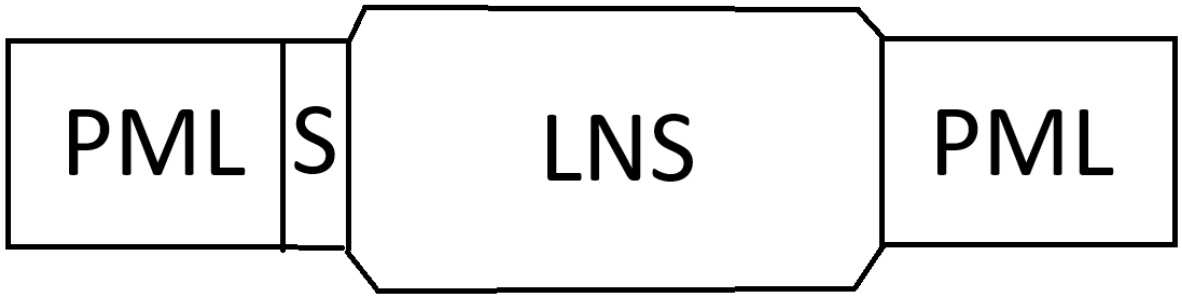

Figure 18: Domains of LNS mean flow study. PMLs are Perfectly Matched Layer domains that absorb waves exiting the geometry, S is an acoustic source domain and LNS is the domain where Linearised Navier-Stokes equations are solved. Flow and source excitations move from left to right.

Unlike the linear acoustics in the validation study (Chapter 4.2), the LNS calculation does not define boundaries to allow for various mode shapes. Instead, PMLs allow for various modes to exit without reflection.

The excitation is an incident plane wave defined in a source domain at the inlet by

$$k_0 = \frac{\omega}{c + U_{flow}} \tag{17}$$

and

$$p_b = 1\ \text{Pa} * e^{i*k_0*z}, \tag{18}$$

where k_0 is the convected wave number, ω the angular frequency, c the speed of sound, U_{flow} the mean speed of the flow through the component, p_b the specified background source, e Euler's number, i the imaginary unit and z the axial direction in which the flow goes through

the pipe. Note that using Comsol notation, the background pressure represents a wave travelling in the negative z-direction, whereas U_{flow} is positive for when acoustic propagation is in the same direction as the flow. The signs change depending on the chosen coordinate system.

Acoustic temperature and velocity are then calculated based on the acoustic pressure exactly as can be seen in [97].

The LNS study is calculated on a frequency range of approximately $10 - 100$ Hz. According to [36, Ch. 1.5], the cut-off frequency is lowered by a factor $(1 - M^2)^{\frac{1}{2}}$ in circular tubes with flow, with M being the Mach number. Using this formula, it was calculated that with the flow present within the mixing silencer at the studied frequencies, no higher order modes can propagate in the pipes. Thus, having only plane wave excitation is physically correct.

The TL is defined by integrating over circular surfaces at the inlet and the outlet. Referencing Figure 18, the power of the incoming wave is calculated at the intersection of the leftmost PML and the source domain. The power of the outgoing wave is calculated at the intersection of the LNS and rightmost PML domains.

4.3.4 Meshing and mesh mapping

The CFD mesh is created with internal Wärtsilä scripts that create a configuration for snappyHexMesh, which is a 3d hexahedral meshing utility included with OpenFOAM v13 [101]. Boundary layers are added, with first layer thickness estimated to reach y_+ values of $30 - 300$ in the log-law region for the k-Omega-SST wall functions (kqRWallFunction, nutkWallFunction, omegaWallFunction and alphatWallFunction) used in the CFD case. More specifically, the y_+ target value used in the estimations was 100.

The y_+ estimation was done according to the procedure shown in [102], and thus a value for the first-layer thickness was gained. y_+ is used as a dimensionless wall distance metric in boundary layer theory, and this methodology only works as a rough estimation. The formulas assume a flat plate in flow, but they give a rough value around the correct order of magnitude for the thickness of the first boundary layer.

SnappyHexMesh, the mesher used to create hex-dominant geometry for the simulation was setup to create the same boundary layers on all walls. This naturally means that the cavity of the quarter-wave resonator will have extremely low values, as there is no flow through the

cavity. This on the other hand should not be a great concern, because a small error in the wall modelling does not really matter if there is no flow. As the geometry is almost cylindrical, a cylindrical background mesh was used for the meshing.

The Acoustic mesh is created in Comsol. Minimum and maximum element sizes are set manually for a free tetrahedral mesh of the domain. This domain is then extended by a swept mesh to accommodate PMLs for the inlet and outlet. The PMLs were set to be meshed into 16 pieces in the axial direction, similarly to the Comsol tutorial [97].

Boundary layers are added to walls also in Comsol, using the same parameters and number of layers as in snappyHexMesh to allow for the CFD data to be fully represented in the simulation.

As we are targeting high y_+ values, the CFD simulation does not fully resolve the wall boundary layers but uses wall functions. This means that the CFD results and therefore also LNS results do not account for all effects in the acoustic or fluid flow boundary layers.

The Comsol FEM mesh for a generic mixing silencer can be seen in Figure 19. The OpenFOAM CFD mesh for a generic mixing can be seen in Figure 20.

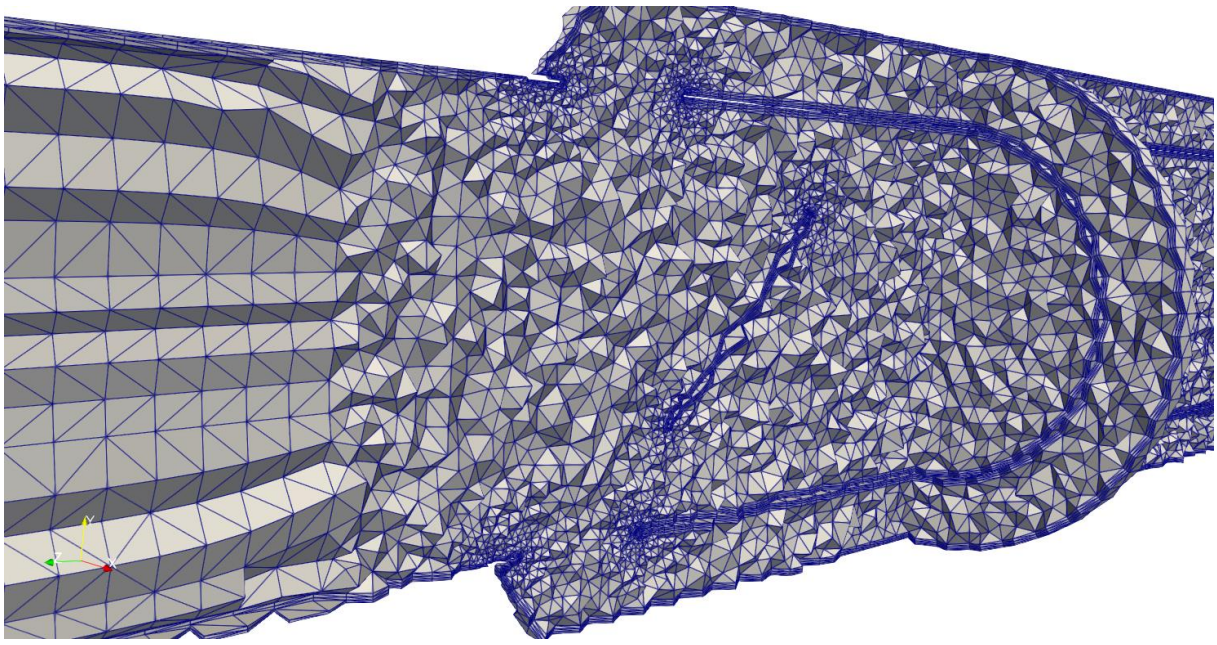

Figure 19: Slices through the tetrahedral FEM Mesh used in the mean flow study. Swept PML mesh visible on the left. Full tetrahedral elements intersecting the slice plane were visualised for clarity.

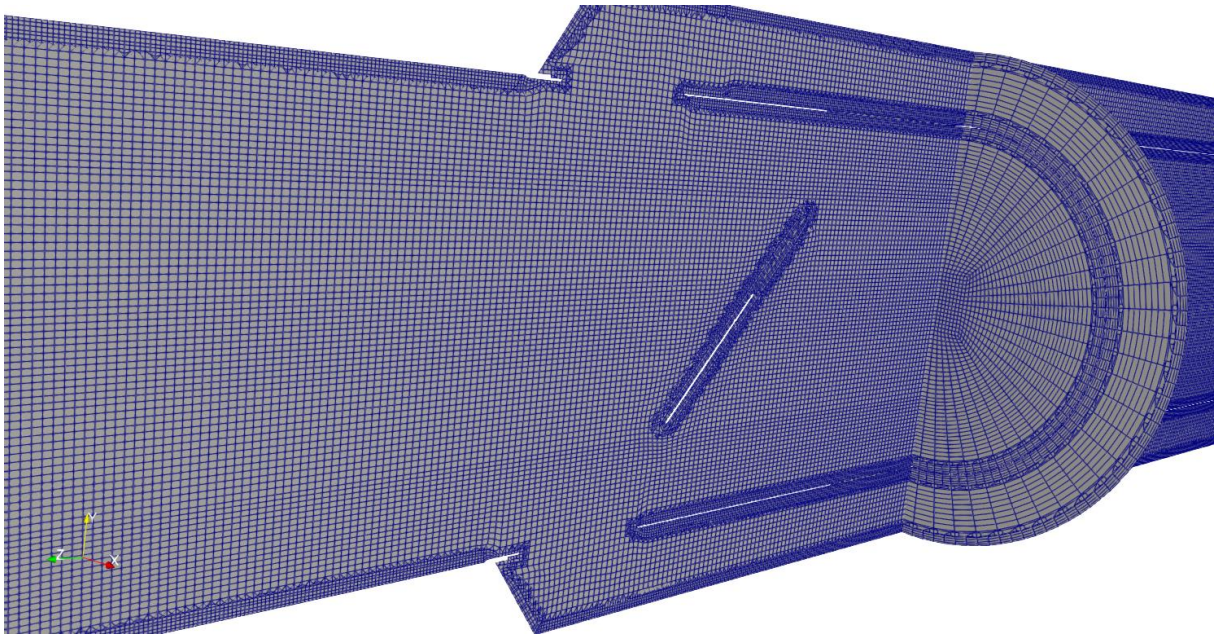

Figure 20: Slices through the hex-dominant CFD Mesh used in the mean flow study.

The boundary layer meshes might visually look thicker in Figure 20, but this is just a side effect of how the boundary layers and the main mesh are blended. The actual boundary layer thicknesses are identical.

The mapping study itself solves the problem of how a point cloud, where every point is a cell centre from the FVM CFD mesh (in Figure 20), can be correctly mapped on to the FEM mesh used by Comsol in (Figure 19) [103].

4.3.5 Theoretical considerations

This chapter presents an idea that could explain some of the convection effects of the flow on the TL.

If we ignore all complex behaviour at boundaries and only account for convection, we can think of the mixing silencer as two separate domains: Assume that in the main pipe, we have a flow speed of u_{flow}, and in the quarter-wave resonator there is zero flow. As there is no flow in the resonator, we assume that the resonant frequency, meaning the maximum attenuation, would have the same wavelength in the resonator as the static case. This would also lead to the frequency being the same f_{rs}.

Since we are treating the resonator as having no flow, we need to think about how the resonator is affected by the excitations from the main pipe. If there is an incoming frequency of f_{in} coming to the main pipe, it will be convected by the flow. Thus, the convected

frequency observed by the resonator can be treated as an approaching source and calculated with the Doppler effect formula

$$f_r = f_{in} \cdot \frac{c}{c - U_{flow}}, \tag{19}$$

where c is the speed of sound.

The approach in Equation 19 should be sound with the assumptions, as we know that the quarter-wave resonator works by the superposition principle. Thus, when the frequency observed by the resonator matches its resonant frequency, we should have maximum attenuation. This also means that the TL spike should move to a lower frequency.

The described method functions a rough analytical approximation to provide an understanding of the magnitude of possible convection effects and ignores several variables included in the three-dimensional LNS FEM used in the mean flow study. Note also that the frequency-domain simulations do not calculate this kind of frequency change, but instead the convection is seen as a change in wavenumber and wavelength with constant frequency.

5 Results

The results of all simulations described in Chapter 4 are presented here.

5.1 Validation

First, the results of the mesh sensitivity study are presented and a parameter for the mesh density target is chosen. Then, the validation study results are compared to measurement results for three different components.

5.1.1 Mesh sensitivity study

The results of the mesh sensitivity study are used to determine a balanced target value for the number of elements per wavelength and to verify that the meshing process does not affect results. This is done to find a good balance between computational cost, accuracy and practicality. The setup for the experiment is described in Chapter 4.2.3.

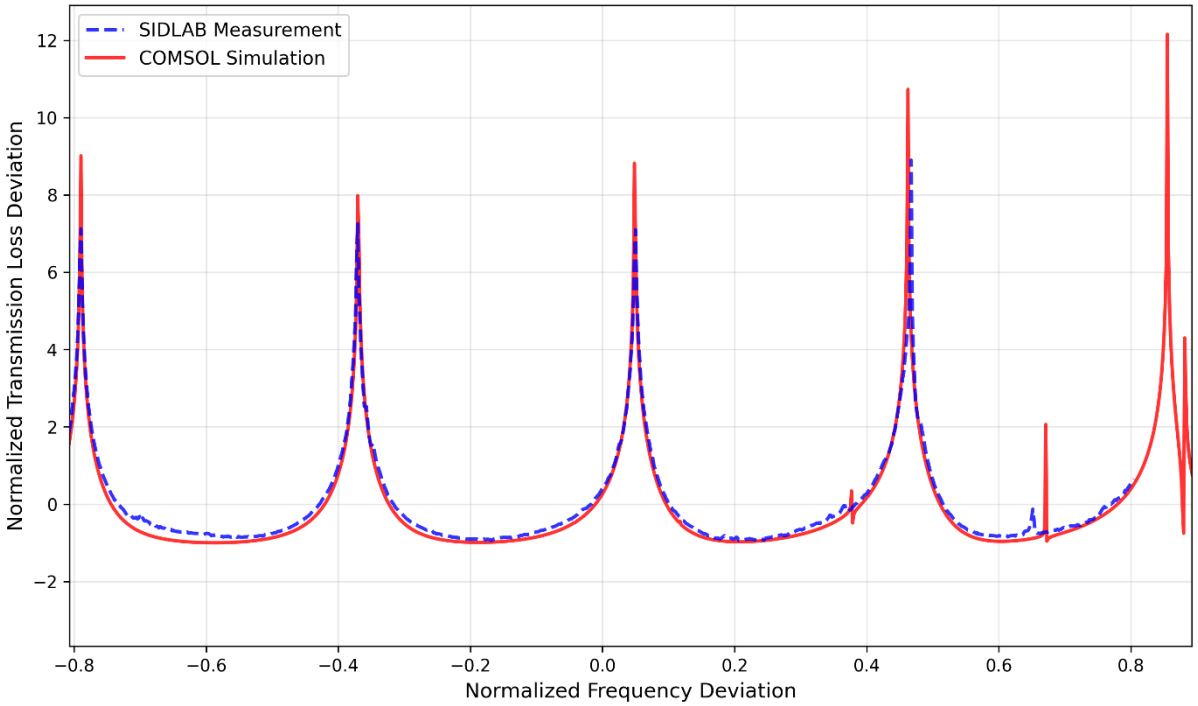

Figure 21: A graph showing a simulation using the overly dense Mesh 1 compared to measurement results for Component 1 at 18°C. To comply with confidentiality requirements, both the measured and simulated data were normalized using a fractional-deviation transformation. A common reference point was derived from the measurement dataset's mean values (with a small arbitrary offset applied to the frequency reference), and all data points were expressed as relative deviations from this reference. This linear transformation preserves the shape of the acoustic response curves and the validity of the measurement-simulation comparison while concealing the absolute frequency range and transmission loss magnitudes. This method preserves the shape and comparability of results.

From Figure 21, we can see that the simulation behaves as expected and predicts the behaviour of Component 1 accurately with the overly dense mesh. The peaks are situated exactly in the same frequencies within the used measuring resolution, except that on right-most spike, the simulation underpredicts by one frequency step. Thus, the behaviour of Meshes (2-5) will be evaluated by plotting the difference between Mesh 1 and the other meshes with a 1 Hz simulation step. It is assumed that the solution of Mesh 1 is correct. The results for various mesh densities are shown below.

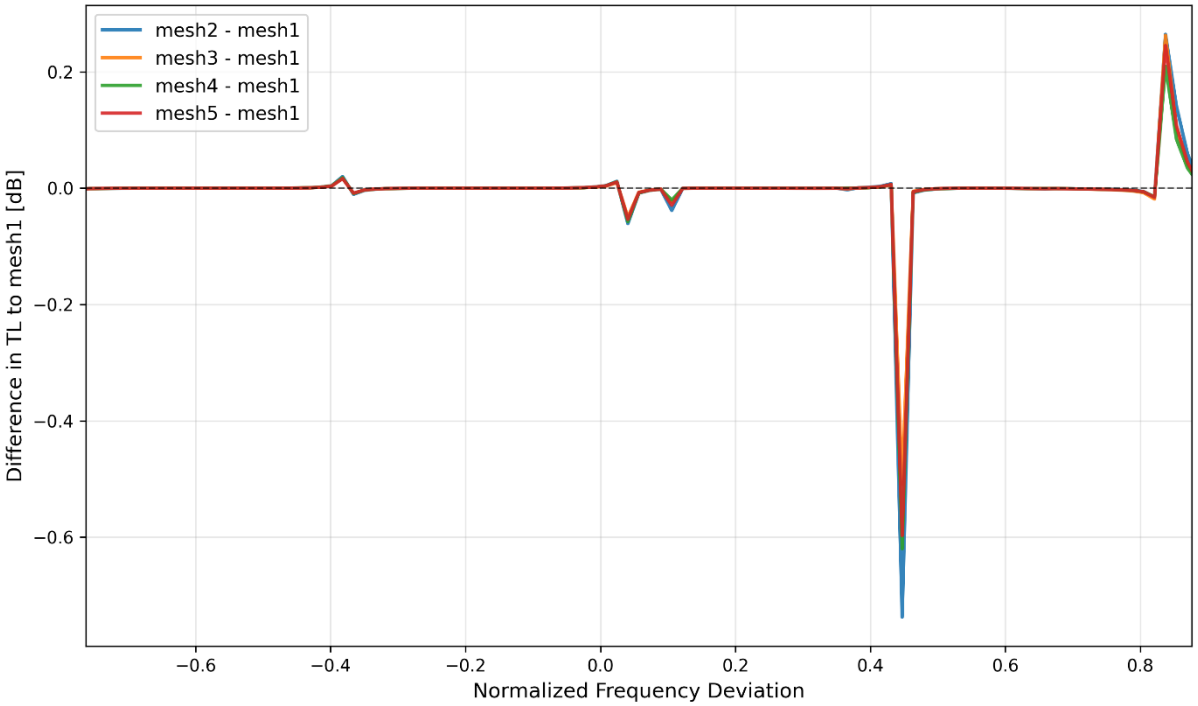

Figure 22: Differences of transmission results produced by various meshes. The y-axis shows the absolute difference in transmission loss in dB, preserving the true magnitude of mesh-induced deviations. To comply with confidentiality requirements, the frequency axis was normalized using a fractional-deviation transformation: a reference frequency was derived from the mean of the common even-integer evaluation frequencies (with a small arbitrary offset), and all frequency points were expressed as relative deviations from this reference. Only even-integer frequencies common to all five mesh datasets were used, ensuring direct point-by-point comparison without interpolation. This transformation conceals the absolute frequency range while showing the effects of mesh density.

Based on Figure 22, we can verify that reducing the targeted $n_{\frac{nodes}{\lambda}}$-value does not meaningfully affect accuracy for any of the various meshes. For the exact parameters of the meshes, refer to Table 8. As hypothesised, we can note that the targeted element size has a small effect here compared to more theoretical studies where all elements are sized exactly according to a target value. More importantly, this indicates that the meshing procedure is not prone to causing meaningful errors to our solution.

Based on the result and literature suggestions, we will use the target value of $n_{\frac{nodes}{\lambda}} = 5$ in the meshing for the validation study described in Chapter 4.2. Due to the meshing process, the meshes created will be much denser than the target value in most areas, and the $n_{\frac{nodes}{\lambda}} = 5$ serves as a minimum density for the mesh. This decision should lead to mesh-related inaccuracies being minimal in the validation study.

5.1.2 Validation study - comparison to measurement results

Three components were simulated and measured using the methodology in Chapter 4.2 and mesh size determined from the mesh sensitivity study. The results are presented in Figures 23-25 for Components 1-3, respectively.

For Figures 23-25, an identical procedure has been applied to the data. The upper panel shows the measured and simulated transmission loss curves, where both the frequency axis and the transmission loss axis have been normalised using a fractional-deviation transformation to comply with confidentiality requirements. A common reference point was derived from the mean of the measurement dataset (with a small arbitrary offset applied to the frequency reference), and all data points were expressed as relative deviations from this reference. The lower panel shows the absolute difference between simulation and measurement in decibels, computed in the original (non-normalised) domain by linearly interpolating the simulation data onto the measurement frequency grid. Positive values indicate that the simulation overpredicts the transmission loss relative to the measurement. This approach preserves the shape of the acoustic response curves and the validity of the measurement–simulation comparison while concealing the absolute frequency range and transmission loss magnitudes.

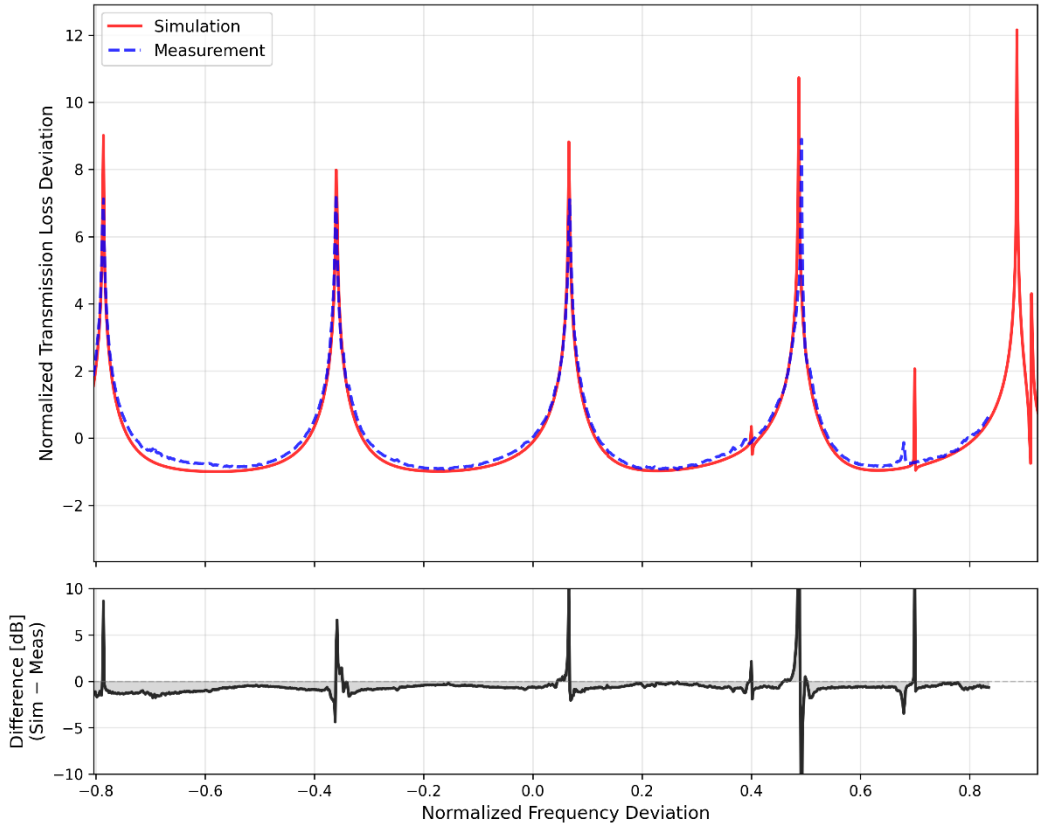

Figure 23: Comparison of measured and simulated transmission losses for Component 1. Refer to the beginning of Chapter 5.1.2 for an explanation of the data normalisation process.

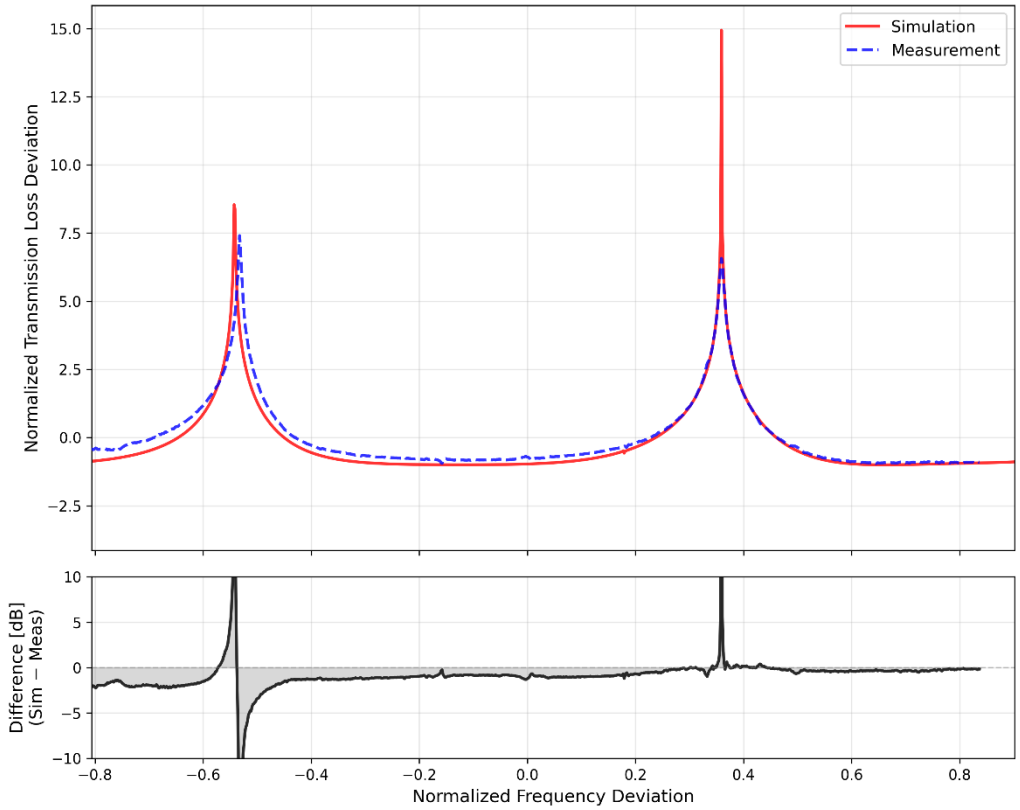

Figure 24: Comparison of measured and simulated transmission losses for Component 2. Refer to the beginning of Chapter 5.1.2 for an explanation of the data normalisation process.

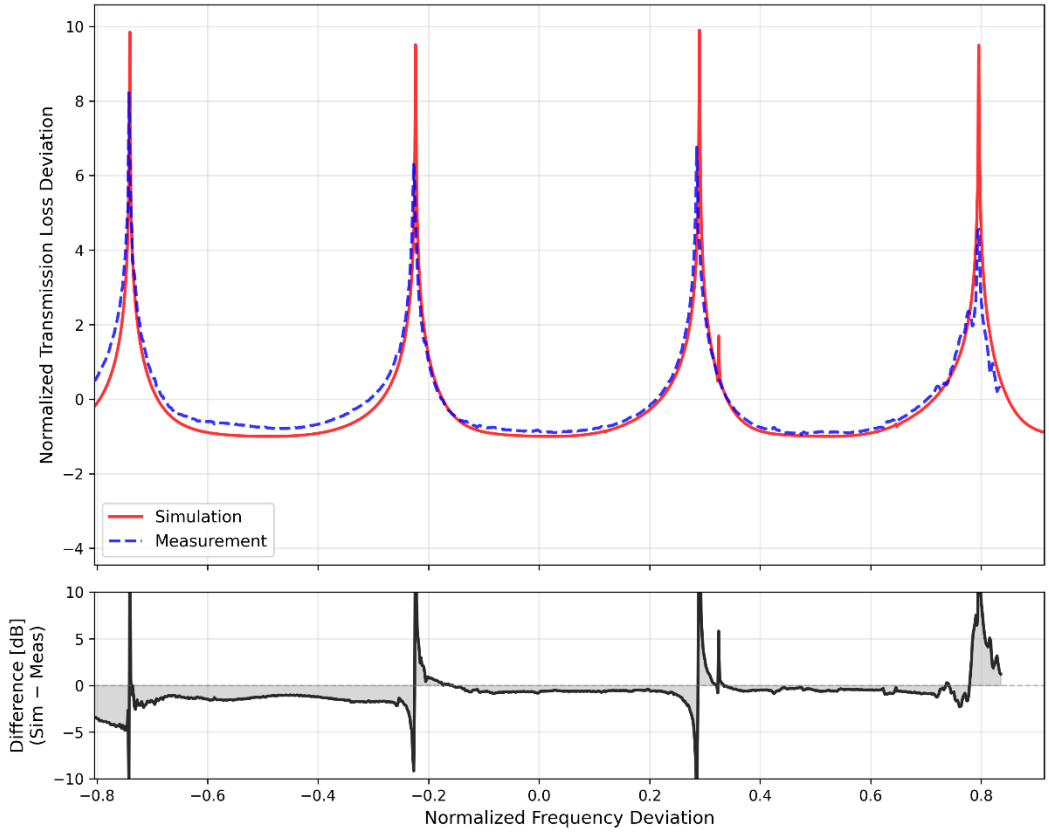

Figure 25: Comparison of measured and simulated transmission losses for Component 3. Refer to the beginning of Chapter 5.1.2 for an explanation of the data normalisation process.

As expected, the simulations predict the experimental measurements well. Especially the frequencies of the TL peaks, which are the parameters that dimensioning is based on, are predicted very accurately.

An interesting break of the general good performance of the models can be seen in the lowest (left-most) peak of Component 2 in Figure 24. The first peak location has an error in the order of 1 Hz, which is ten times higher than any other error regarding the location of the peaks. It is also interesting that the second peak is predicted correctly (considering the resolution of the measurement). Since the frequency of all other peaks is predicted almost perfectly, I would have to assume that there is some phenomenon not included in the simulations happening at the first peak frequency. Perhaps there is some coupling with vibration in the measurement, a small air leak in the component or the measurement setup itself is somehow affecting the behaviour of the quarter-wave resonator.

The behaviour of Component 2 is the most complex also from another standpoint, with comparison to Equation 9 that predicts that the peaks should repeat with a pattern $n = 1, 3, 5 \ldots$

Components 1 and 3, both when measured and simulated follow the rule, that $f_{firstpeak} * 3 = f_{secondpeak}$ with $\pm 1\%$ relative accuracy. Component 2, on the other hand has a relative error of $+3{,}0\%$ in the measurement, compared to the formula. This supports the theory that for some reason, Component 2 exhibits more complex behaviour or measurement error.

The created method is a clear success, as these results are very useable for engineering purposes. There will always be uncertainty regarding temperature and flow conditions that far exceeds the error of these simulations. The simulations are also much more accurate than the analytical methods widely used for mixing silencer dimensioning. Based on previous experience at Wärtsilä, the analytical formulas have had up to $\pm 10\%$ error compared to measurements. The differences between analytical methods and FEM are also evident in the test case results in Figure 14.

5.2 Mean flow

In this chapter, results of the mean flow study are evaluated. First, the quality of the meshing and mesh mapping are evaluated. Second, the effects of the simplification of geometry on the linear acoustic performance of a single mixing silencer are quantified. Finally, the results of LNS cases using both steady-state, single timestep and averaged CFD fields are presented and compared with each other and the static cases. An additional subchapter is devoted to challenges that appeared during the simulation process. Note that only one mixing silencer geometry, Component 1, is evaluated in this chapter.

For the work in this thesis, OpenFOAM is run on a Linux cluster, whereas Comsol is run on a separate Windows server.

Multiple CFD cases are used as input to the LNS; A steady state solution, three singular timesteps from a transient solution and an averaged solution, where an average over the timesteps is calculated.

Various CFD cases are investigated, because the flow through the mixing silencer is oscillatory by nature. In the steady state, this is visible as oscillation in the residuals over iterations. In other words, the steady state does not converge properly, as can be seen from the residual plot in Figure 26.

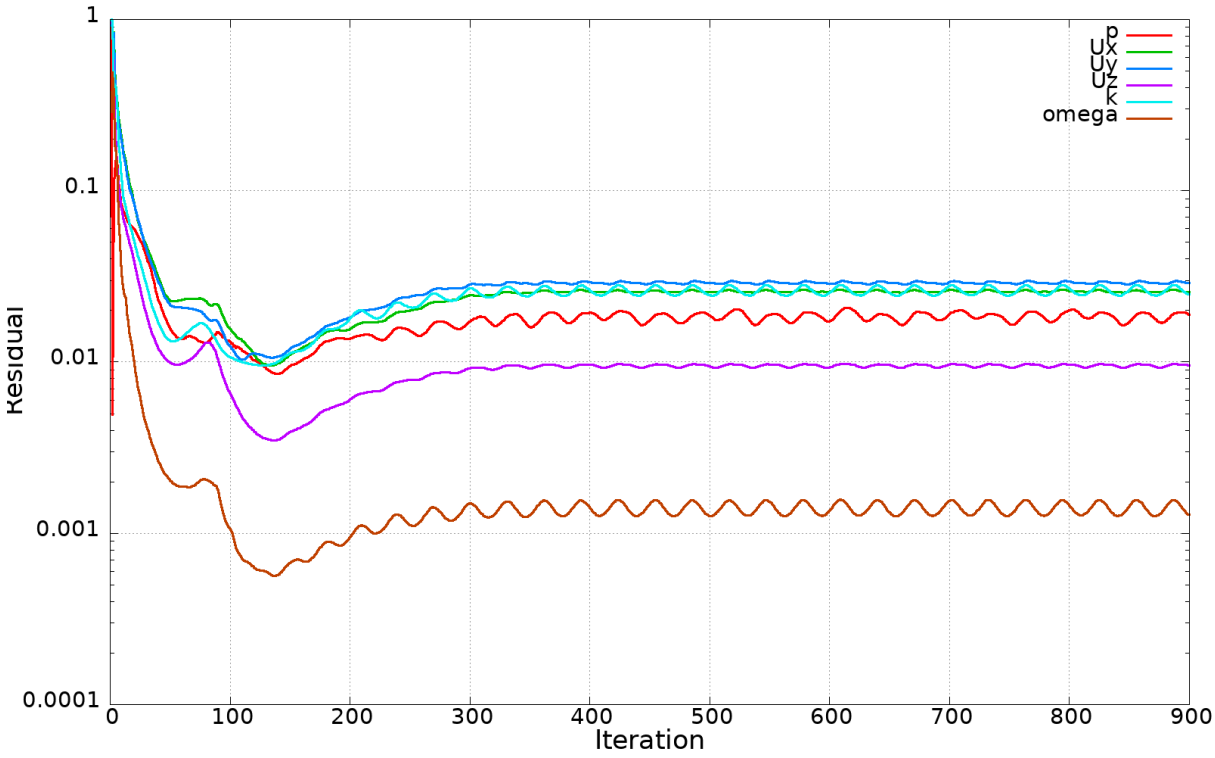

Figure 26: Residuals from a steady-state CFD calculation. It is clear that the solution does not converge well, which is explained by the oscillatory flow seen in the temporary solution. p is pressure, Ux, Uy and Uz components of velocity, k the turbulent kinetic energy and omega the specific dissipation rate of turbulent kinetic energy.

Therefore, the steady-state case is used as an initial condition for a transient simulation to model the flow in the mixing silencer.

A pressure probe was placed in the transient simulation, and FFT was used to verify that there is a pressure oscillation caused by the geometry in the mixing silencer. FFT results can be seen in Figure 27.

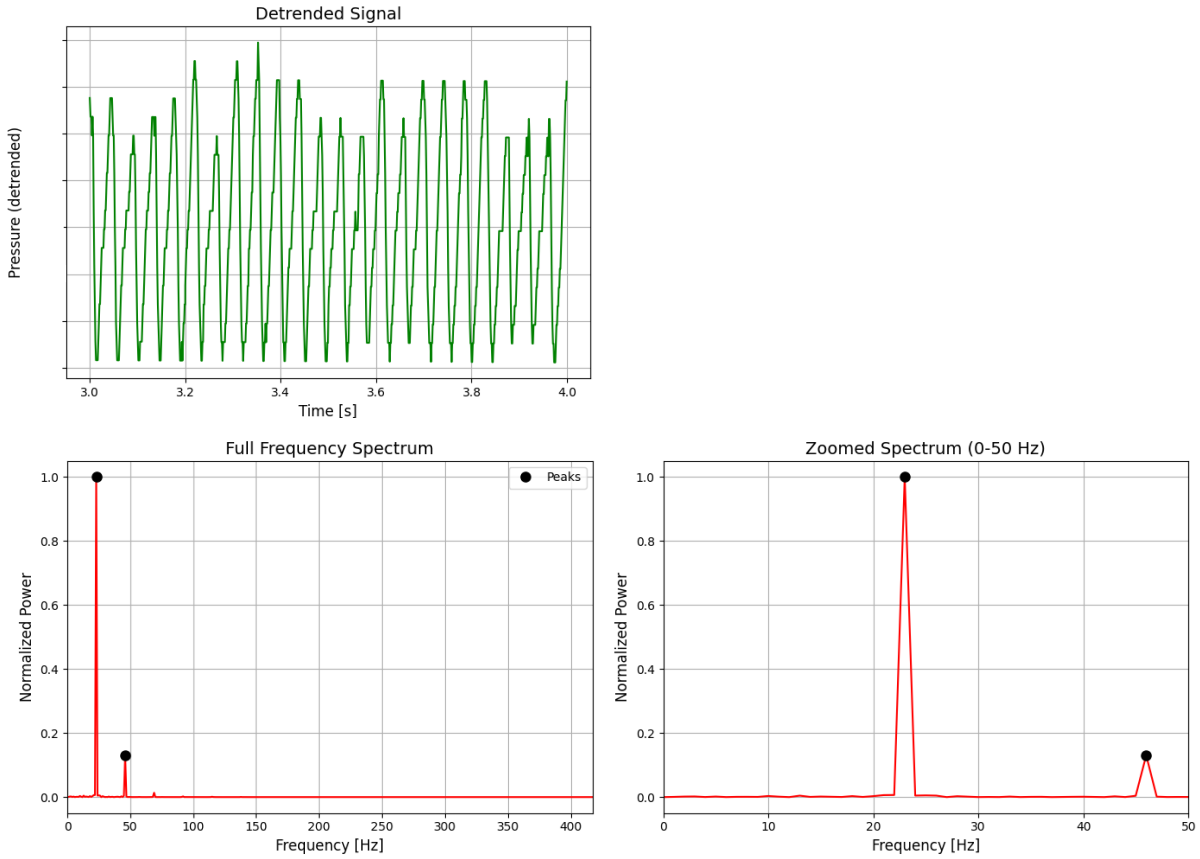

Figure 27: Detrended pressure wave after the mixing plate and FFT results for the signal. Exact pressure values removed due to confidentiality. Note the 23Hz frequency peak.

Due to this behaviour, the mean flow study was run with multiple CFD solutions to observe possible differences in results:

1. A randomly chosen singular iteration from the steady state.
2. Three singular timesteps at three different phases of oscillation to identify if the temporal oscillation meaningfully affects results.
3. An average solution where the fields are averaged over ten oscillations to calculate an average flow.

As a note, separate from this thesis, the oscillatory behaviour caused by the mixing plate brings up a question of whether this oscillation functions as a source for vibrations, leading to possible failures within the system. This could be an interesting question for future studies.

To test of the mesh and solving procedure, the inlet and outlet were switched on the geometry used in the CFD solutions, with everything else being the same. For this reverse flow, all properties seen in the residual plot converge at 580 iterations with residuals under 1e-4. This

behaviour is interesting and could serve as a basis for a new study regarding the CFD of the component.

5.2.1 Meshing and mapping evaluations

As noted in Chapter 4.3.4, estimation formulas for a plate in flow were used to calculate a first-layer thickness targeting y_+ values of 100. The walls of the quarter-wave resonator chamber are excluded from the evaluation, as there is very little flow there, and meshing was targeted for the main pipe flow.

Figure 28 shows a histogram of the y_+values, based on the steady solution. Instead of the targeted average of $y_+ = 100$, the average is 51,01. This is explained by an error in the meshing parameters: For an FVM code like OpenFOAM, the location used in wall functions is not one cell thickness away from the wall, but instead it is half a cell thickness away from the wall, as the middle of the cell is what we are solving for. Due to this, the first layer thickness should have been two times the estimated wall distance, but it was mistakenly set to be the wall distance.

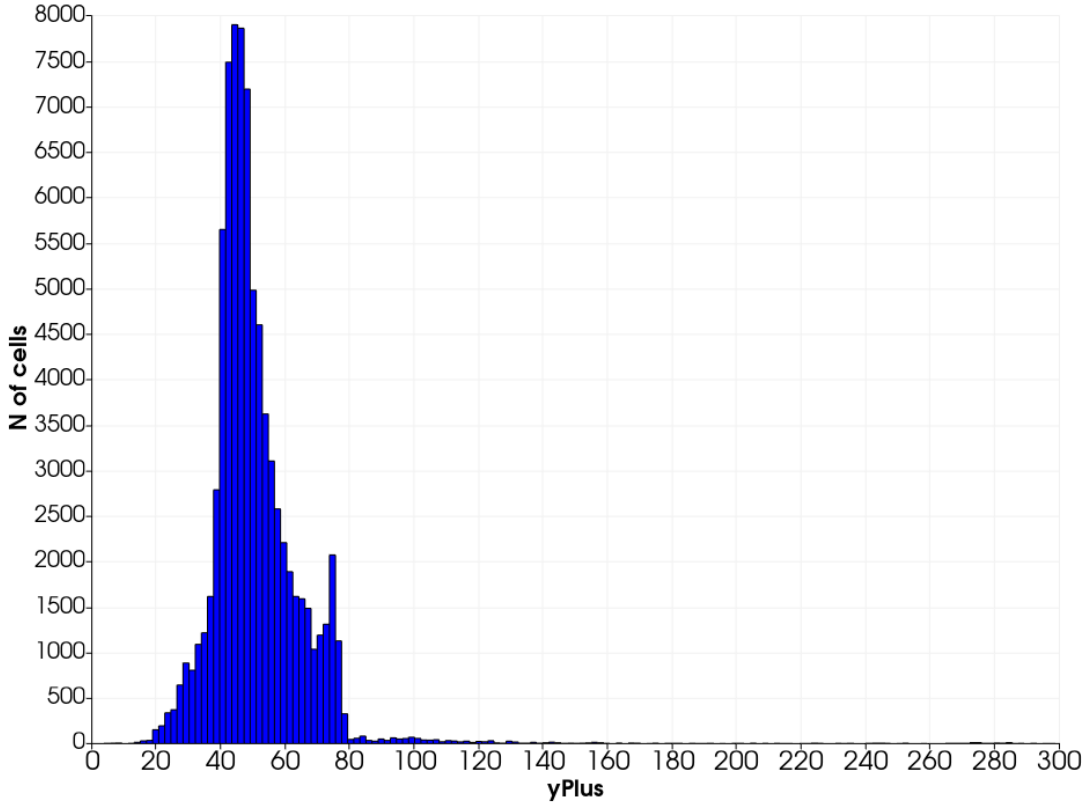

Figure 28: Histogram of the y+ values of the steady solution, excluding the quarter-wave chamber, where flow is negligible. Average value is 51,01. 96,8% of values are over 30.

Despite the error, 96,8% of the y_+ values are above 30, meaning that the results should be physically accurate. Figure 29 shows a similar evaluation averaged over timesteps of the transient simulation.

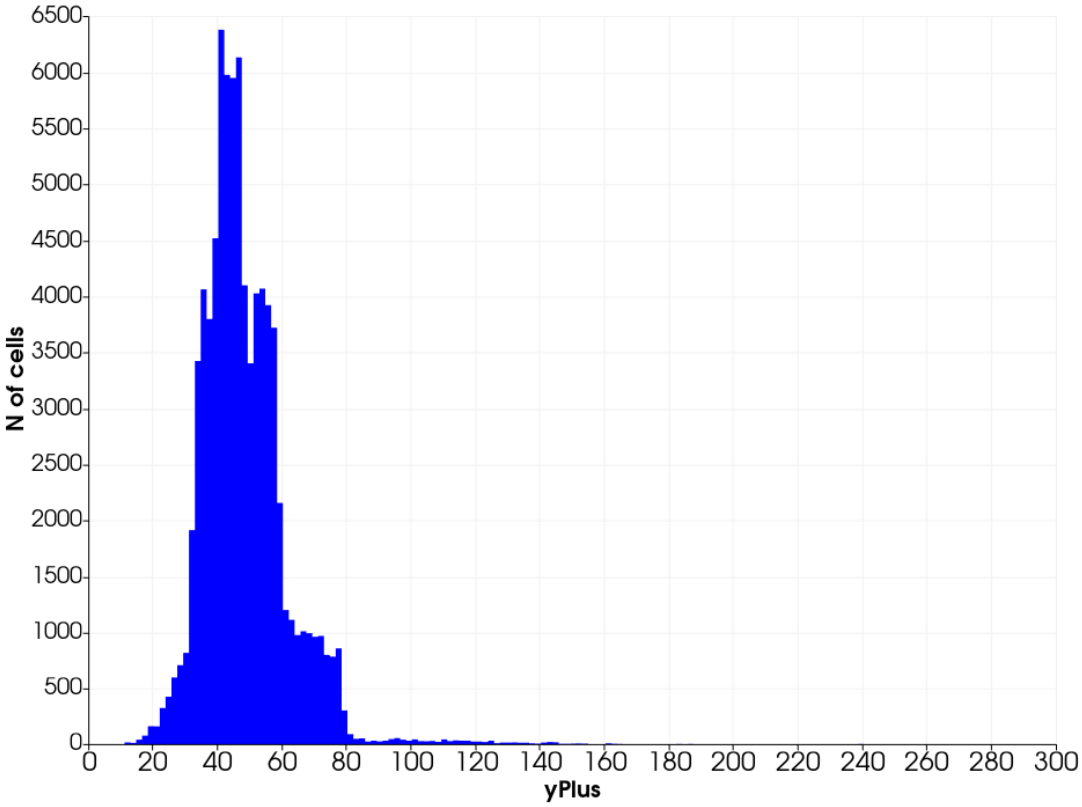

Figure 29: Histogram of the averaged y+ values of the transient solution between timesteps t=3,0 and t=3,2. The quarter-wave chamber, where flow is negligible, is excluded. Average value is 49,2. 96,5% of values are over 30.

Similar conclusions can be made from Figure 29. The results should be mostly physically accurate despite the error in boundary setup. The mesh is identical for all CFD simulations.

To evaluate the results of the mapping study, where CFD fields are mapped onto the FEM mesh in Comsol, plots over a line will be shown for the two meshes. A line is drawn through the geometry, downstream of the mixing plate, as can be seen in Figure 30.

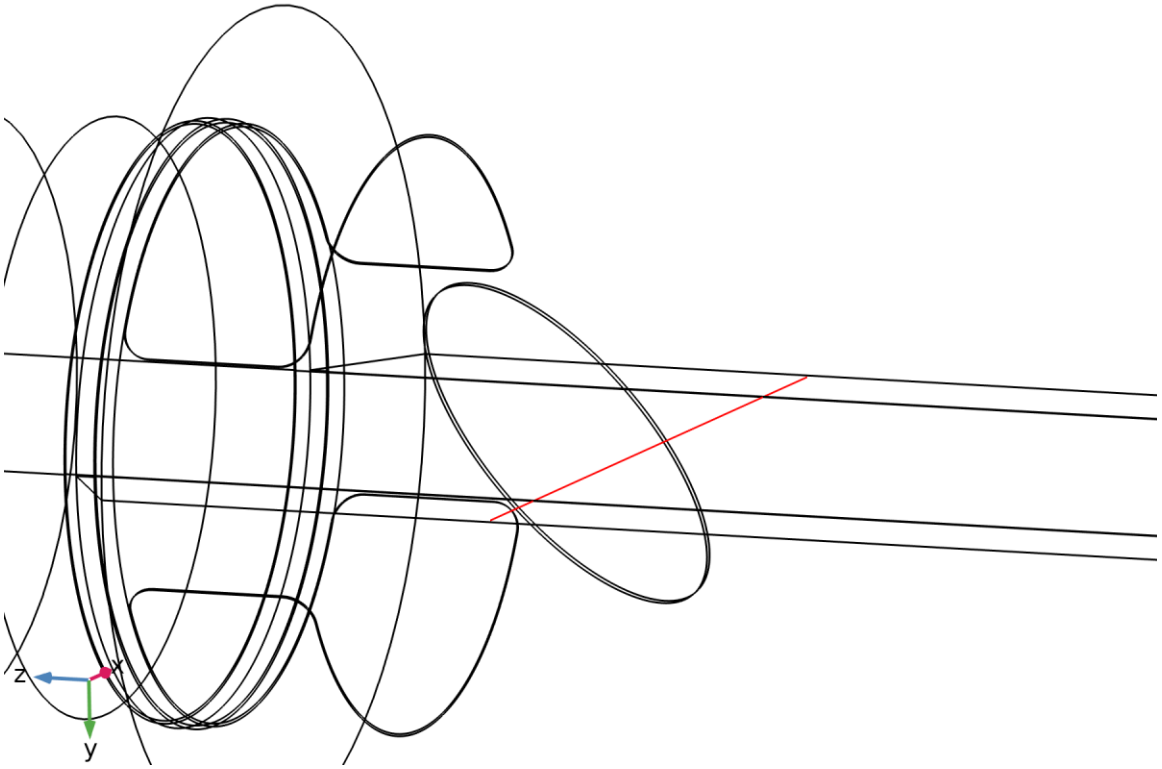

Figure 30: Red line depicts the line used for evaluating the success of the mapping study. Note that the line goes through the whole geometry, including the reactive chambers.

A comparison between the normalised z-component of velocity for the CFD results and mapped values are shown in Figure 31 for the various CFD fields.

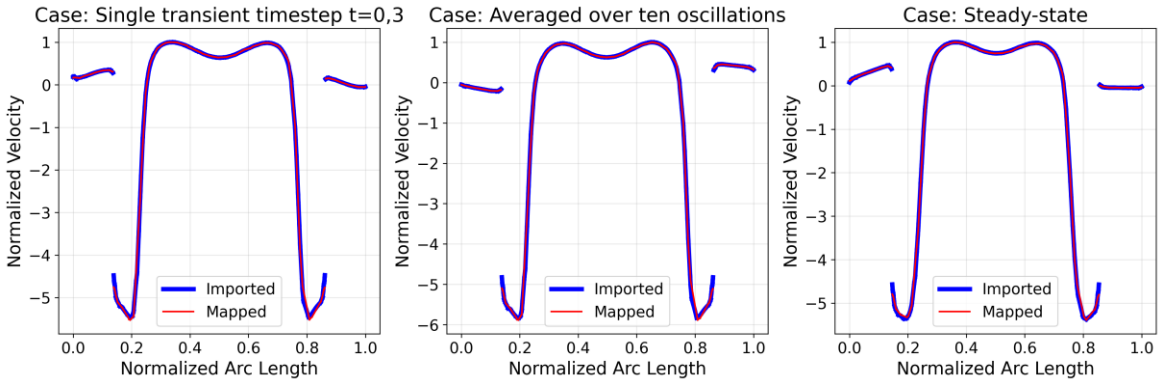

Figure 31: Normalised z-directional velocity over the line visualised in Figure 30 for a single CFD timestep, an averaged solution and a steady-state solution, both imported and mapped data. Mapped field matches well with the imported field. Velocity was normalised by dividing by its maximum positive value, meaning that negative values indicate flow in negative Z-direction.

Based on Figure 31, the mapped results match well with the CFD data being imported. This means that the mapping study is solved correctly and that the mesh sizes are suitable.

To show differences between the various CFD solutions, Figure 32 visualises original CFD data for the three cases.

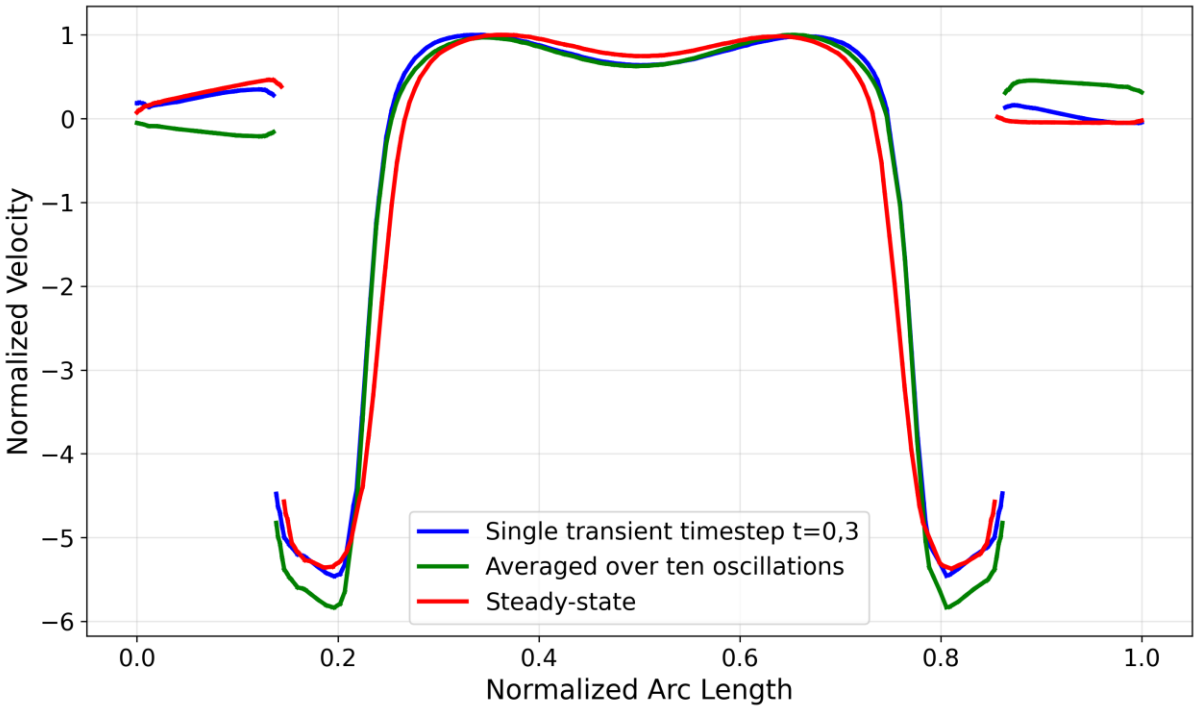

Figure 32: Comparison of z-direction velocities of the various CFD solutions, meaning imported data. Velocity was normalised by dividing by the maximum positive value of all datasets, meaning that negative values indicate flow in negative Z-direction.

Based on Figure 32, we can note that there is a meaningful difference between the solutions, both in the middle downstream of the mixing plate and in the quarter-wave chambers near the edges. This is to be expected since the flow is heavily unsteady.

To conclude, the velocity plots in Figures 31 and 32 show that mapping is accurate to the FEM mesh, and that the flow does differ in the various CFD cases.

Discussing the mesh quality metrics produced by OpenFOAM and Comsol is beyond the scope of this work, but the default mesh quality tests do not give any warnings on either software.

5.2.2 Acoustic effects of simplifying the geometry

The fact that the geometry is simplified for the mean flow study, as described in Chapter 4.3.1, means that there will be minor deviations from the real flow. These are considered minor and a reasonably good trade-off for better quality meshing. As the research question is whether flow needs to be considered in the design or not, the small simplification in the flow field is acceptable. However, if the acoustic behaviour is somehow meaningfully changed by the simplifications, the whole experiment loses its value.

The effects of geometry simplification on the acoustics of the mixing silencer are compared by running the linear acoustics case described in Chapter 4.2.2 for the simplified geometry, and comparing results to the complete geometry used in the validation study.

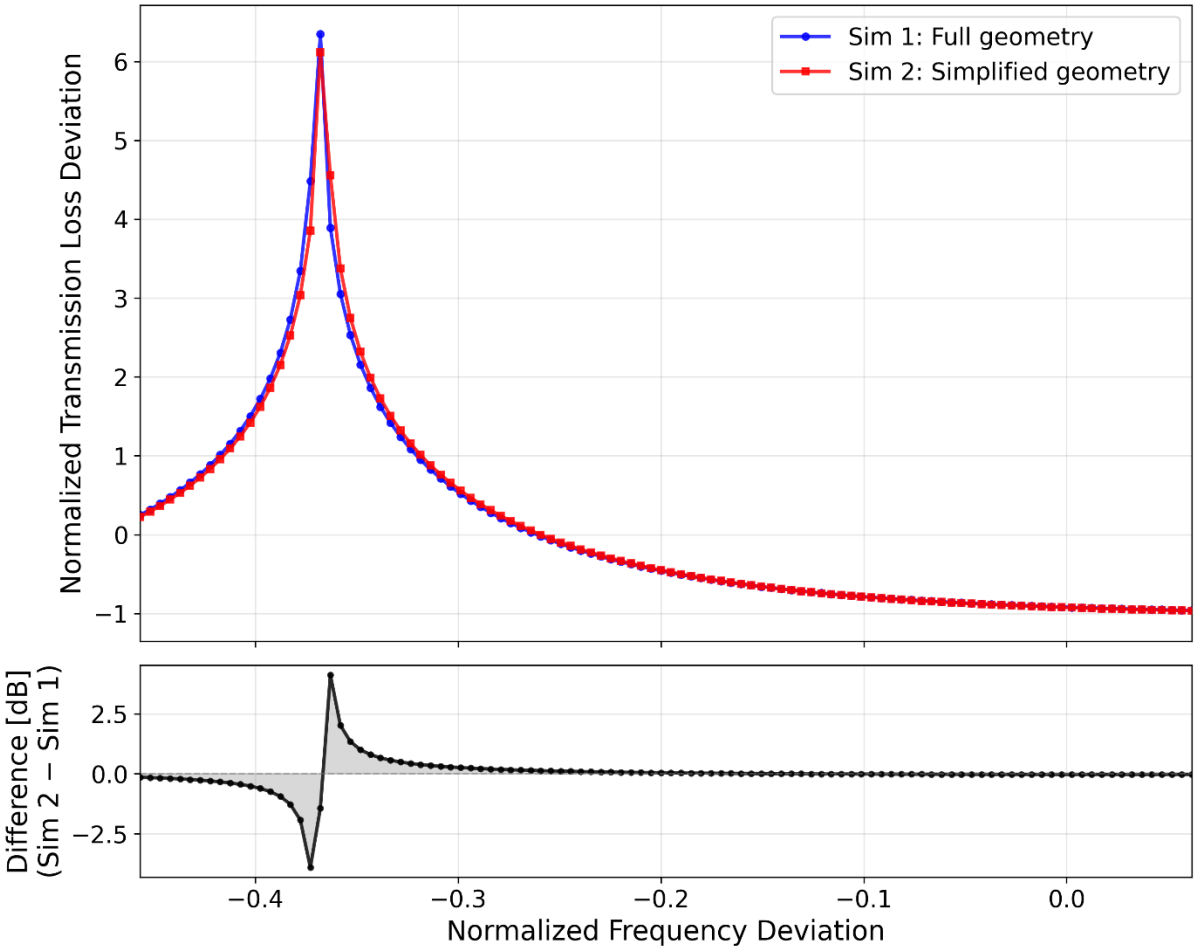

Figure 33: Normalised transmission loss deviation plot for linear acoustics of full and simplified geometries. The upper panel shows the transmission loss curves, where both the frequency axis and the transmission loss axis have been normalised using a fractional-deviation transformation to comply with confidentiality requirements. A common reference point was derived from the mean of the Sim 1 dataset (with a small arbitrary offset applied to the frequency reference), and all data points were expressed as relative deviations from this reference. The lower panel shows the absolute difference between the two simulations in decibels, computed in the original (non-normalised) domain at each common frequency point. This normalisation approach preserves the shape of the acoustic response curves and the validity of the comparison between the two geometries.

Based on Figure 33, we can note that the simplification of the geometry does not meaningfully affect the linear acoustics of the component. Therefore, the simplifications should be acceptable for the purposes of this work.

5.2.3 TL results for mean flow cases

Previous chapters show that the used methodology is based on the validated Comsol example case, that the meshing is done correctly and that the geometry simplification does not

meaningfully affect the acoustics of the component. Thus, the results presented here for the effects of flow on the TL of the mixing silencer are physically correct.

The full TL results for the mean flow case in this work can be seen in Figure 34.

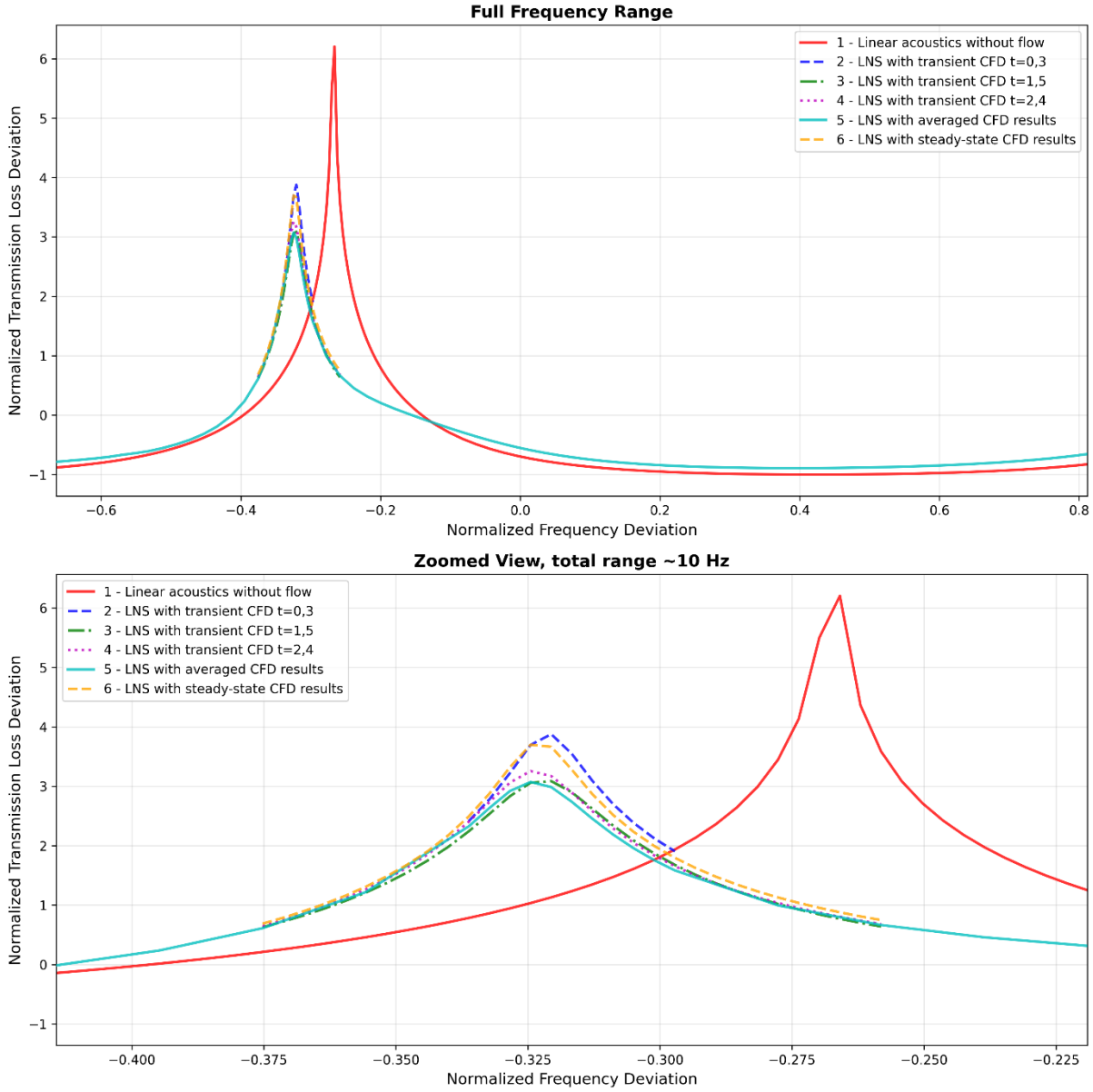

Figure 34: TL results for the mean flow simulations (lines 2-6) and the TL without flow calculated by linear acoustics (line 1). To comply with confidentiality requirements, both the frequency axis and the transmission loss axis have been normalised using a fractional-deviation transformation. A common reference point was derived from the mean of the first dataset (with a small arbitrary offset applied to the frequency reference), and all data points across all six configurations were expressed as relative deviations from this shared reference. This normalisation approach preserves the shape of the acoustic response curves and the validity of the comparison between configurations while concealing the absolute frequency range and transmission loss magnitudes.

Based on Figure 34, the flow moves the peak frequency of the TL graph by multiple Hz.

When discussing the various kinds of CFD solutions used for LNS, the differences are less

meaningful. This is because the various CFD solutions mostly influence the amplitude, not the frequency, which is much more important here. The simulation is thus determined not to be sensitive to the exact CFD solution. Especially the TL peak frequency does not move a lot with the various CFD solutions.

An important practical factor to consider with this kind of data is that the x-axis in Figure 34 represents the un–convected frequency due to the way that the simulation is set up. If acoustic excitation data is measured from a pipe that has flow, one should be careful to see if they are measuring convected frequency or not. As an example, if one is using the Gras 40SC probe microphone [104], they will be measuring the stationary frequency, meaning that the measurement frequency is the same as the LNS frequency.

This happens because the measurement is conducted so that the probe is inserted into the flow. The probe then functions as a waveguide and guides the wave to the actual microphone. There is no flow within the probe, meaning that the wave travels at the static speed of sound. Thus, the result is the stationary frequency. This may change if various microphones are used or if data is taken from simulations, for example.

The transient solutions taken at various phases of the oscillation, described at the beginning of Chapter 5.2, also do not meaningfully affect the result. Transient simulation is still needed in cases that present the kind of oscillatory behaviour, as they allow for gaining the averaged flow solution. If the flow is steady and a good steady-state solution can be obtained, there is no need for transient simulations.

To conclude, the flow through the mixing silencer does affect the TL peak frequency and therefore the tuning and dimensioning of the mixing silencer measurably, while reducing the amplitude of TL. This should be considered during the design phase.

5.2.4 Comparison of mean flow results to literature and simple convection models

Comparable literature results for the patented mixing silencer geometry do not exist. Perhaps the most comparative case study is made in [105], where a similar LNS study is run for much smaller quarter-wave resonators with resonances around 150 Hz. The study results show resonance peaks moving to lower frequencies at 0.05 Mach, but towards higher frequencies at 0.1 Mach. The results of the comparable study [105] are consistent to what is seen in this work.

In the documentation of the example case by Comsol [106], it is claimed that “the additional attenuation due to turbulence will shift the resonance toward a lower frequency, while the convective flow effects will shift it to a higher frequency”. Note that this text is in the context of a Helmholtz resonator, though the same principle could be theorised to also work in the case of the quarter-wave silencer. The convective flow might reduce the effective length of the silencer, thus shifting the peak to a higher frequency.

In [107], Actran is used with a combined CFD/FEM approach to quantify how the quarter-wave resonator peak attenuation frequency is affected by Mach number in the range of 0-0.1 Mach, determining that the frequency is reduced proportionally by $-\Delta f$ to the square of the Mach number M: $\Delta f = 1918.16M^2 - 24.21M$. The exact scale is not mentioned in the work but based on the mentioned maximum frequency of recorded data and size of the resonators from the pictures, the resonant frequencies of the studied quarter-wave resonators are in the range of thousands of Hertz, meaning that the formula is not directly applicable to this work. Interestingly, using the formula in [107] lead to only around 30% of error when measuring the frequency shift compared to the results in this work. This is not statistically significant, as only one flow condition has been studied in this thesis.

Generally, it is logical that the resonant frequency is reduced according to the following simplified analytical model:

For a constant frequency, as is assumed in the frequency-domain analysis, we can write $\frac{c_1}{c_2} = \frac{\lambda_1}{\lambda_2}$, where c is the convected speed of sound, and λ is the convected wavelength. Because the speed of sound is convected downstream, the downstream propagating wavelength will be longer in the pipe flow than it is in the quarter-wave silencer, where flow is approximately zero.

Thinking similarly about frequency instead of wavelength, we can model the flow as a source moving relative to the quarter-wave resonator. This method is also described in Chapter 4.3.5. Then, we can use the formula for the Doppler effect from Equation 19. This leads to the frequency observed by the resonator to be higher than the real acoustic frequency. To correct for this effect, the input frequency should then be lower than the resonant frequency of the component for maximal attenuation at the resonator, just as we see in the results.

Note that these basic formulas underpredict the frequency reduction by about 50%. They ignore all 3D effects, the transition from the pipe flow to the resonator and the turbulence and thermodynamic effects. They are mentioned just to somehow get a grasp on what might be happening in the component, and in which direction the frequency should move when convection is the dominant effect.

One hypothesis is that the additional effect on the TL spike comes from the flow affecting the end correction of the quarter-wave resonator, meaning the behaviour at the opening of the resonator.

5.2.5 Convergence challenges

During this work, convergence issues were sporadically encountered when solving the LNS equations at higher frequencies, typically in the range of 80-120 Hz. Some simulations failed to converge entirely, while others ran successfully through the entire frequency range. The inconsistency of these failures suggests that the problem is sensitive to specific combinations of flow field characteristics, mesh configuration or solver settings.

A systematic investigation into the root cause of these convergence failures is beyond the scope of this thesis. However, several potential contributing factors were identified through observation:

While the mesh quality metrics in Comsol did not produce warnings, it is possible that local refinement is needed in regions with high flow gradients or acoustic activity at higher frequencies. The wavelength decreases with increasing frequency, potentially requiring finer mesh resolution than what was used.

As discussed in the Comsol documentation [108], the LNS equations can develop Kelvin-Helmholtz instabilities when solved in the frequency domain with an iterative solver. These instabilities can prevent convergence, particularly in regions with strong shear flows. The Gradient Term Suppression GTS stabilization method was not tested in this work.

Although the Perfectly Matched Layers functioned correctly when results were obtained, improper PML settings or insufficient PML thickness could contribute to convergence failures at certain frequencies.

The default iterative solver settings may not be optimal for this combination of geometry, flow field, and frequency range. Adjustments to solver tolerances, preconditioning methods, or iterative algorithms might improve convergence.

Despite these convergence challenges, sufficient data was obtained in the frequency range of interest to answer the research question. The failures occurred sporadically and did not prevent the analysis of the mean flow effects on TL. This thesis does not include data from simulations that fail to converge.

6 Conclusions

This thesis successfully validates a FEM-based linear acoustics model for Transmission Loss (TL) calculations in exhaust components, achieving results that can be considered exact for engineering decision-making in cases where flow is negligible.

The work also establishes a state-of-the-art complementary model: A LNS model combining CFD and FEM, incorporating mean flow effects, and allows for evaluation of whether flow effects need to be considered in the design. Simulation and validation are done on the patented mixing silencer geometry.

A summary for properties of the two simulation methods is shown in Table 10.

Table 10: Summary of the properties of the liner acoustic and aeroacoustic simulation methods. $p_{fluid}, \boldsymbol{u}, T, \rho$ and ν_t refer to fluid pressure, velocity, temperature, density and turbulent viscosity fields, respectively.

	Linear acoustics model	**Aeroacoustics model**
Software	COMSOL 6.4	COMSOL 6.4 and OpenFOAM v13
Assumptions	Lossless ideal gas, no flow	Steady flow, all physics present
Geometry	No restrictions	Meshing for CFD can be a challenge for complicated models
Validity	Validated for the mixing silencer	Validated only for other geometries
Maturity	Industry-standard	State-of-the-art
Input data	Ambient pressure and temperature, incident wave	Incident wave and full CFD solution fields for $p_{fluid}, \boldsymbol{u}, T, \rho, \nu_t$
Output data	Acoustic pressure field	Acoustic variations in pressure, temperature and velocity fields
Equations	Inhomogeneous Helmholtz	Linearised Navier-Stokes (LNS)
Relative computational cost	Minutes to hours	Hours to a day
Measured value	Transmission Loss (TL)	Transmission Loss (TL)

The linear acoustics model demonstrates exceptional accuracy, nearly exactly predicting measurement results for three different components. This model is reliable in cases without flow or with negligible flow effects. The practical workflow requires very few assumptions yet achieves remarkable accuracy, making it immediately applicable for current engineering needs. The model is not constrained to low frequencies and successfully handles high-order

resonances in the ducts, incorporating higher-order modes at the inlet, outlet, and within the domain.

The LNS aeroacoustics model, while not yet experimentally validated, follows established methodologies from validated cases and is correct with high confidence. This model reveals that flow presence measurably affects component dimensioning in the case of the mixing silencer, causing the TL peak to shift to lower frequencies and become less sharp, reducing in amplitude.

Interestingly, in the case of the mixing silencer, the simulations prove insensitive to the exact CFD solution used, especially regarding the frequency of the TL maxima. This should be interpreted so that in cases, where there are no oscillations in the flow and a good steady-state solution can be found, the computationally cheapest steady-state solution is adequate for practical applications. Otherwise, transient simulations should be run, and an average flow should be calculated over multiple oscillation cycles for accurate results. Using a random iteration from an oscillating steady-state solution is not recommended, even though the results in this thesis happen to be acceptable even with this approach. This is because the randomness will always propagate to the results.

The mapping and meshing procedures are performed in a physically sound manner, though wall functions are employed in the CFD rather than fully resolving all boundary phenomena.

An unexpected discovery during the CFD analysis is the identification of oscillatory aspects of the flow around the mixing plate, which has implications for vibro-acoustic behaviour and warrants further investigation.

From a computational perspective, both models are feasible within standard engineering workflows, with simulation times using 36 cores generally measured in hours rather than days. This practicality is achieved without requiring cluster-level computational resources, making the approach accessible for routine engineering use. The models are implementable for any duct component with an inlet and an outlet, though computational cost increases with higher frequencies, more complex flows or if more resolution is needed.

The choice of Comsol as the primary simulation platform proves advantageous, offering equivalent capabilities to Actran while providing superior multi-physics capabilities, technical support, and meshing procedures. This platform flexibility allows for additional modelling

capabilities such as porous media representation, which can be valuable for future product development activities.

Both the linear acoustics and LNS models represent significant improvements over traditional analytical methods that are often inaccurate or case specific. By utilizing modern software and computational capacity, these approaches enable improved and correctly dimensioned products, supported by availability of computational resources. The models move the field forward by providing a practical balance between computational cost and accuracy, particularly through the one-directional CFD-to-FEM coupling approach used in the LNS model. It represents current state-of-the-art for TL simulations, including flow effects and turbulence. Additionally, there is potential for simplifications that can be validated to cases where the component is axisymmetric and a sector mesh approach could be enough, for example.

The extensive theoretical foundation and literature review created for this work ensure that all numerical choices are well justified based on underlying physics. This theoretical understanding extends beyond simulation validation to provide more in-depth insights into the various phenomena within the studied components; Flow oscillations, various approaches for muffling low-frequency acoustic excitations, measurement methods and vibro-acoustics of exhaust components.

6.1 Practical suggestions

The suggested immediate use of the methodologies in this thesis will be running both models for various components in upcoming deliveries to collect data and possibly correct dimensions. This will answer the following questions for various sizes and configurations of components: Whether the tuning is correct regarding excitation frequencies coming from the engine, and how various flow conditions affect the component.

Once data points have been gathered, more general observations can be made. By interpolating the data, questions can be answered about when flow can be ignored, how the quarter-wave chamber lengths should be dimensioned and whether there are differences between the behaviours of various designs. At this point, simulations will only need to be run for cases that are far outside the researched parameters and for verification.

As the LNS model considers the full range of physical phenomena within a silencer with flow, it can be used to prototype innovative designs. Porous media modelling should be easily

added to the model to allow for evaluations of damped Helmholtz resonators or metamaterial mufflers, like some of the concepts referenced in the literature review.

As the models are not constrained to any specific geometry, they can also be used to evaluate TLs in other components of the system to gain a more complete understanding.

6.2 Future work

While this thesis establishes robust methodologies for TL calculations in exhaust components, several promising directions for future research and development emerge from the findings.

In terms of implementing the workflow, the most immediate priority is experimental validation of the LNS model through measurements of large-scale components under flow conditions. Although the model follows validated methodologies and is theoretically sound, experimental confirmation of the predicted flow effects on TL would strengthen confidence in the results and potentially reveal additional physical phenomena not captured in the current simulations. Such validation measurements would also provide valuable data for assessing the accuracy of the steady-state CFD solution assumption for different flow regimes and component geometries, and whether boundary layer phenomena should be modelled with denser meshes.

Sensitivity studies for the LNS model would also be useful. They could answer questions like whether there needs to be inlet and outlet ducts included in the domain or if the domain can start at the ends of the component. The set-up of PML layers and possible effects of having more accurate meshes near walls could be studied.

Once the method is validated, more cases with various flow conditions should be run to collect data that graphs could be fitted onto. Then, fitted graphs should be used for dimensioning of the product.

Identifying the reason for the convergence challenges encountered in the LNS model is naturally important for allowing the use of the methodology.

The unexpected discovery of oscillatory flow behaviour around the mixing plate presents an intriguing research opportunity. A dedicated investigation into these oscillations and their vibro-acoustic properties could reveal important implications for component design and performance. Understanding whether these flow oscillations contribute to structural excitation

or acoustic phenomena could inform both the acoustic and mechanical design of mixing silencers and similar components.

Model simplification represents a significant opportunity for improving computational efficiency. The current work demonstrates that the LNS model is insensitive to the exact CFD solution for the mixing silencer geometry, suggesting that simpler flow models might be sufficient. Future studies should systematically investigate whether convection models (like the linearised Euler equations) that neglect turbulence yield comparable TL results, and whether potential flow approximations or two-dimensional flow representations can adequately capture the relevant physics. Such simplifications could dramatically reduce computational costs while maintaining sufficient accuracy for engineering applications. They would also keep the whole process contained within the Comsol environment, allowing better automation/integration of the solvers. The boundary between when simplifications are acceptable and when full LNS treatment is necessary remains to be established across different component types and operating conditions. A sector mesh-based symmetry approach could also make the linear acoustics model much faster, making its accuracy worth studying.

From a practical deployment perspective, developing a Comsol application would enable company-wide use of these methodologies by engineers who are not specialists in acoustics or CFD. Such an application could incorporate standardised workflows, automated meshing procedures, and guided parameter selection based on the sensitivity studies conducted in this work. This democratization of the modelling capability would accelerate its adoption and maximize its impact on product development activities.

The methodology's applicability extends beyond the mixing silencer geometry studied here. Future work should systematically apply these models to other exhaust component types to build a comprehensive library of validated approaches and component-specific insights. Each new geometry may reveal unique characteristics or require specific modelling considerations, and documenting these findings would benefit the broader engineering community.

Integration with structural simulations represents another valuable extension. The Comsol environment facilitates coupling between acoustic and structural domains, enabling comprehensive vibro-acoustic analyses. Such coupled simulations could address questions about structure-borne noise transmission, component fatigue due to acoustic loading, and the interaction between flow-induced vibrations and acoustic performance. Given that low-frequency excitations are problematic from both acoustic and vibration standpoints, as

discussed in the theoretical foundation, these coupled analyses could provide holistic design guidance.

From the work in this thesis, it is extremely difficult to create rationalizations or physical interpretations for why the TL is affected by the flow. Various experiments like reversing the acoustic propagation to be from the outlet to the inlet and modifying various parameters one by one could be used to identify these connections. This knowledge could then be used to improve or create new silencer designs.

Finally, as the methodology matures and more case studies accumulate, developing standardised procedures and guidelines for model setup and result interpretation would ensure consistent application across different users and projects. These standards could specify meshing requirements for different frequency ranges, convergence criteria, best practices for CFD-to-FEM mapping, and protocols for validating new component types. Such documentation would reduce the learning curve for new users and improve the reliability of results across different applications.

References

[1] "Tacoma Narrows Bridge history - Bridge - Lessons from failure." Accessed: Sep. 17, 2025. [Online]. Available: https://wsdot.wa.gov/tnbhistory/bridges-failure.htm

[2] C. A. Silva, R. Vilaça, A. Pereira, and R. J. Bessa, "A review on the decarbonization of high-performance computing centers," *Renew. Sustain. Energy Rev.*, vol. 189, p. 114019, Jan. 2024, doi: 10.1016/j.rser.2023.114019.

[3] J. N. Reddy, *Computational Methods in Engineering: Finite Difference, Finite Volume, Finite Element, and Dual Mesh Control Domain Methods*. Boca Raton: CRC Press, 2024. doi: 10.1201/9781003382812.

[4] R. Guo, W. Tang, and W. Zhu, "Comparison of 1D transfer matrix method and finite element method with tests for acoustic performance of multi-chamber perforated resonator," *Appl. Acoust.*, vol. 112, pp. 140–146, Nov. 2016, doi: 10.1016/j.apacoust.2016.05.018.

[5] M. J. Crocker and J. P. Arenas, *Engineering acoustics: noise and vibration control*. in Wiley series in acoustics noise and vibration. Hoboken, NJ: John Wiley & Sons, Inc, 2021.

[6] Y. Chen and L. Lv, "Design and evaluation of an Integrated SCR and exhaust Muffler from marine diesels," *J. Mar. Sci. Technol.*, vol. 20, no. 3, pp. 505–519, Sep. 2015, doi: 10.1007/s00773-014-0302-1.

[7] G. Kyaw Oo D'Amore, "A Combined FEM-CFD Methodology to Study and Optimize Acoustic Properties of Marine Exhaust Lines," PhD Dissertation, Università degli Studi di Trieste, 2021. Accessed: Sep. 03, 2025. [Online]. Available: https://arts.units.it/handle/11368/3030492

[8] M. Kheybari and S. Ebrahimi-Nejad, "Dual-target-frequency-range stop-band acoustic metamaterial muffler: acoustic and CFD approach," *Eng. Res. Express*, vol. 3, no. 3, p. 035027, Aug. 2021, doi: 10.1088/2631-8695/ac1989.

[9] International Maritime Organisation, *MARPOL: Articles, Protocols, Annexes and unified interpretations of the International Convention for the Prevention of Pollution from Ships, 1973, as modified by the 1978 and 1997 Protocols*. IMO e-Publications, 2022. doi: 10.62454/KF520E.

[10] International Maritime Organization, *Code on Noise Levels on Board Ships*. International Maritime Organization, 2014. doi: 10.62454/K817E.

[11] M. Biot *et al.*, “Quantification of airborne noise emitted by ships based on class notation,” *Ocean Eng.*, vol. 296, p. 117085, Mar. 2024, doi: 10.1016/j.oceaneng.2024.117085.

[12] “ISO 20283-5:2016,” ISO. Accessed: Feb. 06, 2026. [Online]. Available: https://www.iso.org/standard/68125.html

[13] A. Coulon, R. Salanon, and L. Ancian, “Innovative numerical fatigue methodology for piping systems: qualifying Acoustic Induced Vibration in the Oil&Gas industry,” *Procedia Eng.*, vol. 213, pp. 762–775, Jan. 2018, doi: 10.1016/j.proeng.2018.02.072.

[14] S. Liu, C. Gu, Q. Tian, D. Huang, and Y. Guo, “Research on the vibration mechanism of compressor complex exhaust pipeline based on transient flow,” *Int. J. Hydrog. Energy*, vol. 139, pp. 886–894, Jun. 2025, doi: 10.1016/j.ijhydene.2023.12.203.

[15] Y. Zhao, Y. Fan, K. Fagerholt, and J. Zhou, “Reducing sulfur and nitrogen emissions in shipping economically,” *Transp. Res. Part Transp. Environ.*, vol. 90, p. 102641, Jan. 2021, doi: 10.1016/j.trd.2020.102641.

[16] O. Shaketange, “Exhaust scrubber systems onboard vessels,” Bachelor’s Thesis, Satakunta University of Applied Sciences, 2024.

[17] K.-O. Rönnback, “An Exhaust Gas Silencer for an Exhaust System of an Internal Combustion Engine, and the Exhaust System,” EP3707355A1, Sep. 16, 2020

[18] R. Y. Vidana Morales, S. Ortega Cisneros, J. R. Camacho Perez, F. Sandoval Ibarra, and R. Casas Carrillo, “3D Simulation-Based Acoustic Wave Resonator Analysis and Validation Using Novel Finite Element Method Software,” *Sensors*, vol. 21, no. 8, p. 2715, Jan. 2021, doi: 10.3390/s21082715.

[19] J. Wall, “Dynamics Study of an Automobile Exhaust System,” Licentiate dissertation, Blekinge Institute of Technology, 2003.

[20] Alaa Ismail, Abdalla Mostafa Elmarhomy, Abd El-Aziz Morgan, and Ashraf Mostafa Hamed, “Numerical Modeling and Geometry Enhancement of a Reactive Silencer,” *J. Adv. Res. Fluid Mech. Therm. Sci.*, vol. 106, no. 1, pp. 147–157, Jun. 2023, doi: 10.37934/arfmts.106.1.147157.

[21] Ben S. Cazzolato, Carl Q. Howard, and Colin H. Hansen, “Finite element analysis of an industrial reactive silencer,” in *Proceedings of The Fifth International Congress of Sound and Vibration*, 1997. Accessed: Sep. 12, 2025. [Online]. Available: https://www.researchgate.net/publication/235923166_Finite_element_analysis_of_an_industrial_reactive_silencer

[22] M. R. Jokandan, A. safari Variani, and S. Ahmadi, “Study of acoustic and aerodynamic performance of reactive silencer with different configurations: Theoretical, modeling and experimental,” *Heliyon*, vol. 9, no. 9, Sep. 2023, doi: 10.1016/j.heliyon.2023.e20058.

[23] M. Haghighi, R. Mirzaei, A. Putra, and E. Taban, “A comprehensive review of advances and techniques in muffler acoustics and design,” *Int. J. Environ. Sci. Technol.*, vol. 21, no. 13, pp. 8695–8716, Sep. 2024, doi: 10.1007/s13762-024-05686-6.

[24] J.-L. Migeot, J.-P. Coyette, and G. Lielens, *Acoustics: essential concepts, theory and models of linear acoustics for engineers*. Bruxelles: IJK Numerics, 2016.

[25] Comsol, “Introduction to the Governing Equations and Scope of Acoustics.” Accessed: Jan. 22, 2026. [Online]. Available: https://www.comsol.com/multiphysics/acoustics

[26] N. J. Lass and J. J. Donai, *Hearing science fundamentals*, Second edition. San Diego, CA: Plural Publishing, Inc, 2023.

[27] L. J. Eriksson, “Higher order mode effects in circular ducts and expansion chambers,” *J. Acoust. Soc. Am.*, vol. 68, no. 2, pp. 545–550, Aug. 1980, doi: 10.1121/1.384768.

[28] M. J. Crocker, *Handbook of Acoustics*. New York: John Wiley & Sons, 1998.

[29] L. E. Kinsler, Ed., *Fundamentals of acoustics*, 4th ed. New York: Wiley, 2000.

[30] M. J. Crocker, A. J. Price, and F. M. Kessler, *Noise and noise control. Volume I*. Boca Raton, Florida: CRC Press, Inc., 1975.

[31] M. Möser, *Engineering acoustics: an introduction to noise control*, 2nd ed. Dordrecht New York: Springer, 2009.

[32] M.-H. Park, S. Yeo, J.-H. Choi, and W.-J. Lee, “Review of noise and vibration reduction technologies in marine machinery: Operational insights and engineering experience,” *Appl. Ocean Res.*, vol. 152, p. 104195, Nov. 2024, doi: 10.1016/j.apor.2024.104195.

[33] T. Nakada, “Excitation mechanism for engine vibration of half-order components,” *JSAE Rev.*, vol. 17, no. 4, pp. 387–393, Oct. 1996, doi: 10.1016/S0389-4304(96)00047-1.

[34] W. Zhang and F. Xin, “Broadband low-frequency sound absorption via Helmholtz resonators with porous material lining,” *J. Sound Vib.*, vol. 578, p. 118330, May 2024, doi: 10.1016/j.jsv.2024.118330.

[35] S. Kumar, “Linear Acoustic Modelling And Testing of Exhaust Mufflers,” Master of Science Thesis, Royal Institute of Technology, Stockholm, 2007.

[36] M. L. Munjal, *Acoustics of Ducts and Mufflers*. Newark, UNITED KINGDOM: John Wiley & Sons, Incorporated, 2014.

[37] Z. Tao and A. F. Seybert, “A Review of Current Techniques for Measuring Muffler Transmission Loss,” presented at the SAE 2003 Noise & Vibration Conference and Exhibition, May 2003, pp. 2003-01–1653. doi: 10.4271/2003-01-1653.

[38] “ISO 10534,” ISO. Accessed: Sep. 16, 2025. [Online]. Available: https://www.iso.org/standard/81294.html

[39] C. J. Young and M. J. Crocker, “Prediction of transmission loss in mufflers by the finite−element method,” *J. Acoust. Soc. Am.*, vol. 57, no. 1, pp. 144–148, Jan. 1975, doi: 10.1121/1.380424.

[40] “ACTRAN 2022.1 User’s Guide - Volume 1 : Installation, Operations, Theory and Utilities.” Hexagon AB, 2022.

[41] P. K. Kundu, I. M. Cohen, P. S. Ayyaswamy, and H. H. Hu, *Fluid mechanics*, 4th ed. London: Elsevier, 2007.

[42] R. J. Astley, “Numerical Acoustical Modeling (Finite Element Modeling),” in *Handbook of Noise and Vibration Control*, 1st ed., M. J. Crocker, Ed., Wiley, 2007, pp. 101–115. doi: 10.1002/9780470209707.ch7.

[43] M. F. Hamilton and D. T. Blackstock, Eds., *Nonlinear Acoustics*. Cham: Springer Nature Switzerland, 2024. doi: 10.1007/978-3-031-58963-8.

[44] “COMSOL Documentation - Acoustics Module User’s Guide.” Accessed: Oct. 01, 2025. [Online]. Available: https://doc.comsol.com/6.3/doc/com.comsol.help.aco/AcousticsModuleUsersGuide.pdf

[45] S. Bilawchuk and K. R. Fyfe, “Comparison and implementation of the various numerical methods used for calculating transmission loss in silencer systems,” *Appl. Acoust.*, vol. 64, no. 9, pp. 903–916, Sep. 2003, doi: 10.1016/S0003-682X(03)00046-X.

[46] “COMSOL Documentation - Basics of Acoustics.” Accessed: Oct. 13, 2025. [Online]. Available: https://doc.comsol.com/6.3/docserver/#!/com.comsol.help.aco/aco_introduction.02.04.html

[47] N. Atalla and F. Sgard, *Finite element and boundary methods in structural acoustics and vibration*. Boca Raton: CRC press, 2015.

[48] C. Weng, S. Boij, and A. Hanifi, "The attenuation of sound by turbulence in internal flows," *J. Acoust. Soc. Am.*, vol. 133, no. 6, pp. 3764–3776, Jun. 2013, doi: 10.1121/1.4802894.

[49] H. Zhirong, J. Zhenlin, and F. Yiliang, "Acoustic attenuation prediction and analysis of perforated hybrid mufflers with non-uniform flow based on frequency domain linearized Navier-Stokes equations," *Adv. Mech. Eng.*, vol. 16, no. 1, p. 16878132231226055, Jan. 2024, doi: 10.1177/16878132231226055.

[50] C. D. Field and F. R. Fricke, "Theory and applications of quarter-wave resonators: A prelude to their use for attenuating noise entering buildings through ventilation openings," *Appl. Acoust.*, vol. 53, no. 1–3, pp. 117–132, Jan. 1998, doi: 10.1016/S0003-682X(97)00035-2.

[51] U. Ingard, "On the Theory and Design of Acoustic Resonators," *J. Acoust. Soc. Am.*, vol. 25, no. 6, pp. 1037–1061, Nov. 1953, doi: 10.1121/1.1907235.

[52] K. S. Andersen, "Analyzing Muffler Performance Using the Transfer Matrix Method," in *Proceedings of the COMSOL Conference 2008*, Hannover, 2008.

[53] L. Gaul, J. Herrmann, and M. Junge, "Vibro-Acoustic Simulation of Automotive Piping and Exhaust Systems," in *Proceedings of the 43rd DAGA*, Kiel, 2017.

[54] M. F. Calton and S. D. Sommerfeldt, "Modeling acoustic resonators: From theory to application," in *INTER-NOISE and NOISE-CON Congress and Conference Proceedings*, San Francisco, CA: Institute of Noise Control Engineering, 2015.

[55] D. P. Jena and S. N. Panigrahi, "Numerically estimating acoustic transmission loss of a reactive muffler with and without mean flow," *Measurement*, vol. 109, pp. 168–186, Oct. 2017, doi: 10.1016/j.measurement.2017.05.065.

[56] H. Huang, Z. Chen, and Z. Ji, "One-way fluid-to-acoustic coupling approach for acoustic attenuation predictions of perforated silencers with non-uniform flow," *Adv. Mech. Eng.*, vol. 11, no. 5, p. 1687814019847066, May 2019, doi: 10.1177/1687814019847066.

[57] Z. Chu, F. Kuang, R. Kang, and X. Gao, "Effects of airflow on the acoustic attenuation performance of reactive muffler," *J. Vibroengineering*, vol. 18, no. 1, pp. 637–648, Feb. 2016.

[58] H. Huang and Z. Ji, "Acoustic attenuation analysis of circular dual-chamber mufflers with non-uniform flow," in *Proceedings of Inter-Noise 2019*, Madrid: Institute of

Noise Control Engineering, Sep. 2019. Accessed: Dec. 03, 2025. [Online]. Available: https://ince.publisher.ingentaconnect.com/contentone/ince/incecp/2019/00000259/00000009/art00108#expand/collapse

[59] D. Zhang, X. Su, Y. Sun, Y. Luo, X. Sun, and C. Chen, "Performance study and improvement of space-folded metamaterial muffler for pipe under grazing flow," *Appl. Acoust.*, vol. 220, p. 109984, Apr. 2024, doi: 10.1016/j.apacoust.2024.109984.

[60] J. Tyndall, *Sound: A Course of Eight Lectures Delivered at the Royal Institution of Great Britain*. in Cambridge library collection. Physical sciences. Cambridge: Cambridge University Press, 1867. doi: 10.1017/CBO9781107360686.

[61] J. Y. Chung, J. Pope, and D. A. Feldmaier, "APPLICATION OF ACOUSTIC INTENSITY MEASUREMENT TO ENGINE NOISE EVALUATION," presented at the 1979 Automotive Engineering Congress and Exposition, Detroit, Michigan, United States, Feb. 1979, p. 790502. doi: 10.4271/790502.

[62] M. J. Crocker, P. K. Raju, and B. Forssen, "Measurement of Transmission Loss of Panels by the Direct Determination of Transmitted Acoustic Intensity," *Noise Control Eng.*, vol. 17, no. 1, p. 6, 1981, doi: 10.3397/1.2832181.

[63] M. C. Mcgary and M. J. Crocker, "Surface acoustical intensity measurements on a diesel engine," presented at the Acoust. Soc. of Am. Meeting, Atlanta, Apr. 1980. Accessed: Oct. 06, 2025. [Online]. Available: https://ntrs.nasa.gov/citations/19800016610

[64] T. E. Reinhart and M. J. Crocker, "Source Identification on a Diesel Engine Using Acoustic Intensity Measurements," *Noise Control Eng.*, vol. 18, no. 3, p. 84, 1982, doi: 10.3397/1.2832203.

[65] "ISO 266:1997," ISO. Accessed: Feb. 06, 2026. [Online]. Available: https://www.iso.org/standard/1350.html

[66] "ISO 354:2003," ISO. Accessed: Feb. 06, 2026. [Online]. Available: https://www.iso.org/standard/34545.html

[67] "ISO 3744:2025," ISO. Accessed: Feb. 06, 2026. [Online]. Available: https://www.iso.org/standard/80866.html

[68] "ISO 3745:2012," ISO. Accessed: Feb. 06, 2026. [Online]. Available: https://www.iso.org/standard/45362.html

[69] "ISO 3746:2010," ISO. Accessed: Feb. 06, 2026. [Online]. Available: https://www.iso.org/standard/52056.html

[70] “ISO 9614-3:2002,” ISO. Accessed: Feb. 06, 2026. [Online]. Available: https://www.iso.org/standard/24012.html

[71] “ISO 10534-2:2023,” ISO. Accessed: Feb. 06, 2026. [Online]. Available: https://www.iso.org/standard/81294.html

[72] “ISO 15186,” ISO. Accessed: Feb. 06, 2026. [Online]. Available: https://www.iso.org/standard/26097.html

[73] “IEC 61043:1993.” Accessed: Feb. 06, 2026. [Online]. Available: https://webstore.iec.ch/en/publication/4353

[74] “ANSI/ASA S12.12-1992 (R2020) - Engineering Method for the Determination of Sound Power Levels of Noise Sources Using Sound Intensity.” Accessed: Feb. 06, 2026. [Online]. Available: https://webstore.ansi.org/standards/asa/ansiasas12121992r2020?srsltid=AfmBOoqSSXgGybH3eKX60Kbs4onK2iS60gJUH_iOSNE3gIT5WPg-d3wX

[75] “Standard Test Method for Laboratory Measurement of Airborne Transmission Loss of Building Partitions and Elements Using Sound Intensity.” Accessed: Oct. 06, 2025. [Online]. Available: https://store.astm.org/e2249-02.html

[76] “ISO 21984:2018,” ISO. Accessed: Feb. 06, 2026. [Online]. Available: https://www.iso.org/standard/72304.html

[77] “MEPC.1/Circ.833 - GUIDELINES FOR THE REDUCTION OF UNDERWATER NOISE FROM COMMERCIAL SHIPPING TO ADDRESS ADVERSE IMPACTS ON MARINE LIFE - Netherlands Regulatory Framework (NeRF) – Maritime.” Accessed: Oct. 06, 2025. [Online]. Available: https://puc.overheid.nl/nsi/doc/PUC_763894_14/1/

[78] “MEPC 74-INF.28 - Ship underwater radiated noise technical report and matrix (Canada).”

[79] “Class notations – noise and vibration,” DNV. Accessed: Oct. 06, 2025. [Online]. Available: https://www.dnv.com/services/class-notations-noise-and-vibration-4712/

[80] “NR636.” Accessed: Oct. 06, 2025. [Online]. Available: https://erules.veristar.com/dy/data/bv/pdf/636-NR_2016-12.pdf

[81] American Bureau of Shipping, “Guidance Notes on Noise and Vibration Control for Inhabited Spaces.” 2017.

[82] Korean Register, “Guidance for Noise and Vibration.” Accessed: Oct. 06, 2025. [Online]. Available:

https://www.krs.co.kr/KRRules/KRRules2025/data/data_other/ENGLISH/Guidance%20for%20Noise%20and%20Vibration_2020.pdf

[83] Korean Register, *Guidelines for the Identification of Vibration Issues and Remedial Measures on Ships*, GL-0031-E, 2018.

[84] "LR-GN-31 Guidance Notes | LR." Accessed: Oct. 06, 2025. [Online]. Available: https://www.lr.org/en/knowledge/lloyds-register-rules/guidance-notes/guidance-notes-general-overview-of-ship-structural-vibration-problems/

[85] J. Jiang, F. Gu, R. Gennish, D. J. Moore, G. Harris, and A. D. Ball, "Monitoring of diesel engine combustions based on the acoustic source characterisation of the exhaust system," *Mech. Syst. Signal Process.*, vol. 22, no. 6, pp. 1465–1480, Aug. 2008, doi: 10.1016/j.ymssp.2007.12.003.

[86] Z. Gao and K. Saine, "Exhaust pipeline influence on large engine exhaust noise measurement and the countermeasure," in *Proceedings of Akustiikkapäivät 2023*, Tampere, 2023.

[87] "ACTRAN 2022.2 User's Guide - Volume 2: Extended DAT Input File Syntax." Hexagon AB, 2022.

[88] "About - SIDLAB." Accessed: Oct. 30, 2025. [Online]. Available: https://www.sidlab.se/about-us

[89] "silencers for engines – shipbuilding industry – marine industry | JTK Power » JTK-Power." Accessed: Apr. 07, 2026. [Online]. Available: https://www.jtk-power-group.com/group-products-and-services/silencer-solutions-en-us

[90] "OpenFOAM 13 | OpenFOAM." Accessed: Nov. 03, 2025. [Online]. Available: https://openfoam.org/version/13/

[91] W. Na, "A Linearized Navier-Stokes Equations Methodology for Aeroacoustic and Thermoacoustic Simulations," Doctoral Thesis, KTH Royal Institute of Technology, Stockholm, 2021.

[92] H. K. Versteeg and W. Malalasekera, *An introduction to computational fluid dynamics: the finite volume method*, 2. ed., [Nachdr.]. Harlow: Pearson/Prentice Hall, 2007.

[93] Eero Virtanen, "OpenFOAM-for-Investigation-of-Aeroacoustic-Flow-Effects." Accessed: Jan. 09, 2026. [Online]. Available: https://github.com/mineero01/OpenFOAM-for-Investigation-of-Aeroacoustic-Flow-Effects/tree/main

[94] F. R. Menter, M. Kuntz, and R. Langtry, “Ten Years of Industrial Experience with the SST Turbulence Model,” *Heat Mass Transf.*, vol. 4, 2003.

[95] F. R. Menter, R. Lechner, and A. Matyushenko, “Best Practice: RANS Turbulence Modeling in Ansys CFD.” Ansys Inc., 2021.

[96] “COMSOL Documentation - The Linearized Navier–Stokes, Frequency Domain Interface.” Accessed: Jan. 05, 2026. [Online]. Available: https://doc.comsol.com/6.4/docserver/#!/com.comsol.help.aco/aco_ug_aero.08.031.html%23688934

[97] “Helmholtz Resonator with Flow: Imported Fluid Flow from CGNS Data,” COMSOL. Accessed: Jan. 07, 2026. [Online]. Available: https://www.comsol.com/model/helmholtz-resonator-with-flow-imported-fluid-flow-from-cgns-data-143941

[98] J. Gikadi, S. Föller, and T. Sattelmayer, “Impact of turbulence on the prediction of linear aeroacoustic interactions: Acoustic response of a turbulent shear layer,” *J. Sound Vib.*, vol. 333, no. 24, pp. 6548–6559, Dec. 2014, doi: 10.1016/j.jsv.2014.06.033.

[99] “COMSOL Documentation - Coupling to Turbulent Flows (Eddy Viscosity).” Accessed: Jan. 07, 2026. [Online]. Available: https://doc.comsol.com/6.4/docserver/#!/com.comsol.help.aco/aco_ug_aero.08.123.html?highlight=spf.mut

[100] H. Kim and I. Lee, “Effect of Flow on Various Helmholtz Resonators,” *Int. J. Acoust. Vib.*, vol. 25, no. 1, pp. 73–78, Mar. 2020, doi: 10.20855/ijav.2020.25.11549.

[101] C. Greenshields, “OpenFOAM v13 User Guide,” CFD Direct. Accessed: Jan. 08, 2026. [Online]. Available: https://doc.cfd.direct/openfoam/user-guide-v13/snappyhexmesh/

[102] “Y plus wall distance estimation -- CFD-Wiki, the free CFD reference.” Accessed: Jan. 08, 2026. [Online]. Available: https://www.cfd-online.com/Wiki/Y_plus_wall_distance_estimation

[103] “COMSOL Documentation - Mapping Between Fluid Flow and Acoustics Mesh.” Accessed: Jan. 07, 2026. [Online]. Available: https://doc.comsol.com/6.4/docserver/#!/com.comsol.help.aco/aco_ug_aero.08.122.html

[104] “Products,” GRAS Sound and Vibration. Accessed: Jan. 27, 2026. [Online]. Available: https://www.grasacoustics.com/products/special-microphone/probe-microphones/product/189-40sc

[105] S. Dasila, A. Surendran, V. Subramanian, and C. V. Krishnamurthy, “A Comparative Analysis Of Transmission Loss In Helmholtz Resonators And Quarter Wave Resonators,” in *Proceedings of the 2023 COMSOL Conference*, 2023.

[106] “Helmholtz Resonator with Flow: Interaction of Flow and Acoustics,” COMSOL. Accessed: Feb. 09, 2026. [Online]. Available: https://www.comsol.com/model/helmholtz-resonator-with-flow-interaction-of-flow-and-acoustics-35011

[107] N. Ye, “Noise Reduction of Centrifugal Compressors using Array of Quarter Wavelength Resonators,” Jul. 2014, Accessed: Jan. 20, 2026. [Online]. Available: https://hdl.handle.net/1969.1/153659

[108] “COMSOL Documentation - Linearized Navier–Stokes Model.” Accessed: Jan. 14, 2026. [Online]. Available: https://doc.comsol.com/6.4/docserver/#!/com.comsol.help.aco/aco_ug_aero.08.033.html